ASSESSING THE ROLE OF THE TRANSCRIPTION FACTOR *FOXC1* IN EXPRESSION AND REGULATION OF THE ADHERENS JUNCTION PROTEIN N-CADHERIN DURING CORNEAL ENDOTHELIUM DEVELOPMENT

Viveshree Shalom Govender

A research report submitted to the Faculty of Science and Agriculture, University of KwaZulu-Natal, in partial fulfilment of the academic requirements for the degree of Master of Science in Biological & Conservation Sciences (Molecular Science).

October, 2011

As the candidate's supervisor I have/have not approved this thesis/dissertation for submission.

Signed: _____ Name: Dr. Paula Sommer Date: 14/10/2011

Preface

The experimental work described in this dissertation was carried out in the School of Biological & Conservation Sciences, University of KwaZulu-Natal, Westville, from January 2009 to December 2010, under the supervision of Dr. Paula Sommer.

These studies represent original work by the author and have not otherwise been submitted in any form for any degree or diploma to any tertiary institution. Where use has been made of the work of others, it is duly acknowledged in the text.

Declaration: Plagiarism

I, Viveshree Shalom Govender, declare that

1. The research reported in this dissertation, except where otherwise indicated, is my original research. It is being submitted in partial fulfilment of the requirements for the degree of Master of Science in Biological Sciences (Molecular Sciences) at the University of KwaZulu-Natal.

2. This dissertation has not been submitted for any degree or examination at this or any other university.

3. This dissertation does not contain other persons' data, pictures, graphs or other information, unless specifically acknowledged as being sourced from other persons.

4. This dissertation does not contain other persons' writing, unless specifically acknowledged as being sourced from other researchers. Where other written sources have been quoted, then:
    a. Their words have been re-written but the general information attributed to them has been referenced
    b. Where their exact words have been used, then their writing has been placed in italics and inside quotation marks, and referenced.

5. This dissertation does not contain text, graphics or tables copied and pasted from the Internet, unless specifically acknowledged, and the source being detailed in the thesis and in the References sections.

Signed: .....

Viveshree Shalom Govender 14th day of October, 2011

Dedication

This dissertation is dedicated to my late grandmother, mother and aunt in gratitude of their unwavering support, strength and belief in me during my adventures through academia, and life. To my father, for his steadfast support in all my endeavours during this tumultuous and arduous academic journey, words will never do justice in describing my gratitude for the sacrifices that you have made and the hardships that you have endured in order to allow me the privilege of learning and knowledge. If I can aspire to half the success of my elders, then I have achieved in life.

Abstract

The proper organization and differentiation of the anterior segment is pivotal for normal eye development. Neural crest-derived POM cells are key contributors to correct anterior segment formation, differentiating to form the monolayered corneal endothelium. Mice with homozygous null mutations in the forkhead transcription factor gene, *Foxc1,* fail to develop a proper corneal endothelium stabilized by adherens junctions, with the endothelium adhering to the lens, preventing anterior chamber separation. The aim of this study was to evaluate the interaction between *Foxc1* and the adherens junction protein, N-cadherin, as well as an associated gene, *Msx1,* during key stages in corneal endothelium development. *Foxc1* was over-expressed in E12.5 and E13.5 POM cells and qPCR was carried out to determine the effect of *Foxc1* on *N-cadherin* and *Msx1* gene expression. Data showed over-expression of *Foxc1* in wildtype E12.5 and E13.5 POM cells to cause significant fluctuations in *N-cadherin* and *Msx1* expression ($p < 0.05$). POM cells were then transfected with a *Foxc1* knock-down plasmid or the *Foxc1* over-expression plasmid to evaluate the effect of *Foxc1* on N-cadherin protein expression by Western blot analysis, however, these results were inconsistent with the gene expression analyses with no significant differences in N-cadherin expression detected. N-cadherin protein expression and localization was then further assessed by means of immunocytochemistry (ICC) and confocal microscopy in monolayer and hanging-drop POM cell cultures. Both qPCR and confocal microscopy data showed consistency, indicating increased amounts of N-cadherin in E12.5 cells relative to E13.5 cells, with membrane-bound N-cadherin showing a clear lattice-work pattern in hanging drop culture. *Foxc1* over-expression/knock-down studies on E12.5 and E13.5 POM cells together suggest that N-cadherin is transcriptionally regulated by *Foxc1* and that *Foxc1* has a threshold level at which it is able to exert control over N-cadherin in POM cells. *Foxc1* expression is therefore essential in establishing N-cadherin adhesion junctions in the corneal endothelium. Preliminary data also suggests that *Msx1* may directly interact with *Foxc1* in POM cells, however, further studies must be undertaken to verify and establish the effects of *Foxc1*/*N-cadherin*/*Msx1* interaction in the development of a cohesive, integrated corneal endothelium and functional anterior segment.

Conference contributions from this dissertation

Govender, V.S., Napier, H., Sommer, P., 2010. Analysis of the transcription factor *Foxc1* and junction protein N-cadherin during corneal endothelium development. 48th Meeting of the Microscopy Society of Southern Africa, Bela-Bela, Limpopo.

Acknowledgements

I would like to thank my supervisor, Dr. Paula Sommer, for sharing her wealth of knowledge with me and guiding me during the tenure of this project.

Sincere gratitude is extended to the National Research Foundation for the financial assistance that allowed me to pursue this degree.

Thanks to Dr. J. Wesley-Smith at the Electron Microscopy Unit at UKZN (Westville) for assistance with fluorescence microscopy, as well as to Mrs. S. Mackellar and Mrs. Pat Joubert at the Centre for Electron Microscopy at UKZN (Pietermaritzburg) for their ever-willing assistance with confocal microscopy. Heartfelt thanks go out to my Biochemistry colleagues at UKZN (Pietermaritzburg) – Dr. Celia Snyman, Kyle Goetsch, Dennis 'Chien-Yu' Lin, Daniel Bohnen and Dr. Carola Niesler - for their constructive criticism, technical assistance and candid counsel.

To my associates and lab crew, Nazeera Kasim, Taariq Karim, Zaffar Hussain, Theshnie Naidoo, Taryn Ralph, Muhammad Nakhooda, Roxanne Jane Harris, Nimisha Singh and Kerryn Houston – thanks for the memories, conversations, copious cups of tea, dH_2O and KimWipes ☺.

To my brothers: Vishnu Kevin Govender, thank you for being you; Brendan Anen Govender, your tolerance, endurance and consideration during the past six years are appreciated – thank you for going the extra mile; Alistair Govender, thank you for the philosophical conversations, comic relief and for always lending me your ear; Memphis Adrian Govender, thank you for being my role model and the voice of reason; to my baby brother Lakshan Juno Govender, thanks for being my chauffeur and gopher in times of need, you're a **star**!

A special thank you is extended to Yurisha, Virasha, Savna, Suresh Ramlucken and Sherina Ramautar and the extensive Govender clan for enduring support.

Finally, I would like to thank my parents, Siva and Nagie, for their financial support, tolerance, patience, time and understanding. Thank you to my aunt and second mother, Indrani Govender, for her steadfast moral support, motivation, scoldings, smile, love and breakfast on-the-go. To my uncle Ganes Govender, thank you for allowing me refugee status in your home! To my late grandmother, thank you for your love, care and the gift of your genes; thank you for passing on your tenacity and determination.

Table of Contents

List of Figures

List of Tables

List of Abbreviations

ARS	Axenfeld-Rieger Syndrome
ASD	Anterior segment dysgenesis
ANOVA	Analysis of variance
APS	Ammonium persulfate
BamHI	Restriction endonuclease isolated from *Bacillus amyloli*
BglII	Restriction endonuclease isolated from *Bacillus globigii*
BLAST	Basic Local Alignment Search Tool
bp	Base pairs
BSA	Bovine serum albumin
Ca^{2+}	Calcium
cDNA	Complementary deoxyribonucleic acid
$(C_T)/(C_q)$	Threshold cycle/quantification cycle
DABCO	1,4-diazabicyclo[2.2.2]octane
DAPI	4'-6-diamidino-2-phenylindole
DEPC	Diethyl polycarbonate
DNA	Deoxyribonucleic acid
DMEM	Dulbecco's Modified Eagle's medium
dNTP	Dinucleotide triphosphate
DTT	1,4-dithio-D-threitol
(E)	Embryonic day
ECL	Enhanced chemluminescence
ECM	Extracellular matrix
EcoRI	Restriction endonuclease isolated from Eschericia coli
EDTA	Ethylenediaminetetraacetic acid
eGFP	Enhanced green fluorescent protein
EMT	Epithelial – mesenchyme transition
Foxc1	Forkhead box C1
$Foxc1^{+/+}$	Cells expressing *Foxc1* - wildtype
$Foxc1^{-/-}$	Cells without Foxc1 expression - mutants
GAPDH	Glyceraldehyde 3-phosphate dehydrogenase
GOI	Gene of interest
HAV	Histidine-Alanine-Valine
HindIII	Restriction endonuclease isolated from *Haemophilus influenzae*
HeLa	Human cervical carcinoma cells
HEPES	(4-(2hydroxyethyl)-1-piperazineethanesulfonic acid
HRP	Horseradish peroxidase
ICC	Immunocytochemistry
ICR	Imprinting control region
IOP	Intra-ocular pressure
IPTG	Isopropyl β-D-1-thiogalactopyranoside
LB	Luria-Bertani
MEndT	Mesenchyme-endothelial transition
MET	Mesenchyme-epithelial transition
MIQE	Minimum Information for Publication of Quantitative Real-Time PCR Experiments
MOPS	3-(4-Morpholino)propane sulfonic acid
MP	Megapixel
Msx1	Msh homeobox 1
NCBI	National Centre for Biotechnology Information
NIH3T3	Mouse embryonic fibroblast cell line
NTC	No template control
PCR	Polymerase chain reaction
P	Passage

(P)	Postnatal day
PBS	Phosphate buffered saline
pFoxc1-eGFP	Plasmid vector encoding full length Foxc1 gene sequence and enhanced green fluorescent protein
PMSF	Phenylmethanesulfonylfluoride
POM	Periocular mesenchyme
pshFoxc1.neo/gfp	Plasmid vector encoding a shRNA sequence against Foxc1 and enhanced green fluorescent protein
qPCR	Quantitative real time polymerase chain reaction
RFU	Relative fluorescence units
RIPA	RadioImmunoPrecipitation Assay
RNA	Ribonucleic acid
Rps12	Ribosomal protein subunit S12
SDS	Sodium dodecyl sulfate
SDS-PAGE	Sodium dodecyl sulfate polyacrylamide gel electrophoresis
SEM	Standard error of the mean
shRNA	Short hairpin RNA
T_m	Melting temperature
Taq	DNA polymerase isolated from *Thermus aquaticus*
TBE	Tris/Borate/EDTA buffer
TBS-T	Tris-buffered saline with Tween-20
TEMED	1,2-Bis(dimethylamino)ethane
U6	Human type III polIII promoter
UV	Ultraviolet

CHAPTER 1: INTRODUCTION

The proper organization and differentiation of the ocular tissues comprising the anterior segment of the vertebrate eye (i.e. the lens, cornea, iris, ciliary body, and the trabecular meshwork), is crucial for normal visual function (Hsieh et al., 2002). The tissues of the anterior segment form via a cascade of complex morphogenetic events involving cells derived from several distinct embryonic tissues (Hsieh et al., 2002). These tissues include the surface ectoderm of the head, migrating neural crest mesenchyme, and neural ectoderm.

Several transcription factors (primarily *Pax6, Pitx2, Foxc1* and *Foxe3*) have been identified as playing key roles in the proper differentiation of migrating neural crest mesenchyme cells that give rise to the anterior segment tissues (Baulmann et al., 2002). *Foxc1* belongs to the forkhead box (FOX) family of transcription factors, a group of initiators and repressors that are gaining increased recognition for their critical role in embryonic development and tissue-specific cell differentiation in a vast number of species (Saleem et al., 2003). Structure-function analyses of known mutations in human *FOXC1* have indicated that genetic errors in the gene result in reduced stability of FOXC1-DNA binding, causing the ineffective transactivation of target genes and below-optimal transcriptional regulation (Komatireddy et al., 2003). Function-disabling mutations in the *FOXC1* gene or the abnormal regulation of *FOXC1* expression in humans are cited as one of the primary causes behind malformations seen in the anterior segment of the murine eye (Chakravarti, 2001; Hsieh et al., 2002), and most often give rise to Axenfeld–Rieger syndrome in humans, a range of disease conditions characterized by anterior segment defects in the cornea, the iris, and the trabecular meshwork (Hsieh et al., 2002).

Patients presenting with Axenfeld–Rieger syndrome (ARS) show a high probability of early onset glaucoma - approximately 50% of patients with phenotypic manifestations of Axenfeld-Rieger syndrome develop the disease (Idrees et al., 2006). Glaucoma represents the second most common cause of visual loss and is a disorder responsible for 16 million cases of blindness worldwide. It is conservatively estimated that ± 20% of glaucoma cases have a genetic basis (Lehmann et al., 2000) with most documented congenital glaucomas manifesting as a consequence of poor development of the drainage structures (the ciliary body and trabecular meshwork) of the anterior segment (Davis-Silberman & Ashery-Padan, 2008). Mechanical and functional defects in these drainage structures give rise to abnormal intraocular pressures (a major risk factor for glaucoma), which may lead to degeneration of the optic nerve, retinal damage and, eventually, the permanent loss of sight (Baulmann, 2002; Hsieh et al., 2002; Davis-Silberman & Ashery-Padan, 2008).

Studies using transgenic mice have demonstrated that proper formation of the posterior corneal surface, the monolayered endothelium, is necessary for normal development of the anterior segment (Hsieh et

al., 2002). The corneal endothelium is primarily responsible for the hydration of the corneal stroma, with its ordered structure allowing for regulated entry of water and nutrients into the stroma from the aqueous humor (Chakravarti, 2001). The development and separation of this monolayer from the lens is therefore critical to the formation of the anterior chamber space, and the anterior segment as a whole.

In order to comprehensively define the developmental role of *Foxc1* in disease initiation and progression in the eye, potential candidate genes regulated by *Foxc1* must be identified. One family of proteins thought to be regulated by *Foxc1* are the Ca^{2+}-dependent cadherins (Kidson et al., 1999). This group of cell adhesion protein molecules is responsible for maintaining structural integrity between cells at adherens junctions (Braga, 2002). Cadherin-based connections are one of the most influential adhesive interactions in tissue development and maintenance, preserving the structural/architectural properties of the cell while regulating cell differentiation and development (Pontoriero et al., 2009). During development, these differentially expressed molecules control the separation of distinct tissue layers, allowing tissue boundaries to form (Gumbiner, 2005; Pontoriero et al., 2009).

(N)eural-cadherin is a transmembrane cell-cell adhesion molecule belonging to the classical cadherin subfamily (Van Aken et al., 2000). This cell adhesion protein is expressed mainly in adherens junctions in cells of neural origin but are also found in junctions between individual corneal endothelial cells, stromal fibroblasts (keratocytes) and myofibroblasts (Chen & Ma, 2007; Van Aken et al., 2000). Within the anterior eye, N-cadherin proteins are regarded as being crucial for proper formation of the corneal endothelium monolayer. In murine studies, it is postulated that a signal mediated by *Foxc1* is required in order for cadherin proteins to function normally (Kidson et al., 1999). In *Foxc1*$^{-/-}$ mice, the posterior mesenchyme of the cornea fails to develop into the corneal endothelium (Chakravarti, 2001) as the mesenchymal cells do not form the typical junctions. Formation of the anterior chamber is prevented, as the endothelium remains closely attached to the lens (Chakravarti, 2001). *Foxc1* expression is therefore essential for corneal endothelium development to occur successfully, with such data suggesting that *Foxc1* is either involved in the regulation of the cadherins expressed in the corneal endothelium, or in the delivery of these adhesion proteins to the plasma membrane in the stages prior to junction formation.

In vitro experimentation has shown another element to play a role in the regulation of cadherin expression. The *Hox* (homeobox) genes have been put forward as regulatory genes expressing proteins with the potential to bind at regulatory homeodomain binding sites (Hatta et al., 1988). Such binding sites are located within specific regions on adhesion molecule genes, allowing for homeobox genes to possibly induce transcriptional activation of cadherin genes (Hatta et al., 1988). Both calcium-dependent and -independent adhesion molecules are proposed to be targeted by *Hox* genes for regulation, providing a link between pattern formation and morphogenesis within tissues expressing

both these elements (Hatta et al., 1988). In the eye, it is postulated that down-regulation of the homeobox gene, *Msx1*, is critical to the formation of the corneal endothelium and its subsequent separation from the lens surface. This is due to the fact that the gene is down-regulated at E12.5, precisely when adherens junction formation occurs in the periocular mesenchyme (Lincecum et al., 1998). *Msx1* has been shown to decrease cadherin-mediated adhesion *in vitro* (Hartsock and Nelson, 2008), further implicating it as a candidate gene for investigation in corneal endothelium development.

This research aimed to comprehensively investigate the developmental role played by *Foxc1* in the regulation of *N-cadherin* expression in the adhesion junctions associating the cells of the corneal endothelium in the murine eye. The relationship between *Foxc1* and *Msx1* in periocular mesenchyme (POM) cells was also investigated. A range of techniques were employed in order to determine the effect of *Foxc1* expression on *Msx1* expression and *N-cadherin* expression/localization in cultured mouse mesenchyme. Immortal POM cell lines derived from wildtype embryos at embryonic day (E) 12.5 and E13.5 were used as the model system. To determine whether *Foxc1* regulates N-*cadherin* expression, gene expression was evaluated via quantitative real-time PCR (qPCR). RNA was isolated from wildtype and p*Foxc1*-eGFP transfected E12.5 and E13.5 POM cells and cDNA was synthesized. qPCR was carried out to evaluate the effect of *Foxc1* over-expression on *N-cadherin* and *Msx1* expression at these stages in development. Western blot analysis was carried out on total protein isolated from wildtype E12.5 and E13.5 POM cells, and POM cells transfected with either the psh*Foxc1*.neo/gfp knock-down plasmid (to knock-down gene activity) or the p*Foxc1*-eGFP over-expression plasmid. Foxc1, N-cadherin and the GAPDH reference protein were detected using antibodies to assess the effectiveness of the plasmid vectors in regulating *Foxc1* expression as well as to detect fluctuations in target protein expression between the different developmental stages. N-cadherin expression and localization was detected using immunocytochemistry (ICC) and confocal microscopy in monolayer and hanging-drop cultures of wildtype E12.5 and E13.5 POM cells. Wildtype POM cell monolayers were also subject to transfection with either p*Foxc1*-eGFP or psh*Foxc1*.neo/gfp plasmids and N-cadherin expression and localization was evaluated.

This investigation attempted to elucidate the developmental role played by *Foxc1* in N-cadherin expression and adherens junction formation in the precursor cells that eventually give rise to the corneal endothelium – a component that must develop correctly to attain normal visual acuity. The study will be the first to investigate the links between the expression of the homeobox gene *Msx1* and transcription factor *Foxc1* in periocular mesenchyme. It is hoped that this information will make a significant contribution to the current body of knowledge regarding *Foxc1* expression and gene targets in the eye. Such data may form the groundwork for the development of effective therapeutics that may lessen the effect of the debilitating anomalies that present in anterior segment disorders.

CHAPTER 2: LITERATURE REVIEW

2.1. The eye

The eye is a complex neurosensory organ responsible for vision and is comprised of three major components: a lens system, receptors and a nervous supply. The lens system focuses light toward the photo-receptors while the nervous supply conducts impulses away from the receptors to the brain (Ganong, 2003). Normal visual function necessitates precise spatial organization of and interaction between the individual tissues such that these processes occur flawlessly and with seamless continuity (Hsieh et al., 2002; Pirity et al., 2007). The eye can be divided into two main regions. The anterior eye comprises the sensitive lens system which regulates the amount of light entering the eye while the posterior eye is involved in receiving this focused light and converting the stimulus into an electrical signal which is then conducted to the brain (Figure 1).

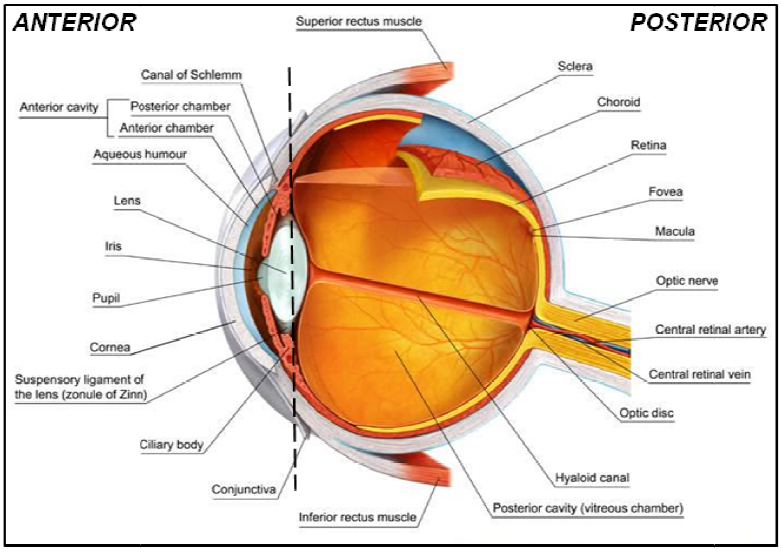

Figure 1: The adult eye. The broken line demarcates the boundary between the anterior segment and the posterior segment. Image adapted from *www.virtualmedicalcentre.com.*

2.1.1. The anterior segment of the eye

The major structures that comprise the anterior segment of the eye include the cornea, limbus, iris, lens, ciliary body and trabecular meshwork (Figure 2) (Hsieh et al., 2002; Gage & Zacharias, 2009). The outermost region of the eye field is specified by the presence of the cornea, a connective tissue responsible for protecting the eye from microbial infections whilst maintaining an optimum degree of transparency and refractive power in order to attain visual acuity (Wu et al., 2008). This tissue possesses an immense tensile strength and is comprised of an outer epithelium (~5-7 cell layers thick) separated from an inner single cell-layer thick endothelium by a stroma (Wu et al., 2008). The stroma is the tissue component responsible for the refractive ability of the cornea. It is composed of a highly organized matrix of collagen fibrils interspersed with fibroblasts (keratocytes), and receives hydration through the regulatory pump mechanism

inherent within the innermost layer, the corneal endothelium (Wu et al., 2008). The ciliary body is responsible for producing aqueous humor (Hsieh et al., 2002; Davis-Silberman & Ashery-Padan, 2008). This slightly hypertonic (relative to plasma), transparent fluid moves through the iris into the anterior chamber region between the lens and corneal endothelium to provide nourishment to and remove metabolic waste from the avascular corneal stroma (Davis-Silberman & Ashery-Padan, 2008). The trabecular meshwork, located in the iridiocorneal angle (region where the cornea and iris converge), serves to channel any excess aqueous humor toward Schlemm's canal and into the venous system (Hsieh et al., 2002). This stringently monitored process ensures that build-up of aqueous fluid and any subsequent damaging increase in intra-ocular pressure is prevented. The muscular, vascular iris is a thin, contractile disc located between the cornea and the lens, and regulates the amount of light that is allowed to pass through the lens and onto the retina (Davis-Silberman & Ashery-Padan, 2008). The ordered, fibrous lens is responsible for focusing the light entering the eye onto the sensitive sensory cells of the retina (Cain et al., 2008).

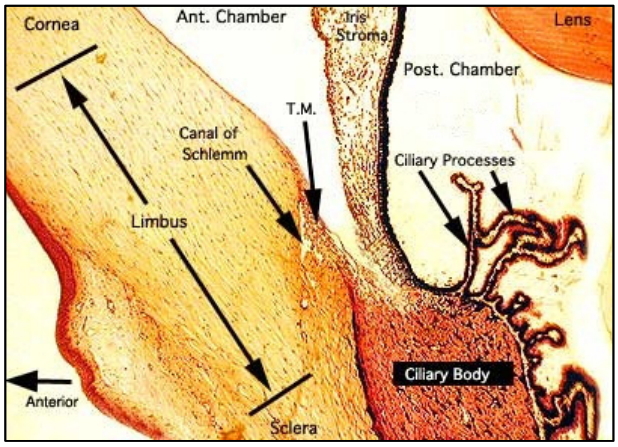

Figure 2: Histological section through the anterior segment of the eye. Abbreviations: TM=trabecular meshwork. Image adapted from *http://faculty.une.edu/com/abell/histo/histolab3b.htm.*

The structures of the anterior segment all interact in a co-ordinated, sequential fashion to ensure that key mechanisms remain in place so that proper visual function is attained. In order for this to occur, light needs to be effectively refracted and focused and the delicate intra-ocular pressure must be maintained within its limits to prevent damage to the photo-sensitive retinal layer of the posterior eye. This functional interaction is dependent on the specific structural attributes of each tissue component. The proper development of these structures is thus pivotal for the correct functioning of the anterior segment, and consequently the eye.

2.1.2. The cornea

The protective corneal tissue provides nearly three quarters of the eye's refractive power; its proper development is thus pivotal in attaining optimum vision (Chakravarti, 2001). The adult

cornea consists of 5 layers:- the outermost epithelium, Bowman's membrane, stroma, Descemet's membrane and the final innermost layer, the corneal endothelium (Figure 3).

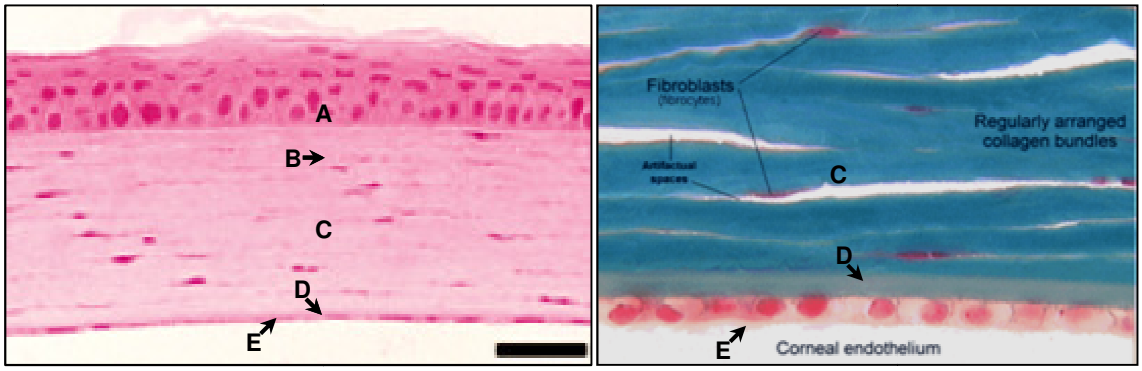

Figure 3: Histological sections through the cornea - corneal epithelium (A), Bowman's membrane (B), stroma (C), Descemet's membrane (D) and the corneal endothelium (E) with a higher magnification of the corneal endothelium showing the tightly arranged, ordered monolayer. Images adapted from *Smith et al. (2000)* and *http://neuromedia.neurobio.ucla.edu/.*

The monolayered corneal endothelium functions to maintain stromal hydration and acts as a fixed barrier between the anterior chamber and the stroma (Chakravarti, 2001; Blixt et al., 2007). This function is effectively carried out by the endothelium's rigidly cohesive and ordered structure, which creates a permeable barrier allowing water and nutrients from the aqueous humor to enter the stroma (Chakravarti, 2001). The active sodium and bicarbonate pumps within the endothelium lining prevent the stroma from swelling, even in the presence of the water-retaining stromal glycosaminoglycans (Chakravarti, 2001). This is due to the ion concentration gradient created by the endothelial cells which pump ions from the stroma to the chamber, creating an osmotic gradient that allows for the passive removal of water while maintaining the relatively dehydrated nature of the stroma, keeping it optically clear and functional (Chakravarti, 2001; Blixt et al., 2007). The endothelial monolayer is highly polarized and the cells are joined by tight junctions. If the integrity of the endothelium is compromised in any way, oedema results, leading to corneal swelling and opacity (Blixt et al., 2007). Thus, the proper differentiation of the corneal endothelium is a vital step in proper eye development, leading to the separation of the lens from the cornea and the subsequent formation of the anterior chamber (Cvekl & Tamm, 2004).

2.2. Embryonic development of the eye

2.2.1. The onset of eye development

Murine embryonic development is, to date, the most well-studied vertebrate model. In this model, the onset of eye development is identified morphologically by the specification of the eye field in the neural ectoderm and lens induction in the surface ectoderm at around embryonic day (E) 8.5 (Gould et al., 2004). Lens induction is initiated by the bilateral evagination of the forebrain and the development of optic pits on the inner surface of the cephalic neural folds at

E8.5 (Davis-Silberman & Ashery-Padan, 2007). By E9.0, the neural folds oppose each other and the optic pits deepen to become the optic vesicles (Figure 4 A) (Gould et al., 2004). The optical vesicles move through a layer of mesenchyme until they reach the surface ectoderm at ~ E9.5 (Davis-Silberman & Ashery-Padan, 2007) with formation of the lens placode in the surface ectoderm being induced by the interaction of the optic vesicle with the surface ectoderm (Figure 4 B). The lens vesicle remains connected to surface ectoderm via the lens stalk (Figure 4 C) until it detaches around E11 (Figure 4 D).

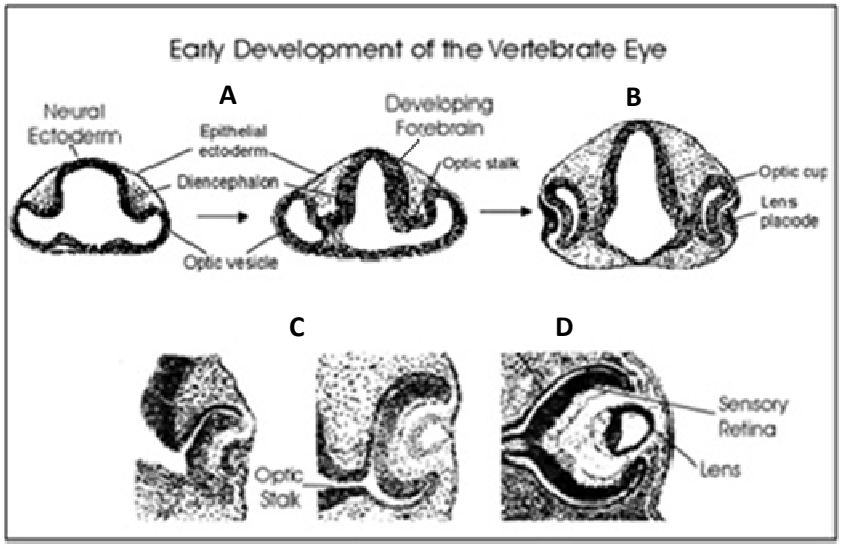

Figure 4: Progression of early development in the vertebrate eye: A – optic vesicles form; B – lens placode formation; C – lens vesicle formation; D – lens vesicle detachment (*O'Day, 2010*).

2.2.2. Development of the anterior chamber structures

The structures of the anterior segment of the eye develop through a series of carefully timed, co-ordinated morphogenetic event cascades: induction and differentiation. These events involve cells derived from three distinct embryonic tissue types; the surface ectoderm, neural ectoderm and migrating POM (Hsieh et al., 2002; Gould et al., 2004). The surface ectoderm forms the corneal epithelium and lens. Tissues derived from the neural ectoderm form the retina and the epithelial tissues of the iris and ciliary body. The periocular mesenchyme are migrant cells predominantly composed of forebrain neural crest cells, however, a small mesoderm mesenchyme contribution has also been shown (Hsieh et al., 2002; MacDonald et al., 2004, Gage et al., 2005). These cells give rise to a number of ocular tissues including the corneal endothelium, keratocytes of the corneal stroma, the muscles and stroma of the ciliary body, sclera, stroma of the iris and the trabecular meshwork (Hsieh et al., 2002; MacDonald et al., 2004). The differentiation of POM cells into these cell types has been confirmed in murine studies by cell grafting and cell-labeling experiments in craniofacial morphogenesis (Cvekl & Tamm, 2004). This has also been confirmed in avian models by fate-mapping experiments, using

specific antibodies against neural crest cells and vital dye-labelling (Davis-Silberman & Ashery-Padan, 2007; Chakravarti, 2001; Cvekl & Tamm, 2004; Gould et al., 2004). Figure 5 depicts the transition of embryonic cell lineages to adult tissues, clearly showing the embryonic tissue types from which the adult ocular tissues are derived.

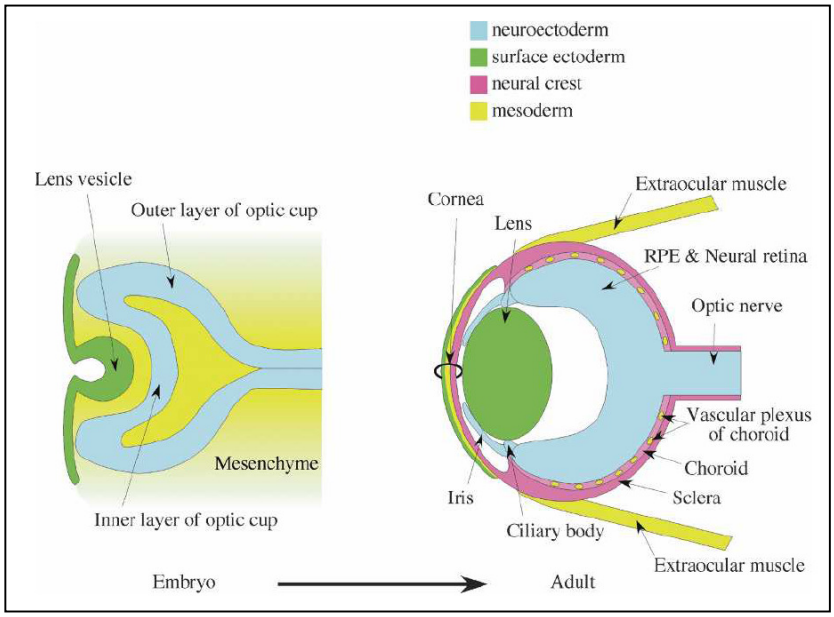

Figure 5: Embryonic lineages that contribute to the development of the mammalian eye: surface ectoderm – green; forebrain neuroectoderm - blue; mesoderm - yellow; neural crest - pink (*Harada et al., 2007*).

Following the detachment of the lens vesicle from the surface ectoderm, the space that is formed between the surface ectoderm and the anterior epithelium of the lens vesicle becomes occupied with migrating POM cells (Chakravarti, 2001; Cvekl & Tamm, 2004; Gould et al., 2004). In mice, approximately 4-7 layers of POM cells migrate in a single wave into the space formed between the surface ectoderm and the anterior epithelium of the lens vesicle at E12.5 (Cvekl & Tamm, 2004; Gould et al., 2004; MacDonald et al., 2004). These stellate, mesenchymal cells multiply and increase in number within the anterior chamber space, until the cells eventually condense to form several layers of flattened mesenchyme cells interspersed and separated by a fibrillar, extracellular. The migrant POM then begins to differentiate to form corneal endothelial cells. The cells eventually become joined to each other via the development of continuous bands of junctional complexes, resulting in the formation of an endothelial monolayer (Cvekl & Tamm, 2004). By E14.5-15.5, the corneal endothelium is fully developed and the anterior chamber is apparent as a small space between the lens and developing cornea. At this point the remaining POM cells begin to differentiate to give rise to the collagen-secreting keratocytes that comprise the corneal stroma.

Development of the eye in humans requires a second wave of mesenchyme cells into the anterior eye at a later stage. These cells appear at the angle between the future cornea and the anterior

edge of the optic cup (Cvekl & Tamm, 2004) and eventually differentiate to give rise to the stroma of the iris and the ciliary body. Figure 6 shows the fully developed anterior region of the adult eye.

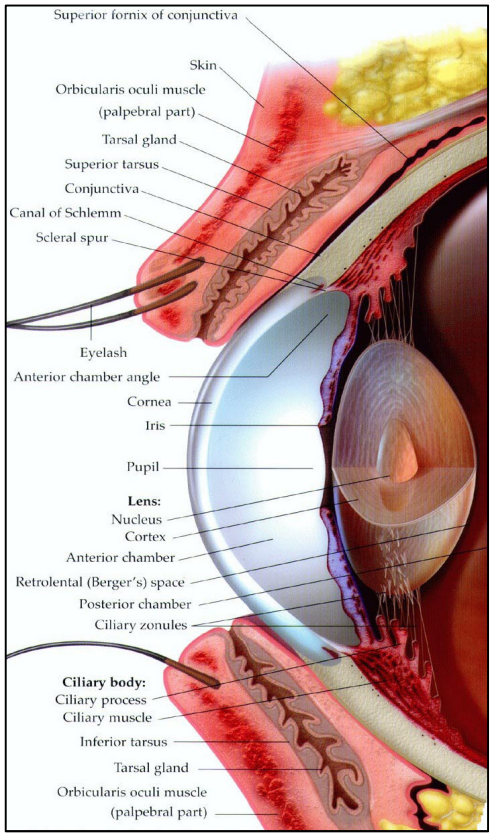

Figure 6: Detailed section through the anterior segment of the fully developed adult eye. Image from *http://eyemakeart.wordpress.com/2010/05/03/large-human-eye-anatomy-diagram/.*

2.3. Signaling in eye development

2.3.1. Cell signaling in anterior segment development

Cell signaling and the regulated expression of genes are crucial for normal embryonic development to occur (Faber et al., 2001). This is no less true for the cells that compose the tissues of the eye. In recent years, the importance of these two activities has been re-iterated by molecular genetics approaches which have identified a string of signaling molecules and transcription factors whose presence in the eye is considered critical for inductive interaction between the optic vesicle and presumptive lens to occur (Faber et al., 2001; Hsieh et al., 2002). The migration of cranial neural crest cells into the developing eye, as well as their proliferation and differentiation, are also under the control and regulation of various signaling pathways and transcription factors (Chung et al., 2010).

Signaling in the anterior segment is initiated early in development by the anterior epithelial cells of the lens vesicle (Gage et al., 2005). These cells act as a "signaling center" that direct multiple key processes during anterior segment development, including the induction of the corneal endothelium and stromal layers (Gage et al., 2005). Classical transplantation experiments

indicate corneal endothelium differentiation and formation to be an essential step in the normal development of the anterior chamber (Hsieh et al., 2002). In order for the corneal endothelium to form correctly, the precursor POM cells require inductive signals from the lens in order to develop junctions and complete their mesenchyme-epithelium transition (MET) (Hsieh et al., 2002; Zhang et al., 2008). It is these inductive tissue interactions that allow the anterior eye to develop and function correctly.

Although the primary function of the periocular mesenchyme in the embryonic eye is to give rise to specifically differentiated cell lineages crucial in the development of normal ocular structures, these cells also generate signals themselves that are essential in directing ocular patterning during development. If the development and/or functioning of the periocular mesenchyme is compromised by genetic disease, irreparable vision loss could result (Gage et al., 2005).

A number of key regulators in periocular mesenchyme development have been identified. Factors associated with the differentiation of the anterior mesenchyme to endothelium in the eye that have been extensively studied include members of the TGF-β, homeobox gene and Fox families (Gould et al., 2004). *Pax6*, *Six3*, *Foxe3*, *Pitx3* and *Sox3* have all been found to play specialized roles during lens development (Pirity et al., 2007), while *Pax6*, *Pitx2*, *Pitx3* and *Foxc1* have been linked specifically to the development and progression of anterior segment dysgenesis (Wurm et al., 2008).

2.3.2. The role of Pax6 in eye development

Highly conserved in vertebrates, the paired homeodomain transcription factor gene *Pax6* is indispensable during development and is most well known for the key regulatory role that it plays during eye development (Davis-Silberman & Ashery-Padan, 2008). *Pax6* is expressed in the surface ectoderm (the precursor tissue of the corneal epithelium), iris, ciliary body, developing retina and the developing lens (Faber et al., 2001; Hsieh et al., 2002; Collinson et al., 2001). The gene is thought to act as a key control point ensuring that the complex interaction between cells of different origins is synchronized, allowing the eye to develop correctly (Kim & Lauderdale, 2008).

Studies have shown that *Pax6* expression is a vital factor in the interaction between the lens placode and the optic vesicle, the eventual differentiation of the lens and retina, and in the proper long-term maintenance of the lens (Collinson et al., 2001). The factor has been cited as being the cause of defects in the anterior segment of the murine and human eye, with heterozygous mutations in *Pax6* resulting in anomalies such as iris hypoplasia (aniridia), cataract, corneal opacification, iridocorneal adhesions, the incomplete separation of the lens from the cornea

(Peter's anomaly) and degenerative aspects such as early onset glaucoma and optic nerve hypoplasia (Hsieh et al., 2002; Collinson et al., 2001). It is hypothesised that *Pax6* plays a functional role in the regulation of expression of specific molecules necessary for directing migrating cells or instigating adhesion in these cells (Collinson et al., 2001; Davis-Silberman & Ashery-Padan, 2008). Support for this hypothesis can be found in the implication of *Pax6* as a regulatory transcriptional control factor directing expression of *N-cadherin*, a key adhesion molecule, in the lens (Davis-Silberman & Ashery-Padan, 2008).

2.3.3. The role of Pitx2 in eye development

In mice, the bicoid-class homeobox protein *Pitx2* is one of the most widely investigated factors expressed in the periocular mesenchyme (Hsieh et al., 2002). *Pitx2* is a homeobox transcription factor gene involved in the normal development of key structures such as the heart, brain and lungs (Gage et al., 2005; Davis-Silberman & Ashery-Padan, 2008). This factor is considered to be essential for ocular development in mice, and is generally associated with ocular defects in humans (Gage et al., 2005; Davis-Silberman & Ashery-Padan, 2008). *Pitx2* defines the multiple tissue lineages derived from the periocular mesenchyme, such as the corneal endothelium and stroma (Gage et al., 2005).

Gage et al. (2005) have shown that *Pitx2* is expressed in neural crest cells immediately after their arrival in the nascent anterior segment region. Subsequently, at around E11.5, expression is rapidly extended into the optic cup periphery (Gage et al., 2005; Davis-Silberman & Ashery-Padan, 2008). By E12.5, *Pitx2* expression is prevalent in all cells derived from the ocular neural crest, such as the presumptive corneal endothelium, iris and iridocorneal angle (Gage et al., 2005; Davis-Silberman & Ashery-Padan, 2008). In mice, *Pitx2* activation, together with the activation of a number of other essential genes, initiates a genetic cascade that results in the specification and differentiation of POM cells into the corneal endothelium and stroma (Gage et al., 2005).

Pitx2 shows similar expression patterns to the forkhead winged-helix transcription factor gene *Foxc1*, with heterozygous mutations in both human *FOXC1* or *PITX2* genes resulting in abnormal development of the anterior chamber of the eye (Hsieh et al., 2002; Gage et al., 2005; Davis-Silberman & Ashery-Padan, 2008).

2.4. ***The role of the transcription factor Foxc1 in eye development***

2.4.1. Physical characteristics

The Forkhead box (FOX) transcription factors are frequently implicated as playing vital roles in the proper execution of development, with a wide number of species ranging from yeasts to humans incorporating FOX proteins as important gene regulators (Panicker et al., 2002; Saleem

et al., 2003). *FOXC1* is the name given to a monoexonic gene 1.6 kb long encoding a 553 amino acid long protein belonging to the FOX family of transcription factor genes (Panicker et al., 2002; Tamimi et al., 2004; Tamimi et al., 2006). The forkhead/winged helix gene family is defined by the presence of an evolutionarily well-conserved 110-amino-acid DNA-binding domain, originally identified as being a homologous region to both the rat hepatocyte nuclear factor 3 protein (*Foxa3*) and the *Drosophila melanogaster* forkhead protein (Kume et al., 2000; Fuse et al., 2007; Panicker et al., 2002; Gould et al., 2004; Tamimi et al., 2004; Tamimi et al., 2006). The DNA-binding motif seen in members of the FOX family is a variant of the helix–turn–helix motif, which is composed of three α-helices and two large loops; these loops form the 'wing' structure - W1 and W2 (Figure 7) (Fuse et al., 2007; Panicker et al., 2002; Tamimi et al., 2006). This domain serves the indispensable function of DNA recognition and initiation/repression of transcription (Tamimi et al., 2006).

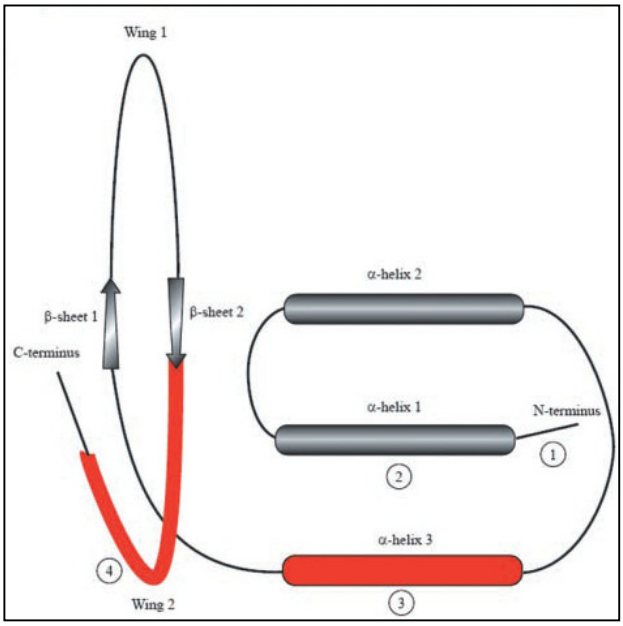

Figure 7: Functional sub-domains of FOXC1 depicted as a simplified wire diagram. 1 & 2 indicate the N-terminus of the forkhead domain incorporating the first α-helix which arranges the forkhead domain for transactivation and DNA binding – this region also serves a nuclear localization function. 3 is the third α-helix which specifies DNA-binding of the domain for high efficiency binding. 4 indicates the second wing region which also serves to organization the forkhead domain for transactivation and DNA binding (*Saleem et al., 2004*).

2.4.2. Foxc1 expression in the developing head

Expression of *Foxc1* in the developing head mesenchyme in the murine model has been well documented, with studies indicating transcripts to be present and detectable as early as the head fold stage, where expression of the transcription factor is localized to the entire non-notochordal mesoderm (Sommer et al., 2006). During development *Foxc1* is highly expressed in tissues such as the paraxial mesoderm, periocular mesenchyme, somites, pre-chondrogenic mesenchyme, as well as in the tissues of the developing cardiovascular system (Kume et al., 2000). *Foxc1* is

expressed in cranial neural crest cells of the first branchial arch in mice between E7.5 and E9.5 (Chakravarti, 2001; Sommer et al., 2006).

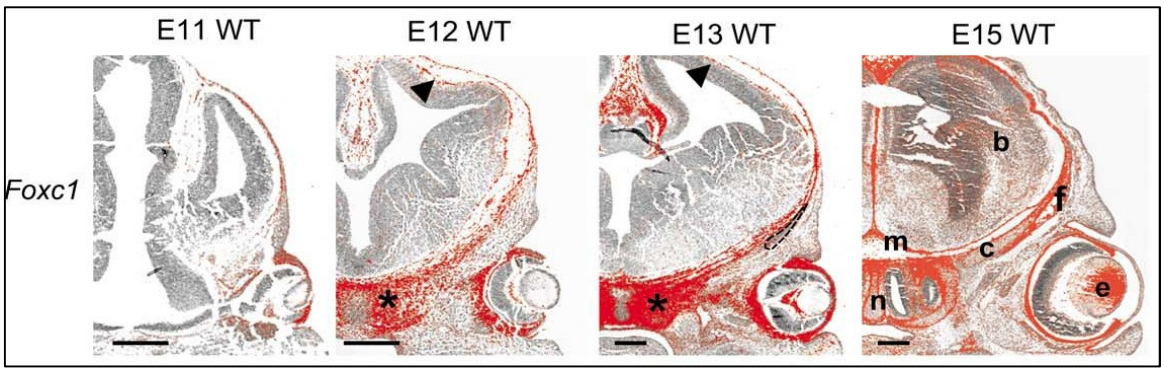

Figure 8: *Foxc1* expression pattern (red) in the heads of mice embryos at different time points in development. * - condensing prechondrogenic mesenchyme; e - eye; c – cranial base cartilage; b - brain; f – frontal bone; m - meninges; n – nasal cartilage. Scale bars = 200 µm. Image adapted from *Rice et al., 2003*.

Variable spatio-temporal expression can be detected in the anterior segment tissues in the developing eye derived from neural crest cells from E11.5 (Cvekl & Tamm, 2004; Gage et al., 2005), and by E12.5 of embryonic development, *Foxc1* expression is established in a number of different areas of the developing head mesenchyme including the developing nasal region, submandibular duct and gland, cartilage primordia of the skull bones, primitive meningeal layers and the cranial mesenchyme and mesenchyme surrounding the optic nerve (Sommer et al., 2006) (Figure 8).

From this point up until E18.5, *Foxc1* is present in significant amounts in the murine eye (specifically in the periocular mesenchyme, presumptive corneal mesenchyme, prospective trabecular meshwork, sclera and future conjunctival epithelium) is considered an essential constituent necessary for the differentiation of the POM-derived tissues (Chakravarti, 2001; Cvekl & Tamm, 2004; Gage et al., 2005; Sommer et al., 2006). Northern blot analyses have shown that *Foxc1* mRNA expression is relatively high in the developed adult trabecular meshwork (the tissue regulating aqueous outflow and intraocular pressure) and optic nerve head (a tissue that is associated with the development of glaucomatous optic neuropathy in the posterior segment of the eye) of the human eye (Wang et al., 2001). Anterior segment tissues in the adult eye such as the ciliary body, iris and cornea also express relatively high levels of *Foxc1* (Wang et al., 2001).

2.4.3. Mutations in Foxc1

Foxc1 is known to play specific key roles in somitic, cardiovascular, renal and ocular development, and also in tumorigenesis (Kume et al., 2000; Wang et al., 2001; Zarbalis et al., 2007). The important role of Foxc1 protein in the development of mesoderm-derived vertebrate

tissues (such as the kidney, eye, heart, bone and cartilage) has been demonstrated by studies targeting deletions of *Foxc1* in the murine model (Cha et al., 2007; Tamimi et al., 2006). In mice, the loss of function associated with mutations in the gene encoding *Foxc1* results in eye and heart defects, and lymphatic and germ cell migration abnormalities (Libby et al., 2003; Mattiske et al., 2006; Seo et al., 2006), whilst the decreased production of effective, viable Foxc1 proteins in zebrafish actively inhibits somitogenesis (Cha et al., 2007). Loss-of-function analyses show *Foxc1* to be an essential transcription factor in *Xenopus sp.,* necessary for the maintenance of cell-to-cell adhesion in the mesodermal germ layer during the early gastrula stage (Cha et al., 2007).

A wide spectrum of human *FOXC1* mutations have been discovered to date; deletions, insertions, duplications, translocations, frameshift mutations and missense mutations are amongst the most well-known, with these anomalies being noted to result in haplo-insufficiency of the FOXC1 transcription factor protein (Komatireddy et al., 2003; Fuse et al., 2007; Saleem et al., 2003). It has also been noted that mutated residues within these altered genes remain highly conserved across species (Fuse et al., 2007). Studies by Strungaru et al. (2007) have shown that patients with *FOXC1* gene mutations are more likely to manifest with systemic malformations than patients with *FOXC1* duplication. Missense mutations have been characterized as being responsible for reducing FOXC1 protein stability by reducing wildtype conformations, limiting the ability of the tertiary structure to bind to DNA by inhibiting transcriptional initiation, or by causing reduced transactivation by *FOXC1* even though the protein is able to bind to DNA (Figure 9) (Komatireddy et al., 2003; Saleem et al., 2003; Tamimi et al., 2006). Such studies on *Foxc1* missense mutations show the extent to which mutations impair *Foxc1* function and shed light onto the functional characteristics of manifesting defects (Saleem et al., 2003).

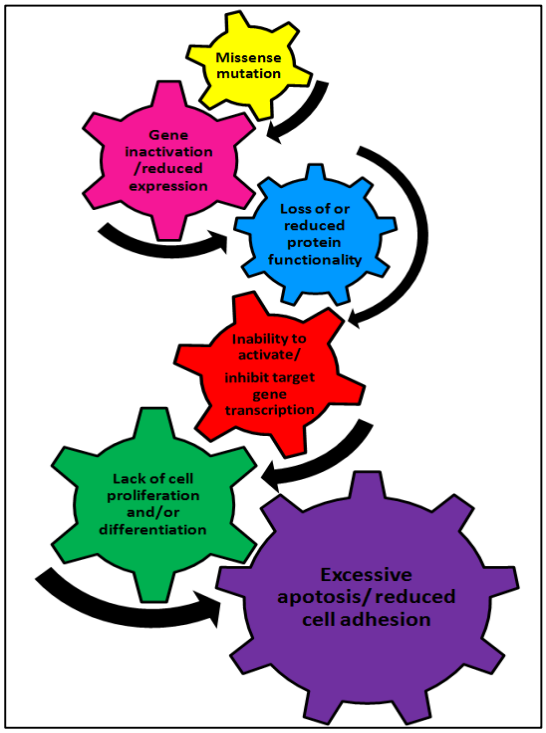

Figure 9: Effect of missense mutations in cell function. Image adapted from *Vieira, 2008.*

The abnormal expression of *Foxc1* (brought about as a result of chromosomal translocations, deletions, duplications, and nonsense or missense mutations) has been implicated in the abnormal development of key ocular structures such as the iris, cornea and trabecular meshwork (Wang et al., 2001). A wide range of phenotypes of variable severity are caused by mutations in *Foxc1*; this may be as a result of mutated proteins retaining partial function, causing milder phenotypes to manifest (Cvekl & Tamm, 2004) or as a result of *Foxc2* expression compensating for loss in *Foxc1* expression (Smith et al., 2000).

In humans, ASD is an umbrella term that refers to a range of structural deformities in the anterior eye. The current body of knowledge includes data from both human and mouse studies, and clearly defines anterior segment dysgenesis to encompass a complex spectrum of disorders (Gould et al., 2004). Heterozygous ($Foxc1^{+/-}$) mice present with abnormalities that show analogy to those in patients presenting with ASD; these include (amongst others) iris hypoplasia, aberrantly developed trabecular meshwork, small or absent Schlemm's canal, severely eccentric pupils, fusion of the lens to the cornea (Figure 10) and displaced Schwalbe's line (Chakravarti, 2001; Kume et al., 2001; Wang et al., 2001; Saleem et al., 2003). These mice possess Foxc1 proteins with reduced stability, and have *Foxc1* activity reduced to a degree that is just sufficient for early developmental events to proceed normally (Zarbalis et al., 2007). Mutant mice showing the absence of the fully functional gene ($Foxc1^{-/-}$) die both pre- and peri-natally, with embryos manifesting outwardly with lethal, combined skeletal, ocular, and genito-urinary defects, and severe haemorrhagic hydrocephalus (Kume et al., 2001; Saleem et al., 2003; Gould et al., 2004; Tamimi et al., 2006; Zarbalis et al., 2007).

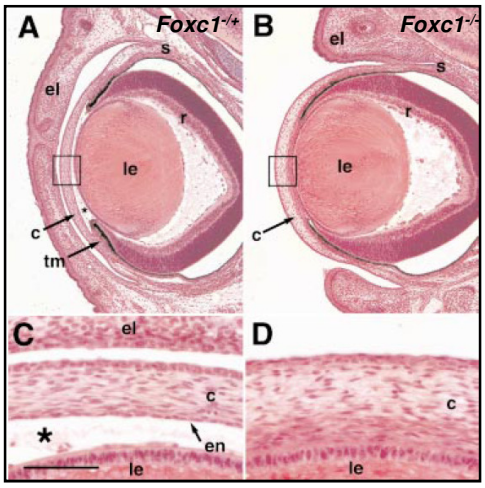

Figure 10: Histology of heterozygous & homozygous *congenital hydrocephalus* ($Mf1^{ch}$) (subsequently renamed $Foxc1^{-/-}$) mouse eyes at E17. Images are original H&E stained sections of embryos by Dr. Hans Gruneberg (1943). (A/C) Heterozygote ($Foxc1^{+/-}$) shows closed eyelids (el) with distinct anterior chamber (*) & endothelial layer (en) along the posterior corneal margin. (B/D) Homozygous mutant ($Foxc1^{-/-}$) with open eyelids & anterior chamber. Abbreviations: c=cornea; el=eyelid; en=endothelium; le=lens; r=retina; s=sclera; tm=presumptive trabecular meshwork. Scale: A/B = 200 µm; C/D = 50 µm (*Kidson et al., 1999*).

Whole mount preparations of the corneas of *Foxc1*$^{-/-}$ mutant eyes mice have a thickened epithelium, disorganized stroma and absent, undifferentiated corneal endothelium. The posterior mesenchyme in the developing cornea of *Foxc1*$^{-/-}$ null mutant mice fail to make the transition to corneal endothelium tissue. Frequently, the lens appears fused to the cornea (corneolenticular adhesions) resulting in the absence of a distinct anterior chamber (Figure 10) (Chakravarti, 2001; Cvekl & Tamm, 2004; Saleem et al., 2003; Gould et al., 2004; Sommer et al., 2006; Zarbalis et al., 2007). Such studies implicate *Foxc1* as a fundamental part of the signaling cascade responsible for the induction of and proper development of the endothelium and other anterior segment tissues (Chakravarti, 2001; Panicker et al., 2002).

2.4.4. Foxc1 and Axenfeld-Rieger Syndrome

Mutations in human *FOXC1* resulting in a loss of protein function have been identified in numerous cases as the cause behind the human disorder Axenfeld–Rieger Syndrome (ARS), a heterogenous, dominantly inherited genetic disorder. ARS is characterized by the dysgenesis of the anterior chamber of the eye (predominantly affecting anterior eye structures derived from the periocular mesenchyme), cranio-facial abnormalities, dental abnormalities (Figure 11), congenital cardiac defects and hearing loss brought about by irregularities in developmental processes (Cha et al., 2007; Fuse et al., 2007; Gould et al., 2004; Kume et al., 2001; Strungaru et al., 2007; Panicker et al., 2002; Tamimi et al., 2004; Tamimi et al., 2006).

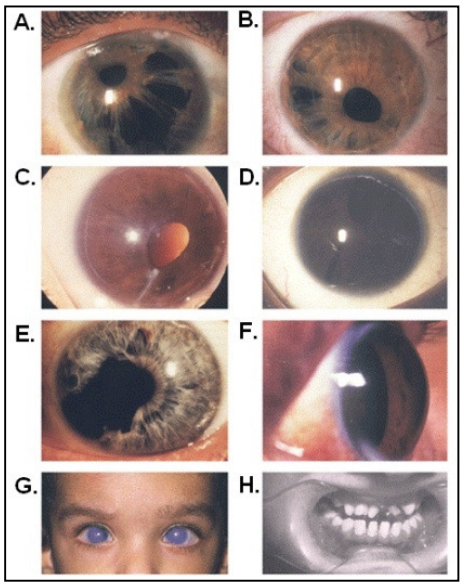

Figure 11: Examples of clinical phenotypes commonly seen in patients presenting with Axenfeld-Rieger Syndrome. A. Displaced pupil, iris atrophy, polycoria (apparent multiple pupils), prominent and anteriorly displaced Schwalbe's line. B. Irregular pupil and pseudopolycoria. C. Anterior segment dysgenesis with posterior embryotoxon and fibrous band bridging pupil and angle. D. Inferiorly drawn pupil, attachments to prominent and anteriorly displaced Schwalbe's line. E. Congenital ectropion of the iris. F. Megalocornea. G. Bilateral glaucoma, corneal opacification. H. Dental hypoplasia (*Hjalt & Semina, 2005*).

Although Axenfeld-Rieger Syndrome is known to desist from manifesting systemic abnormalities, clinical symptoms indicative of developmental defects in the anterior chamber of the eye are frequently documented. These include abnormalities such as a prominent, anteriorly displaced Schwalbe's line, insertion of iris processes in the stroma, hypoplastic iris, polycoria, corectopia, anterior chamber angle anomalies and irregularly formed aqueous drainage structures (Panicker et al., 2002; Komatireddy et al., 2003; Strungaru et al., 2007). In some instances, the corneal endothelium and Descemet's membrane may be absent, and the corneal stroma may appear to be centrally opaque (a condition thought to arise due to oedema associated with the decreased permeability of the corneal endothelial barrier) (Strungaru et al., 2007).

Mutations in genes encoding the transcription factors PITX2 and FOXC1 have been implicated in Axenfeld-Rieger malformations (Tamimi et al., 2006). Such phenotypes are known to map to locus 6p25, the same chromosome that *FOXC1* is located on (Komatireddy et al., 2003; Saleem et al., 2003). Mutations in the *FOXC1* gene are thus thought to cause the Axenfeld-Rieger phenotypes known as ARS that map to this locus (Komatireddy et al., 2003). Roughly 40% of patients presenting with Axenfeld-Reiger mutations are noted to have mutations or duplication in *FOXC1* (Strungaru et al., 2007).

As a result of the characteristic abnormal structural development of drainage tissues in anterior segment dysgenesis categorized as ARS, the functioning of the drainage structures is compromised. An important observation in the study of anterior eye anomalies is that developmental abnormalities of the ocular drainage structures that occur in conditions such as ARS cannot always be detected by clinical assessment. In some instances, this irregular functioning proceeds without a clear, outwardly visible disturbed morphology indicating the severity of the condition. Developmental gene mutations such as those discussed above appear to be a key contributor to the onset of one such ailment: congenital glaucoma. Common forms of glaucoma, such as primary open angle glaucoma, do not manifest with obvious phenotypic developmental abnormalities and, as such, pose a silent risk of developing blindness to many (Gould et al., 2004).

2.4.5. Glaucoma

Any abnormal development of iridocorneal angle structures is considered an initiating factor in the development of elevated intra-ocular pressure (IOP), a factor that is often regarded as the preemptive cause behind the development of congenital glaucoma (Figure 12) (Gould et al., 2004).

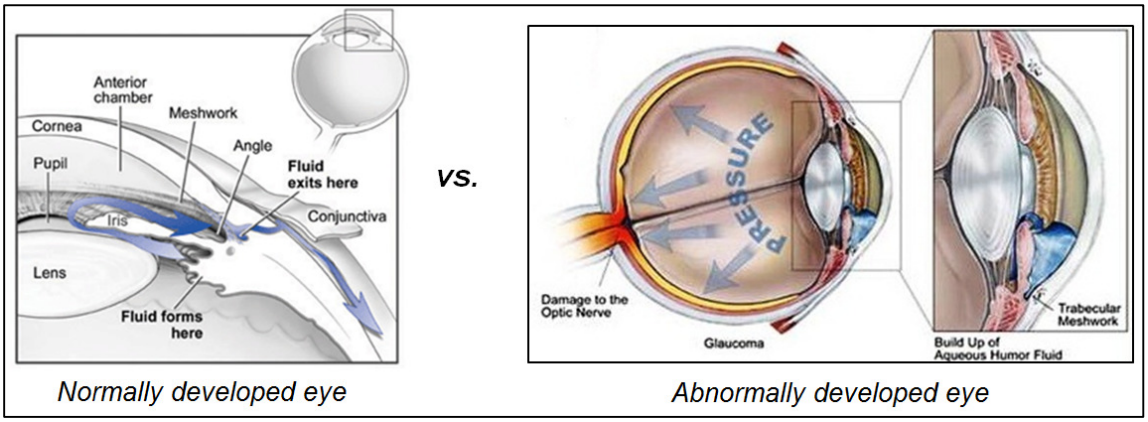

Figure 12: Poorly developed anterior segment drainage structures in the eye result in increased intra-ocular pressure, which could eventually manifest as glaucoma. Images adapted from *http://www.nei.nih.gov/health/glaucoma/glaucoma_facts.asp;http://www.igaveawaythesky.com/know-eye-diseases-glaucoma/.*

Ocular disorders such as Peter's anomaly (an anterior eye disorder characterized by corneal opacity and cornea-lens/iris-lens adhesion) and juvenile-onset glaucoma with iridogoniodysgenesis are anterior segment development disorders strongly associated with the development of congenital glaucoma (Wang et al., 2001; Vincent et al., 2006). A large body of evidence implicates Axenfeld-Rieger syndrome as being strongly associated with the onset and progression of congenital glaucoma (Kume et al., 2001; Tamimi et al., 2006). Over 50% of individuals afflicted by such disorders develop glaucoma, with ARS patients at a slightly more serious risk (at around 50% to 75%) (Fuse et al., 2007; Komatireddy et al., 2003; Panicker et al., 2002; Vincent et al., 2006; Tamimi et al., 2004). Patients manifesting with ARS are noted to develop glaucoma during infancy, adolescence or early adulthood, which can lead to blindness (Strungaru et al., 2007). Rare cases do exist in which ARS patients are seen to develop glaucoma after middle age, suggesting that patients with ARS are at lifelong risk for the development of glaucoma (Strungaru et al., 2007).

Studies propose that mutations in the *FOXC1* gene are responsible for causing a wide variety of disorders in the anterior segment associated with the development of glaucoma, however the precise mechanisms by which *FOXC1* mutations give rise to glaucoma remain unclear (Komatireddy et al., 2003; Panicker et al., 2002; Tamimi et al., 2004; Fuse et al., 2007).

Glaucoma can currently only be effectively treated by significantly reducing intra-ocular pressure, through either medication or surgical treatment (Strungaru et al., 2007). However, in glaucoma patients with genetic defects in *FOXC1*, only 18% of glaucoma patients respond to medical or surgical treatment (Fuse et al., 2007). Alternative treatments targeting the genetic basis of the disease thus need to be developed in order to prevent the critical outcomes of disease progression.

2.5. Potential *Foxc1* Target Genes

Future perspectives in investigating the developmental role played by *FOXC1* in the eye seek to identify specific potential candidate genes targeted for regulation by FOXC1 (Tamimi et al., 2006). This, together with a better understanding of the molecular mechanisms behind the progression of *FOXC1* mutation-mediated anterior segment dysgenesis, would allow for a better understanding of the role played by FOXC1 in disease manifestation and progression. Gaining more knowledge relating to *FOXC1* target genes is a crucial step in understanding embryonic development and the diseases that result upon the impairment of *FOXC1* gene function.

2.5.1. Cell Adhesion Molecules: Junction Protein Interactions

Cell interactions, both with their adjacent counterparts as well as with the extracellular matrix surrounding the cells play an integral role in the control of signal transduction, and the transcriptional/translational gene expression regulatory mechanisms that take place during cell proliferation and differentiation (Balda & Matter, 2008). A number of morphogenetic processes occurring during the growth and turnover of adult tissues, as well as during the development of new tissues, are brought about and controlled by the fine regulation of the formation of adhesive contacts between cell membranes (Gumbiner, 2005). Cell–cell adhesion is regarded as an essential element required for both the proper functioning and maintenance of the morphology of epithelial cells (Braga, 2002). As such, cells possess a number of specialised adhesive structures which allows them to adhere tightly to adjacent cells, and this in turn results in these cells being able to maintain an appropriate degree of structural integrity and tensile strength as they form epithelial sheets (Braga, 2002).

Single cells make contact with each other (i.e., intercellular contact) through morphologically distinct components. Gap junctions, adherens junctions, desmosomes and tight junctions are all elements composed of distinct proteins that allow for contact between cells to occur successfully (Figure 13) (Balda & Matter et al., 2008; Troyanovsky, 1999).

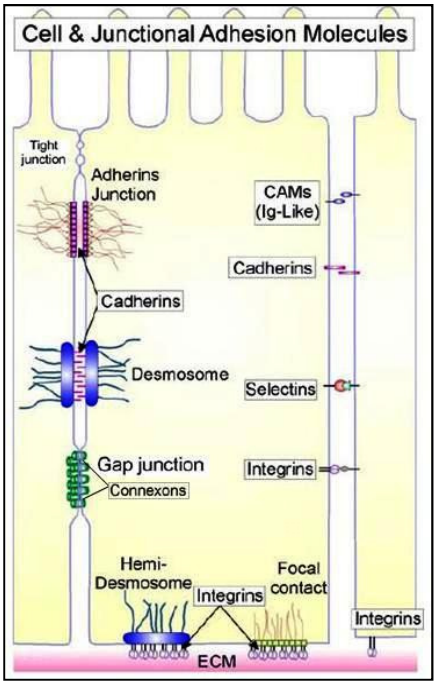

Figure 13: Molecules involved in cell adhesion and junctional contact points (*O'Day 2009*).

Among the different adhesion/contact elements that exist, one of key interest in this study is the adherens junction. Two structurally distinct types of adhesion receptors generally make up the morphologically different adhesion junctions (Troyanovsky, 1999). The cadherins form one group while, connexions, occludins and claudins comprise another (Troyanovsky, 1999). The cadherin proteins can be further divided into classic cadherins and desmosomal cadherins, the former mediating intercellular adhesion via adherens junctions, and the latter present in desmosomes (Troyanovsky, 1999). Although a variety of cell adhesion molecules and cell junctions control the physical interactions that occur at points of cellular contact, the cadherin family of adhesion molecules in particular is regarded as being vitally important in the dynamic regulation of these junctions and as a result the diverse morphogenetic processes associated with them (Gumbiner, 2005).

2.5.2. Adhesion Junction Proteins: The Cadherins

The Ca^{2+}-dependent cadherins are a superfamily of single-pass trans-membrane glycoproteins comprised of no less than 90 members that require calcium in order to maintain their structural and functional integrity (Chen et al., 2005; Gumbiner, 2005; Itoh et al., 1993; Radice et al., 1997; Chen & Ma, 2007; Van Aken et al., 2000; Braga, 2002; Pontoriero et al., 2009). Originally named after the tissue most prominently expressing them, the classical cadherins show diverse and non-restricted expression patterns (Gumbiner, 2005). Cadherins and proteins showing domains with similar activity are seen in a diverse range of organisms, including unicellular choanoflagellates, invertebrates (*Drosophila sp.* and *Caenorhabditis elegans*) and numerous other vertebrates such as mammals and reptiles (*Xenopus sp.*) (Barth et al., 1997; Hulpiau & van Roy, 2009).

Classical cadherins have a primary role in homophilic, homotypic cell–cell adhesion and cytoskeletal anchoring in embryonic and adult tissues (Troyanovsky, 1999; Castro et al., 2004; Gumbiner, 2005; Packer et al., 1997; Radice et al., 1997; Chen & Ma, 2007; Hulpiau & van Roy, 2009; Van Aken et al., 2000). These trans-membrane glycoprotein molecules are regarded as key players in a range of cell signalling events, transducing signals critical in the regulation of cell migration, cell differentiation, proliferation and signalled cell death (Barth et al., 1997). Changes in the expression of cadherins coincide with the advent of major events such as embryonic development (gastrulation and neurulation), tissue morphogenesis (somitogenesis) and organogenesis (cardiogenesis) implicating a mechanistic role for these proteins (Troyanovsky, 1999; Castro et al., 2004; Gumbiner, 2005; Packer et al., 1997; Barth et al., 1997; Radice et al., 1997; Hulpiau & van Roy, 2009). This mechanistic control is exerted by regulating the synthesis of epithelial and endothelial cell junctions. These serve to control the movement of substances across cells, mediate the proper arrangement of developing tissues and ensure maintained stability in organized adult tissues and organs (Gumbiner, 2005).

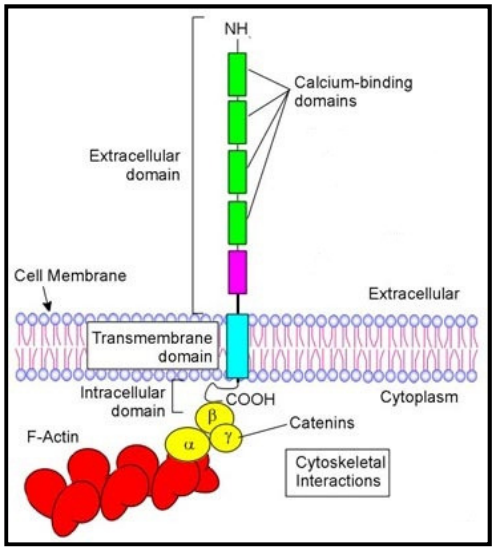

Figure 14: Basic structure of a single cadherin molecule showing the membrane-bound N-cadherin protein and the cytoskeletal elements anchoring the protein intracellularly (*O'Day, 2000*).

The basic cadherin molecule is a parallel or *cis* homodimer with the extracellular domain (the region primarily involved in the adhesive binding function) of classic cadherins consisting of five cadherin-type repeats (EC1-EC5) bound by Ca^{2+} ions to give the protein a rigid, rod-like structure thereby maintaining the integrity of the EC domains (Figure 14) (Troyanovsky, 1999; Gumbiner, 2005). The defining feature of cadherins is the presence of two or more repeated motifs of 110 residues comprising the extracellular domains (Hulpiau & van Roy, 2009). It is the amino terminus of the extracellular domain, consisting of tandem repeats of domains carrying negatively charged amino acids that mediate the specificity of the adhesion function (Radice et

al., 1997; Pontoriero et al., 2009). A conserved Histidine-Alanine-Valine (HAV) cell adhesion recognition sequence located within the first extracellular domain is proposed to control the adhesive activity of the molecule (Van Aken et al., 2000).

2.5.3. (N)eural Cadherin

The most well-characterised of the classical cadherin proteins are undoubtedly E- and N-cadherin, due largely to their roles in development having been assessed by means of loss-of-function analysis as well as dominant-negative gene analysis approaches (Chen & Ma, 2007; Barth et al., 1997). The Ca^{2+}-dependent cell-cell adhesion molecule classified as N(eural)-cadherin was initially identified as a cell adhesion molecule within the central nervous systems of both mice and chickens, and belongs to the "Type I" cadherin family (Hatta et al., 1985; Packer et al., 1997; Chen & Ma, 2007; Van Aken et al., 2000). Named for its extensive expression in the nervous system, it is most commonly linked to the presence of small adherens-type junctions found at the neural synapses, growth cones and other regions along the neuron (Gumbiner, 2005). N-cadherin is expressed in neural cells and mesenchymal cells and instigates the differentiation of undifferentiated embryonic tissues into defined epithelial and neuronal tissues (Chen & Ma, 2007; Van Aken et al., 2000). N-cadherin is associated with the proper assembly of neural tissues during embryonic development, a role that has been reiterated by studies showing antibodies directed against N-cadherin to cause tissues to dissociate (Hatta et al., 1988). The adhesive activity of N-cadherin occurs through a complex non-Ca^{2+} binding site within the EC1 domain composed of residues from β-strands, incorporating the tripeptide HAV sequence at β-strand F (Troyanovsky, 1999). The strength and specificity of the binding interaction of N-cadherin is thought to be brought about by zipper-like interaction between N-cadherin molecules on adjacent cells (Figure 15) (Radice et al., 1997). The expression of N-cadherin results in differentiation, segregation, and migration away from their parent tissue (Hatta et al., 1985; Van Aken et al., 2000).

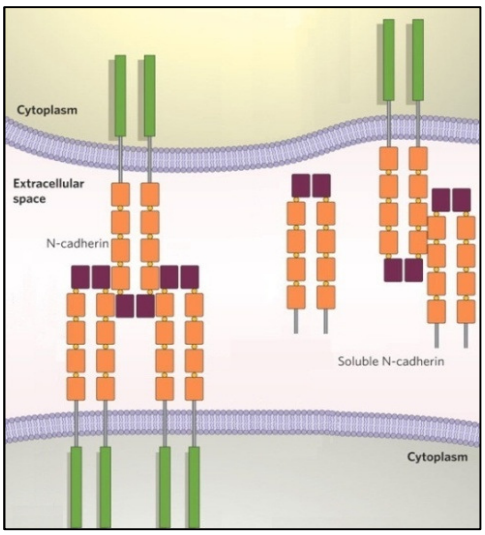

Figure 15: (N)eural cadherin "zipper-like" interaction between membrane-bound and soluble protein fractions. Image adapted from *Christofori, 2006*.

However, N-cadherin expression is not limited to neural tissues only, and a number of non-neural tissues have shown spatiotemporal expression of N-cadherin during embryogenesis (Hatta et al., 1988; Radice et al., 1997; Van Aken et al., 2000). Its expression - examined by *in situ* hybridization and immunofluorescence in the developing chick embryo - is linked to the rearrangement and invasion of embryonic cells during morphogenesis. Subsequently, N-cadherin patterning undergoes a dynamic change during the rapid chain of events that occur during development, with the absence or presence of the protein showing a strong correlated with cellular association or segregation (Hatta et al., 1988). Within the chick embryo, N-cadherin can be noted to show diverse expression patterns, and is found extensively throughout embryonic development in the central and peripheral nervous systems, cardiac and skeletal muscle, somites, the urogenital system, as well as in a number of neural crest-derived and mesenchymal cells (Packer et al., 1997; Barth et al., 1997; Van Aken et al., 2000; Matsuda et al., 2006). N-cadherin is expressed in mouse embryos from around 9.5 days into development, chiefly within the developing heart myocardium due to its involvement in cardiac myocyte adhesion. At E12.5, this expression remains in the neural tube, brain, the umbilical gut, myocardium and the somites (Barth et al., 1997; Blixt et al., 2007; Matsuda et al., 2006; Packer et al., 1997.). N-cadherin expression is absent in the neural arches and in the perichondria and mesenchyme of developing limbs at E12.5, but strong expression is seen in these tissues at E15.5 (Packer et al., 1997). The developing lung mesenchyme uniformly expresses N-cadherin at E12.5, while the embryonic urogenital complex shows expression of N-cadherin around E14.5 (Packer et al., 1997).

In the eye, N-cadherin is prominently localized within the lens, corneal endothelium, stromal fibroblasts (keratocytes) and the neuroretina of the developing eye at day 12.5. In the developed eye, N-cadherin is regarded as being the main cell-adhesion protein in the lens, forming adherens junction complexes. Cadherin-mediated adhesion, such as the kind seen in lens cells is considered a critical element in the maintenance of the epithelial phenotype (Chaffer et al., 2007). Sudden changes in the assembly or the breakdown of adherens junctions during development results in radical changes during cell differentiation (Gumbiner, 2005). Changes in the specific cellular localization of N-cadherin that are seen upon assessment of individual cells have become associated with cellular rearrangement (Hatta et al., 1988). The assembly of cell junctions is thought to be both directly and indirectly influenced by the event of epithelial-mesenchyme transactions and this is due mainly to the process of EMT involving a number of fluctuations in gene expression and post-translational modification mechanisms that directly affect the expression and/or regulation of junction proteins (Gumbiner, 2005).

Murine studies suggest that in order for cadherin proteins - such as N-cadherin - to be expressed, Foxc1 proteins must be actively functional (Chen et al., 2005; Kidson et al., 1999). In *Foxe3* mutant mice, *N-cadherin* expression is increased, resulting in adherent sections between different tissues of

the anterior segment, however this observation is somewhat inconsistent with the lack of N-cadherin and corneal endothelium observed in chick embryos from which the Foxe3- producing lens has been excised (Blixt et al., 2007). *Foxc1* has been implicated as a factor regulating N-cadherin expression and functioning prior to the development of adhesion junctions forming the corneal endothelium monolayer (Kidson et al., 1999). In *Foxc1*$^{-/-}$ mice, the posterior mesenchyme of the cornea fails to develop into the corneal endothelium (Chakravarti, 2001) as the mesenchymal cells do not form the typical junctions. Formation of the anterior chamber is prevented, as the endothelium remains closely attached to the lens (Chakravarti, 2001). N-cadherin and its relationship with *Foxc1* therefore needs to be further assessed in order to determine the functional and mechanist relationship between the two elements.

2.5.4. Potential Foxc1 Target Genes: Msx1

2.5.4.1. Homeobox genes

The homeobox genes are a family of regulatory transcription factors that were initially identified based on their association with the appearance of developmental anomalies (Catron et al., 1995). Homeobox genes belong to an extensive and highly conserved multigene family of transcription factors homologous to the *Drosophila* muscle-segment homeobox (*msh*) gene (Jowett et al., 1993; Blin-Wakkach et al., 2001; Catron et al., 1995; Petit et al., 2009). Members of this gene family were originally implicated as being associated with mutations that resulted in homeotic transformations, i.e. the development of normal, but ectopic organs or tissues (Catron et al., 1995). The structurally and functionally conserved superfamily of homeobox transcription factors can be found in all eukaryotes, where they take on primary roles in the regulation of axis determination, segmental patterning and tissue identity during development. These genes are also known to have analogues in prokaryotes (Katerji et al., 2009; Catron et al., 1995; Boogerd, et al., 2010).

Homeobox proteins possesses a highly conserved homeodomain at the carboxyl terminus within which a DNA binding helix-turn-helix motif can be found, together with a region of variation comprising domains engaging in the regulation and targeted specificity of protein binding (Katerji et al., 2009). The highly conserved homeodomain plays a pivotal role in directing functional specificity within structures and is a common component of numerous proteins that are known to regulate transcription during development (Catron et al., 1995). Proteins expressing the homeodomain play a number of developmental roles, such as directing pattern formation and conservatively determining cell fate in specific regions (Catron et al., 1995). The fundamental role of homeobox genes, however, is the maintenance of normal cell growth and differentiation. As such, the atypical expression of certain homeobox genes is noted to result in cellular transformation (Catron et al., 1995). Genes belonging to this family are expressed in a spatially and temporally restricted way during the initial phases of development (Katerji et al., 2009). Homeogenes have also been nominated as being

candidate regulatory genes - genes which exert regulatory genetic control, and are thought to play an active role in the control of early patterning, predominantly in cranial neural crest cells destined for differentiation into a variety of different cell types such as the neural crest-derived skeleton (Berdal et al., 2002; Katerji et al., 2009; Chung et al., 2010). Support for this hypothesis has been put forward in the form of observed defective developmental phenotypes (such as hypodontia and palatal clefting) in a number of studies (Berdal et al., 2002; Katerji et al., 2009; Chung et al., 2010).

2.5.4.2. Msx genes: Msx1

The *Msx* genes belong to the homeobox gene family and regulate key steps in morphogenesis during all phases of vertebrate development, especially so in the pivotal epithelium-mesenchymal interactions that occur during organogenesis (Lazzarotto-Silva et al., 2005). *Msx1* and *Msx2* (formerly referred to as *Hox-7* and *Hox-8,* respectively) are two members of this diverged homeobox family of proteins, which are regulated developmentally (Jowett et al., 1993). *Msx1* is known to control the fate of cranial neural crest cells (Han et al., 2009), with the primary role of the transcription factor encoded by the *Msx1* gene being the maintenance of progenitor cells in an undifferentiated, proliferative state (Lazzarotto-Silva et al., 2005).

In mice, the homeobox gene *Msx1* possesses the typical traits of both a cell transforming gene and an essential developmental regulator (Catron et al., 1995). *Msx1*'s proposed function as a regulator of differentiation in specific cell populations (assessed in *in vivo* expression studies) is substantiated by Catron et al. (1995). They postulate that *Msx1* has the ability to maintain cells in an undifferentiated state and have shown *Msx1* to be a potent transcription repressor able to repress several genes simultaneously, with repression occurring even if DNA-binding sites for the *Msx1* homeodomain are absent. Recent studies have outlined another important primary function of *Msx* genes to be control of the progression of the cranial neural crest cell cycle (Han et al., 2009). This was brought to light in studies showing that a deficiency of both the *Msx1* and *Msx2* genes gives rise to defective neural crest cell proliferation which consequently results in a decreased chance of survival (Han et al., 2009).

The *Msx* family of homeobox genes and *Msh*-like genes are predominantly expressed in a number of embryonic regions in tissues which develop by epithelial-mesenchymal interactions, i.e. the neural tube, limb buds and cell derivatives of the cranial neural crest (such as the vertebrate eye, limbs and heart), where their primary role is to specify differential fates of these initial mesenchymal cells (Chung et al., 2010; Jowett et al., 1993; Lazzarotto-Silva et al., 2005; Boogerd, et al., 2010). *Msx1* expression in mice is detected early in development (from around E7) and is localized to several sites, such as in the cephalic neural crest (from which the craniofacial structures form), the cells contributing to the neural folds, the somites, limb buds, craniofacial bones, teeth, hair follicles, the embryonic tail and the heart (Catron et al., 1995; Lazzarotto-Silva et al., 2005; Blin-Wakkach et al.,

2001; Petit et al., 2009). *Msx* genes are also noted to be expressed in the pharyngeal arches, which also contribute to the formation craniofacial structures such as the mandible, maxilla, zygoma and ear (Katerji et al., 2009). *Msx1* expression in the cranial neural crest is noted to continue during cell migration and colonization of first pharyngeal arch from which these tissues arise. *Msx1*-expressing cells share a common characteristic element, even though they have incongruent origins – cells expressing the homeobox protein are considered to be developmentally plastic or in an actively proliferating state – in fact, these genes and the expression of the protein transcription factors encoded by them is limited to proliferating cells (Catron et al., 1995; Chung et al., 2010).

Screening of *Msx1* expression during a number of stages in development (including the early antenatal, postnatal and late adulthood stages) has established the maintained life-long expression of this homeoprotein in mammals (Berdal et al., 2002). *Msx1* expression is limited in adult mice to cells capable of self-renewal and constant, permanent regeneration such as the tissues comprising the mammary and uterine organs, as well as the basal dermal epithelium (Lazzarotto-Silva et al., 2005; Petit et al., 2009). Interestingly, *Msx* genes show synchronicity in their expression in a variety of cell lineages during cellular differentiation and proliferation, both in embryonic and adult developmental events (Chung et al., 2010). *Msx1* gene expression is thus regarded as being important not only during early embryonic patterning, but also in the maintenance of adult stem cells in specific areas of the adult skeleton (Berdal et al., 2002).

Even though *Msx1* has a diverse expression pattern, only a handful of abnormalities have been described in $Msx1^{-/-}$ mutants (Lazzarotto-Silva et al., 2005). However, a number of gene mutations seen in mammalian studies (in both mice models and humans) demonstrate the importance of the transcription factor gene in cranio-facial development (Berdal et al., 2002). *Msx1* gene expression patterns are closely related to the development of neural crest cells in a number of species, with reports suggesting that mesenchymal differentiation and the establishment of certain cranio-facial structures is defective in the homozygous absence of *Msx1* (Katerji et al., 2009). Cranio-facial malformations seen in the absence of the *Msx1* gene include abnormal phenotypes such as cleft palate, deformities of the nasal, frontal and parietal bones, shortened mandibular length, inner ear malformations and stunted tooth development (Lazzarotto-Silva et al., 2005; Blin-Wakkach et al., 2001; Boogerd, et al., 2010). In humans, the phenotype that is commonly seen in mutations of the *Msx1* gene are tooth agenesis and cleft palate, with the manifestation of both deformities being proposed to be brought about as a result of the dose effect of the Msx1 protein (Blin-Wakkach et al., 2001; Katerji et al., 2009; Han et al., 2009; Petit et al., 2009). The abnormal phenotype seen in the facial regions of $Msx1^{-/-}$ mutant mice cannot explain the lethality of the null mutation in mouse neonates (which die within 24 hours of birth) or the role played by *Msx1* expression at such a range of sites (Lazzarotto-Silva et al., 2005). The role of the Msx family in differentiation can be illustrated

by studies showing mutations in Msx1 to result in Witkop syndrome (hypodontia with nail dysgenesis) (Catron et al., 1995; Petit et al., 2009).

Gene expression analysis of *Msx1* at sites undergoing epithelium-mesenchymal interactions has implicated a number of factors as having involvement in *Msx1* regulation; these include the Tgf-β family proteins BMP2, BMP4 and BMP7, which show overlap in expression with *Msx1* at a number of tissue sites in vertebrate embryos (Lazzarotto-Silva et al., 2005). *Msx1* down-regulation appears to be a vital precursor step to terminal differentiation in cell types such as cartilage and muscle, acting presumably by inducing expression of tissue-specific master-genes, triggering the synthesis of phenotypic markers (Blin-Wakkach et al., 2001; Katerji et al., 2009; Berdal et al., 2002). *Msx1* is therefore implicated as a transcription factor gene able to inhibit differentiation (maintaining cells in an undifferentiated state) and increase proliferative ability of cells by controlling gene expression (Blin-Wakkach et al., 2001; Catron et al., 1995; Lazzarotto-Silva et al., 2005).

In the eye, *Msx1* expression during embryonic development in the mouse model has been well established (Petit et al., 2009). Within the tissues of the eye, *Msx1* is expressed in the ciliary bodies, iris, corneal endothelial cells, with the lens showing the strongest expression (Figure 16) (Petit et al., 2009).

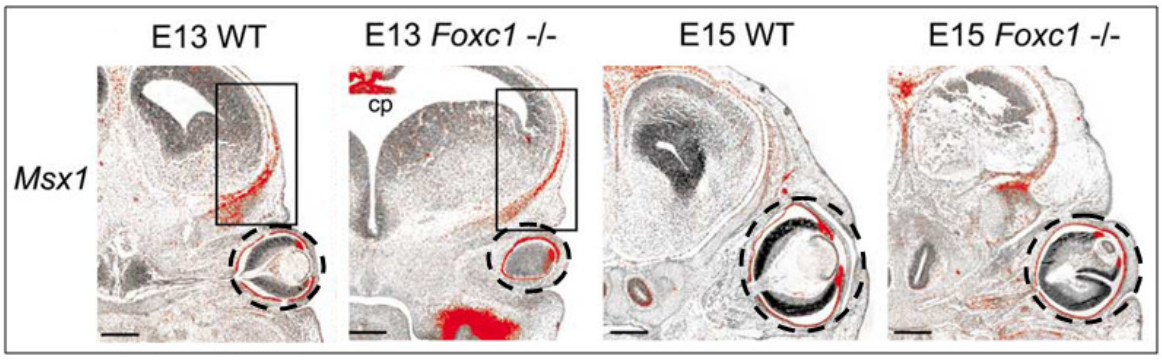

Figure 16: *Msx1* and *Msx2* expression patterns (red) in the developing mouse head of $Foxc1^{+/+}$ and $Foxc1^{-/-}$ embryos at E13.5 and E15.5. *Msx2* is down-regulated in $Foxc1^{-/-}$ embryos but *Msx1* is not. cp - choroid plexus. The developing eye region is indicated with broken lines. Scale bars = 200 µm. Image adapted from *Rice et al., 2003.*

In the eye, it is postulated that down-regulation of the homeobox gene *Msx1* is critical to the formation of the corneal endothelium and its subsequent separation from the lens surface. This is due to the fact that the gene is down-regulated at E12.5, precisely when adherens junction formation occurs in the periocular mesenchyme (Lincecum et al., 1998). *Hox* genes have been nominated as regulatory genes expressing proteins with the potential to bind sites within specific regions located on adhesion molecule genes, and induce regulatory transcriptional activation of cadherins (Hatta et al., 1988). This hypothesis thus serves to link both *Hox* genes and cadherins in a co-operative role during pattern formation/morphogenesis within tissues expressing these elements (Hatta et al., 1988). *Msx1*

has previously been shown to decrease cadherin-mediated adhesion *in vitro* (Hartsock and Nelson, 2008), further implicating it as a candidate gene in corneal endothelium development. Additionally, *Msx2* (a homologue of *Msx1*) has been shown to be a downstream target of *Foxc1* in the calvarial mesenchyme. Evidence suggests that *Msx1* is also a downstream target of *Foxc1* in periocular mesenchyme tissue (Figure 16) (Rice et al., 2003). These links all point towards *Msx1* playing a significant role in the development of the anterior segment. Further studies therefore need to be carried out in order to fully understand the functional link between N-*cadherin*, *Foxc1* and *Msx1* in order to gain a better understanding of these factors in eye development.

2.6. Aims & Objectives

FOXC1 mutations in humans result in anterior segment defects in the cornea and the trabecular meshwork, leading to ARS (Hsieh et al., 2002). The corneal endothelium is regarded as the primary component that must develop correctly in order to attain normal vision. In the absence of Foxc1, the corneal endothelium fails to develop correctly. In order to define the role of *Foxc1* in eye development and disease initiation/progression, genes regulated by *Foxc1* must be identified. The cadherin family of junction proteins is thought to undergo regulation by *Foxc1* (Kidson et al., 1999). N-cadherin is considered crucial for proper formation of the corneal endothelium and anterior eye. Chakravarti (2001) has shown that in *Foxc1*$^{-/-}$ mice, the posterior mesenchyme of the cornea fails to develop into the corneal endothelium and remains closely attached to the lens. Kidson et al. (1999) have postulated that in order for N-cadherin to function normally, a *Foxc1*-mediated signal is required, without which the formation of the anterior chamber is prevented.

In vitro experimentation has also implicated the *Hox* (homeobox) genes as being regulators of cadherin expression. The up-regulation of the homeobox gene *Msx1* has been shown decrease cadherin-mediated adhesion. The gene shows decreased expression and is down-regulated at E12.5 when the corneal endothelium develops, a process marked by adherens junction formation between POM cells (Lincecum et al., 1998). *Msx1* may thus be a downstream target of *Foxc1*.

This study thus aims to:

a. develop effective vector systems targeting *Foxc1* to either increase or ablate gene expression.

b. comprehensively ascertain the role played by *Foxc1* in adherens junction formation in corneal endothelium development by using the above vector systems to determine whether *Foxc1* regulates *N-cadherin* expression in POM cells.

c. assess N-cadherin expression and localization in periocular mesenchyme cells in a 3-dimensional model.

d. investigate the effect of *Foxc1* expression on the expression of the homeobox gene *Msx1*.

CHAPTER 3: MATERIALS & METHODS

3.1. Cell lines: Overview

The cell lines used in this study were generated by other members in the laboratory in order to provide a means of understanding the mechanisms behind the differentiation of the corneal endothelium. Cell lines were generated by immortalizing POM cells (cells that give rise to the corneal endothelium) dissected from E12.5 and E13.5 embryos – the point in development during which the corneal endothelium begins to differentiate.

To create the POM cell lines, wedges (±0.05 mm^3) of POM cells were micro-dissected from the anterior region of E12.5 and E13.5 *Foxc1*$^{+/+}$ and *Foxc1*$^{-/-}$ embryos (animal ethics number: 019/10/Animal) as described by Sommer et al. (2006). The *Foxc1*$^{lacZ+/-}$ transgenic mice (ICR background) used in this study were a kind gift from Prof. Susan H. Kidson, from the University of Cape Town. These mice contain the *LacZ* cassette encoding the β-galactosidase reporter gene in place of one *Foxc1* allele (Figure 1). These wedges were allowed to proliferate in culture for 48 – 72 h at 37˚C in DMEM supplemented with 20% foetal bovine serum (FBS) (both supplied by Gibco-Invitrogen, California, USA). Cells were subsequently immortalised by infection with a retrovirus encoding the mutant SV40 large T-antigen (Frederiksen *et al.*, 1988; Jat & Sharp, 1989).

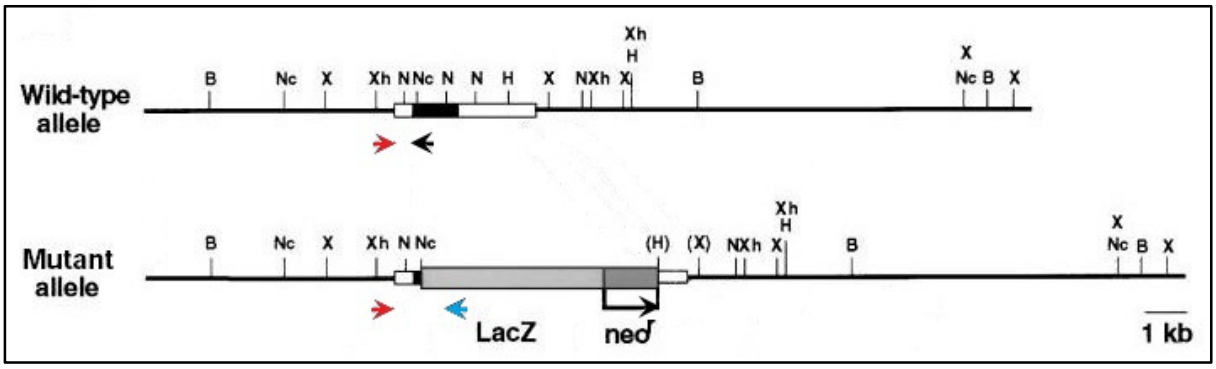

Figure 1: Targeting strategy employed to generate the *Foxc1*$^{lacZ+/-}$ mice.

The immortalized cell lines used in this study include E12.5 *Foxc1*$^{+/+}$ and E13.5 *Foxc1*$^{+/+}$ cell lines. NIH3T3 cells were used to initially optimise PCR cycling conditions and microscopy techniques. To determine the effects of a lack of *Foxc1* expression, shRNAs were designed to target and knock-down *Foxc1* gene expression. An existing plasmid vector incorporating the full-length *Foxc1* sequence was used to determine the effects of Foxc1 over-expression in the POM cell lines. Stable transfected cell lines incorporating the plasmids were not established, thus data were gathered from experiments using transiently transfected immortalized wildtype cells.

3.2. Maintenance of Cell Lines

All tissue culture procedures were performed in a sterile tissue culture room using a Labconco Purifier Biological Safety Cabinet laminar flow. The POM cell lines were cultured and maintained in a sterile, humidified water-jacketed incubator (Forma Scientific Inc.) at the replication permissive temperature of 33°C with a constant feed of 5% CO_2 in Dulbecco's Modified Eagle's medium (DMEM) supplemented with 10% heat-inactivated fetal bovine serum and 2% 0.5µg/mℓ penicillin-streptomycin (all supplied by Gibco-Invitrogen, California, USA). Cells in 6 or 10 cm tissue culture dishes and T75 culture flasks (Corning) were monitored using a Nikon TMS-F inverted light microscope (Nikon, Tokyo, Japan) at 100x total magnification. Cells were maintained until monolayers reached 80% - 100% confluency, at which point cells were either passaged, treated, transfected or trypsinized for further use. Trypsinizing and passaging involved the addition of 800µℓ trypsin-EDTA (Invitrogen, USA) to the culture vessel followed by a 3-5 minute incubation at 33°C to enhance trypsin activity. Trypsin was deactivated by addition of 200µℓ DMEM to the culture vessel. Cells were adjusted to an appropriate concentration and seeded into new culture vessels.

Cells were imaged during culture to establish if any visible differences in cell morphology across the cell lines existed. Images were captured using a Nikon TMS-F inverted light microscope (Nikon, Tokyo, Japan), ScopeTek DCM130 1.3MP camera and the ScopePhoto (version 3.0.12.867) imaging software (ScopeTek, 2008).

3.3. Plasmid preparations

3.3.1. Generation of shRNA sequences targeting *Foxc1*

3.3.1.1. *Overview: shRNA*

shRNA (short hairpin RNA) is a term used in reference to a sequence of RNA that forms a tight hairpin structure able to silence the expression of a specific gene by RNA interference. The shRNA sequence is cloned into an expression vector together with the human U6 promoter sequence, to ensure the continuous expression of the sequence. shRNAs were generated using reverse primers incorporating the shRNA sequence and the 3' end of the human U6 promoter, and a forward primer incorporating the 5' end of the human U6 promoter. Human genomic DNA was used a template to generate a PCR product containing the full-length U6 promoter and shRNA sequence.

3.3.1.2. Primer design

With the help of Dr. Marco Weinberg from the University of the Witwatersrand, five putative shRNAs to *Foxc1* were chosen from the MIT/Harvard Broad Institute's murine shRNA library database (http://www.broad.mit.edu/rnai/trc/lib). Oligo primers were designed to incorporate the following, as shown in Figure 2:

1. 21 bp sequence corresponding to the 5' end of the human U6 promoter

2. 22 bp sequence corresponding to the sense sequence of the shRNA
3. 9 bp loop sequence
4. 21 bp sequence corresponding to the anti-sense sequence of the shRNA
5. 6 bp termination sequence

These primers were used in conjunction with a forward primer designed to amplify the 5' end of the human U6 promoter in a PCR reaction using human genomic DNA. The resulting amplicons therefore contained the full-length U6 promoter and the shRNA sequence. All primer sequences are given in Table 1.

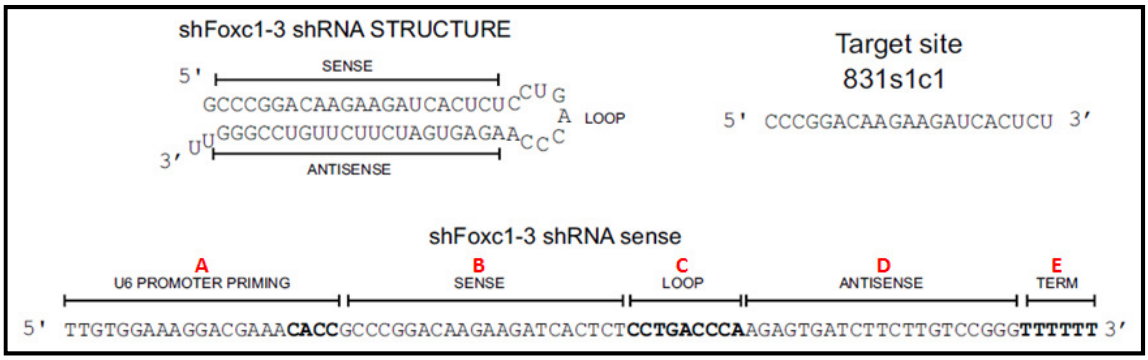

Figure 2: Structure of shRNA3 sequence: the U6 promoter (A), the sense (B) coding sequence, a 9bp loop sequence (C), the antisense (D) coding sequences, and the Pol III transcription terminator sequence (E).

Table 1: Primers generated to amplify shRNA sequences

Target gene	Forward Primer	Reverse Primer
U6 Promoter-Xho1 Site	5' GATCTCGAGAAGGTCGGGCAGGAAGAGGGGCC 3'	
ShFoxc1-1		5' AAAAAACGTCTATGACTGTAGCAAATTTGGGTCAGGAATTTG CTACAGTCATAGACGCGGTGTTTCGTCCTTTCCACAA 3'
ShFoxc1-2		5' AAAAAATGGGAATAGTAGCTGTCAGATTGGGTCAGGATCTGA CAGCTACTATTCCCACGGTGTTTCGTCCTTTCCACAA 3'
ShFoxc1-3		5' AAAAAACCCGGACAAGAAGATCACTCTTGGGTCAGGAGAGTG ATCTTCTTGTCCGGGCGGTGTTTCGTCCTTTCCACAA 3'
ShFoxc1-4		5' AAAAAAGCGGGAAATGTTCGAGTCTCATGGGTCAGGTGAGAC TCGAACATTTCCCGCGGTGTTTCGTCCTTTCCACAA 3'
ShFoxc1-5		5' AAAAAAGAGCAGAGCTACTATCGCGCTTGGGTCAGGAGCGCG ATAGTAGCTCTGCTCGGTGTTTCGTCCTTTCCACAA 3'

3.3.1.3. Amplification of shRNAs

Genomic DNA extracted from HeLa cells (human cervical carcinoma cells) using a Qiagen DNA Extraction Kit (QIAGEN, USA) was used as a template to carry out PCR amplification in a BioRad MyCycler PCR ThermoCycler. Each 20µℓ reaction incorporated the following reagents: 11 µℓ DNAse-free H_2O (Invitrogen, USA), 2 µℓ 10x NH_4 Buffer (Fermentas, Canada), 1.8 µℓ 25mM $MgCl_2$ (Fermentas, Canada), 2 µℓ 2mM dNTPs (Promega, USA), 1 µℓ 10µM reverse primer, 1 µℓ 10 µM forward primer, 0.2 µℓ *Taq* polymerase (Fermentas, Canada) and 1 µℓ HeLa cell genomic DNA. Prepared PCR reactions were amplified by 1 initial cycle of 94°C for 4 minutes followed by 35

cycles of 94°C for 30 seconds, 55°C for 1 minute, and 72°C for 1 minute, with a final cycle of 72°C for 7 minutes.

3.3.1.4. Gel Excision & Extraction

Amplified PCR products were separated out alongside a 100 bp GeneRuler molecular weight marker (Fermentas, Canada) on a 1% (w/v) agarose gel (Roche, New Jersey, USA) via electrophoresis in 1 x TBE buffer (Appendix 1) for 90 minutes at 80V. The resultant bands were visualized by staining the agarose gel with ethidium bromide for 10 minutes followed by destaining in 1 x TBE buffer (Appendix 1). Bands specific to each shRNA sequence were excised from the agarose under UV light (Uvitech, Petach Tikva, Israel) and the DNA was purified using the Qiagen Gel Extraction Kit (QIAGEN, USA). The purified DNA was quantified on a NanoDrop ND-1000 Spectrometer using the ND-1000 V3.5.2 software.

3.3.1.5. Plasmid ligation and transformation into competent cells

These purified short hairpin sequences were ligated into the pGEM-T Easy plasmid vector (Promega, USA) (Appendix 2) in overnight reactions at 4°C. Briefly, DH5α competent cells (Invitrogen, USA) were transformed using the ligated shRNA plasmid vectors or the PUC19 vector as a control (Appendix 3), and plated onto Luria agar (Sigma-Aldrich, USA) plates containing Ampicillin Ready Made Solution (Sigma, USA) and X-gal/IPTG (Promega, USA) selective markers (Appendix 4). Prepared plates were incubated at 37°C overnight and stored at 4°C thereafter. Single putatively positive bacterial colonies were selected (based on white/blue selection), from each shRNA plate and innoculated into 5 mℓ of Luria-Bertani broth containing 5μℓ of 100mg/μℓ Ampicillin Ready Made Solution (Sigma, USA). Innoculated cultures were allowed to grow at 37°C in a shaking incubator at 200 rpm for 12-16hrs until bacterial growth reached logarithmic phase.

3.3.1.6. MiniPrep Plasmid Purificaton & Restriction Enzyme Digest

Cells were harvested by centrifugation at 4000 x *g* for 10 minutes at 4°C in an Eppendorf Centrifuge 5810R, following which the plasmid DNA incorporating the shRNA sequences was purified using the QIAPrep Spin Miniprep Kit (QIAGEN, USA) as per the manufacturer's instructions. The resulting purified plasmid DNA was quantified using a NanoDrop ND-1000 Spectrometer and the ND-1000 V3.5.2 software package. The presence of the shRNA sequences in the plasmid was verified by restriction enzyme digest using the *EcoR1* restriction enzyme (Fermentas, Canada) (Appendix 5). The digest products were separated out alongside a 100 bp GeneRuler molecular weight marker (Fermentas, Canada) on a 1% agarose gel by electrophoresis in 1 x TBE buffer (Appendix 1) for 90 minutes at 80V. The resultant bands were visualized by staining the gel with ethidium bromide for 10 minutes followed by destaining in 1 x TBE buffer (Appendix 1). Images were captured and analysed using the ChemiDoc XRS Imaging System (BioRad, USA) and the Image Lab imaging software (V

2.0.1) (BioRad, USA). Positive clones were sent for sequencing (Inqaba Biotech) and these sequences were subject to BLAST analysis to confirm homology to the desired shRNA oligo sequence (Appendix 6).

3.3.1.7. Glycerol Stock Generation

In order to maintain a stock of the plasmid clones, 800µl of the cultured growth medium was inoculated into 200µl of sterile, autoclaved glycerol in labeled cryo-vials. The suspension was vortexed to ensure homogeneity and then flash-frozen in liquid nitrogen and immediately transferred to a -80°C ultrafreezer for long-term storage. When required for culture, 5µl of this stock was inoculated into 50ml of LB broth at room temperature and allowed to grow at 37°C in a shaking incubator at 200 rpm for 12-16hrs until bacterial growth reached logarithmic phase.

3.3.2. Cloning functional shRNA targeting *Foxc1* into a mammalian expression vector

Two of four shRNA sequences generated to knockdown *Foxc1* gene activity were shown to effectively silence *Foxc1* expression via qPCR analysis. One of these sequences (shRNA3) was shown to knockdown *Foxc1* activity by > 98%. Because the shRNA sequence could not be directly sub-cloned into the mammalian vector due to a lack of compatible restriction sites, a pair of custom oligonucleotide sequences specific to this shRNA was purchased from IDT (USA), designed such that *BglII* (*BamHI*) and *HindIII* restriction enzyme target sites were incorporated into the oligo ends (Figure 3). A 10 mg/mℓ stock oligo was reconstituted in sterile, nuclease-free H_2O to a final working concentration of 3 mg/mℓ.

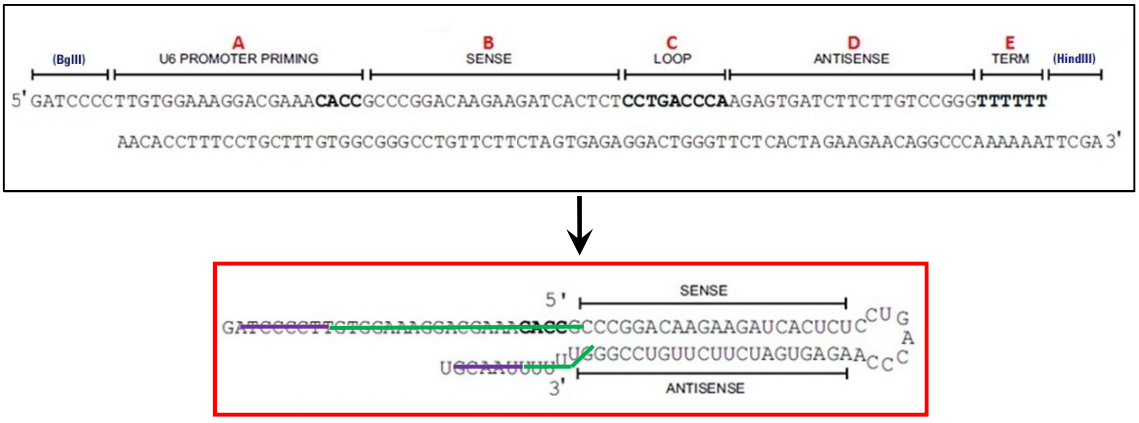

Figure 3: shRNA oligo sequences incorporating the restriction enzyme sites *BglII* and *HindIII* and the (A) U6 promoter, (B) sense coding sequence, (C) 9 bp loop sequence, (D) antisense coding sequence, and (E) the *PolIII* transcription terminator sequence. The final functional hairpin structure is shown below, outlined in red. Portions of the hairpin sequence struck out in purple show digested restriction enzyme sites, while those struck out in green indicate the U6 promoter (5' end) and termination sequence (3' end).

3.3.2.1. Annealing Oligonucleotides

An annealing reaction incorporating 1 µl 3mg/ml sense and antisense oligo and 48 µl annealing buffer (Appendix 7) was set up for the shRNA sequence. The reaction was subjected to incubation in a

BioRad MyCycler PCR ThermoCycler as follows: 90°C for 4 minutes, and then at 70°C for 10 minutes. The annealed oligonucleotide was step-cooled to 37°C for 15-20 minutes, and then to room temperature.

3.3.2.2. Ligation and transformation into competent cells

The annealed oligo insert was ligated into the linearized, purified pSuper.gfp/neo vector (OligoEngine, USA) at room temperature in an overnight reaction (Appendix 8). Prior to transformation, the ligated plasmid was treated with *BglII* (Appendix 9) to reduce the level of background in the transformation. This is because the *BglII* site on the 5' overhang of the oligo and plasmid is destroyed to form a *BamHI* site upon ligation. *BglII* treatment thus enables for a more efficient screening of positive clones.

DH5α competent cells (Invitrogen, USA) were transformed as per manufacturer's instructions (Appendix 3) using the ligated pshFoxc1.gfp/neo vector, and plated onto a Luria agar plate containing the selective antibiotic ampicillin (Sigma, USA) (Appendix 4). The prepared plate was incubated at 37°C overnight and stored at 4°C thereafter. Single putatively positive bacterial colonies were selected from the shRNA plate and inoculated into 5mℓ of Luria-Bertani broth containing 5μℓ of 100mg/μℓ ampicillin at room temperature. Inoculated cultures were grown as per section *3.3.1.5*.

3.3.2.3. MiniPrep Plasmid Purification & Restriction Enzyme Digest

Cells were harvested and the pSuper.gfp/neo vector DNA incorporating the shRNA sequences was purified as outlined in section *3.3.1.6*. The plasmid DNA was quantified using a NanoDrop ND-1000 Spectrometer and the ND-1000 V3.5.2 software package and the presence of the sh*Foxc1* sequences in the vector was verified by restriction enzyme double digest using the *EcoRI* and *HindIII* restriction enzymes (Fermentas) (Appendix 10). The digest products were subject to electrophoresis and visualized as per Section *3.3.1.6*.

3.3.3. Amplification of pFoxc1-eGFP Vector

To determine the effects of over-expression of *Foxc1*, an existing p*Foxc1*-eGFP clone containing the full length *Foxc1* sequence cloned into the peGFP-N1 plasmid vector (BD Biosciences Clontech, Canada) in frame with eGFP (enhanced green fluorescent protein) at the *BamHI* and *EcoRI* restriction enzyme sites (Appendix 11) was used to transform DH5α competent cells (Invitrogen, USA). Transformed cells were plated onto a prepared Luria agar plate (Sigma-Aldrich, USA) (Appendix 4) containing the antibiotic kanamycin (Gibco, USA) as a selective marker and incubated overnight and stored at 4°C thereafter. A single colony was selected from the plate and inoculated into 5ml of Luria-Bertani broth at room temperature containing 5μℓ of a 1:1000 working solution of kanamycin (Gibco, USA). Inoculated cultures were grown as per section *3.3.1.5*. Cells were harvested and the vector

DNA incorporating the *Foxc1* sequence was purified as per section *3.3.1.6*. The digested/amplified products were subject to electrophoresis and visualized as per Section *3.3.1*.6. Plasmid DNA was quantified using a NanoDrop ND-1000 Spectrometer and the ND-1000 V3.5.2 software package and the presence of the *Foxc1* sequence in the vector was verified by conventional *Foxc1* PCR (see section *3.7.2.2*) using 1:100 and 1:1000 dilutions of purified plasmid.

3.4. Cell Transfection

10cm tissue culture plates (Corning) holding cells at ~70-80% confluency were transiently transfected with 4µg of either the p*Foxc1*-eGFP; psh*Foxc1*-GEM-T Easy or psh*Foxc1*-eGFP vector DNA using the transfection reagent FuGene6 (Roche Diagnostics, Germany) as per the manufacturer's protocol. After 24 hours in a sterile, humidified incubator at 33°C with a constant feed of 5% CO_2, cells were harvested by trypsinization or with cell scrapers.

3.5. RNA isolation

Total RNA was extracted from wildtype and transfected cells using the QIAGEN RNeasy™ Plus Mini Kit (QIAGEN, Germany) as per the manufacturer's instructions. RNA was also isolated using TriReagent (Appendix 12). The concentration and purity of the product was determined using a NanoDrop ND-1000 Spectrophotometer and the ND-1000 V3.5.2 software package (Nanodrop Technologies). RNA quality was assessed on an RNA gel (Appendix 13). RNA samples were aliquoted and stored at -80°C until further use.

3.6. cDNA synthesis

Two separate methods were used to synthesise cDNA from isolated total RNA. Sample cDNA was either synthesized using SuperScript™ III (Invitrogen, USA) or the RNA to cDNA 2-Step MasterMix (Applied Biosystems, USA). RNA was defrosted on ice prior to synthesis and all incubation steps were carried out in a BioRad MyCycler™ PCR thermal cycler. A starting concentration of 2µg of total isolated RNA was used to synthesise cDNA for both the methods outlined below.

cDNA synthesised for the purpose of *N-cadherin* and *Msx1* PCR/qPCR was subject to DNAse treatment and synthesis using the RNA to cDNA 2-Step MasterMix (Applied Biosystems, USA). cDNA synthesised for the purpose of *Foxc1* qPCR was not subjected to DNAse treatment as an optimization measure, but was synthesised using SuperScript™ III (Invitrogen, USA).

Total RNA used in the synthesis of cDNA, and the resultant cDNA for use in PCR/qPCR analysis was always aliquotted in volumes sufficient for single usage, and never subject to continuous freeze-thaw cycles.

3.6.1. cDNA synthesis: DNAse treatment of RNA

RNA was DNase treated by the addition of one unit (1µℓ) of RNAse-free DNAse1 (Promega, USA) and 2µℓ of RNAse-free DNAse buffer (Promega, USA) per 2µg of RNA. The reaction was brought up to a volume of 10µℓ by the addition of nuclease-free water (Invitrogen, USA) and incubated for 5 minutes at 37°C to remove contaminating genomic DNA. Samples were immediately plunged into ice following this incubation and 2µℓ of Stop Buffer (Promega, USA) was added to each reaction to cease activity of the DNAse 1 enzyme. The reactions were transferred back to the thermal cycler for a 10 minute incubation at 65°C to inactivate the enzyme.

3.6.2. cDNA synthesis: SuperScript™ III method

3.6.2.1. Poly(A)-tail priming with Oligo-dT

Oligo-dT primers were annealed to the 3'-end of mRNA strands to define initiation sites for SuperScript™ III reverse transcriptase activity following DNAse treatment of the RNA samples (carried out depending on the target being amplified). 1µℓ 50µM Oligo-dT primer (Promega, USA) together with 2µℓ 2mM dNTP mastermix (Fermentas, Canada) was added to the RNA samples and incubated for 5 minutes at 65°C in the thermal cycler. Primed samples were immediately plunged into melting ice to super-cool the reaction and ensure rapid hybridization of Oligo-dT primers to the mRNA template.

3.6.2.2. First-strand cDNA synthesis

A mastermix incorporating 4µℓ 5X First-Strand Synthesis Buffer, 1µℓ 0.1M DTT, 1µℓ RNaseOUT Recombinant RNase Inhibitor and 1µℓ Superscript™ III reverse transcriptase (all Invitrogen) per reaction was made on ice. 7µℓ of this mastermix was added to each reaction vessel subsequent to the Oligo-dT hybridization. The reactions were then exposed to sequentially incubations of 50°C for 60 minutes, 55°C for 15 minutes and 70°C for 15 minutes in a pre-programmed thermal cycler.

A cDNA synthesis negative control "no-Reverse Transcriptase" (no-RT) sample was also prepared for each RNA sample by substituting nuclease-free water (Invitrogen, USA) for SuperScript™ III reverse transcriptase to ensure the absence of random amplicons and purity of the cDNA. This sample was evaluated alongside the treatment samples in all PCR and qPCR analyses.

Synthesised cDNA was briefly centrifuged, diluted in a 1:1 ratio with nuclease-free water (Invitrogen, USA), aliquoted and stored at -20°C.

3.6.3. cDNA synthesis: RNA to cDNA 2-Step MasterMix method

Following the DNAse treatment of the RNA samples, cDNA was synthesized using the RNA to cDNA 2-Step MasterMix (Applied Biosystems, USA) as per the manufacturer's protocol. 4µℓ of

nuclease-free water (Invitrogen, USA) and 4µℓ of RNA to cDNA 2-Step MasterMix (Applied Biosystems, USA) was added to the 12 µℓ DNAse-treated total RNA samples.

Negative control "no-Reverse Transcriptase" (no-RT) samples were prepared for each RNA sample in a similar manner as above. This was done by substituting nuclease-free water (Invitrogen, USA) for the RNA to cDNA 2-Step MasterMix (Applied Biosystems, USA) in these samples. No-RT samples were evaluated alongside the treatment samples in all PCR and qPCR analyses.

3.7. Polymerase Chain Reaction

3.7.1. Primers and primer design

Primer sets targeting amplicons within the N-cadherin (*N-cad*), Muscle-segment homeobox (*Msx1*), Forkhead box C1 (*Foxc1*), green fluorescent protein (eGFP) and Ribosomal protein S12 (*RpS12*) genes were used in gene expression analyses via conventional PCR and qPCR (Table 2). Primers amplifying *Msx1*, *Foxc1*, *eGFP* and *RpS12* sequences were sourced from literature, however, one set of primers amplifying the N-cadherin gene were designed using the primer design programme Primer3 (Rozen and Skaletsky, 2000) and the NCBI database (www.ncbi.nlm.nih.gov). Unfortunately, these primers, together with the literature-source *Msx1* primers ceased to amplify the target sequences during experimentation, and a new primer sets amplifying respective amplicons in the *N-cadherin* and *Msx1* genes had to be sourced.

Where possible, intron-exon boundary primers were used for qPCR in order to eliminate amplification of any unwanted transcript-contaminating genomic DNA. To ensure primer specificity, all primer sets were subjected to sequence alignment against the *Mus musculus* genome on the NCBI database using the Basic Local Alignment Search Tool (BLAST).

All primer sets were subject to optimization protocols, including annealing temperature gradient analysis, reagent variation and varied template concentrations. Primers amplifying GC-rich templates, such as the *Foxc1* domain, were subject to further optimization considerations including the addition of a range of PCR enhancers to increase specificity of primer binding. Primers sets were initially optimized, if possible, by means of conventional PCR subsequent to which they were applied in qPCR analysis.

All primers were reconstituted in nuclease-free water (Promega, USA) to a 100µM stock concentration, while a 10µM working dilution was utilized in both PCR and qPCR reactions. Both stock and working aliquots were stored at -20°C.

3.7.2. Conventional Polymerase Chain Reaction (PCR)

To determine the optimum annealing temperature and to verify specificity of each primer set, conventional PCR amplification was optimized in 20µℓ reactions incorporating the following reagents: 11 µℓ nuclease-free water (Promega, USA), 2 µℓ 10x NH_4/ KCl Buffer (Fermentas, Canada), 1.8 µℓ 25mM $MgCl_2$ (Fermentas, Canada), 2 µℓ 2mM dNTPs, 1 µℓ 10µM reverse primer, 1 µℓ 10µM forward primer, 0.2µℓ *Taq* polymerase (Fermentas, Canada), and 1 µℓ of cDNA template. A negative, no-template control sample incorporating nuclease-free water (Promega, USA) instead of cDNA was run alongside samples for each primer set in order to confirm the absence of contaminating amplicons.

Table 2: Primer sets amplifying target genes of interest.

Target gene	Forward/Left Primer	Reverse/Right Primer	Product Size	Ref. Sequence (NCBI)	Intron -Exon	Source	Manufacturer
Ribo S12 *(Rps12)*	5' GGAAGGCATAGCTGCTGGAGGT 3'	5' CGATGACATCCTTGGCCTGAG 3'	365 bp	NM_011295.5	Yes	Sommer et al., 2005	Inqaba Biotechnology
N-cadherin *(N-cad)* Set 1	5' TTAAAAGCTGCTTGGCTTGG 3'	5' AACATTTCCATCCTGCGTGT 3'	205 bp	NM_007664.4	Yes	Primer3 v. 0.4.0 Rozen & Skaletsky, 2000	Inqaba Biotechnology
N-cadherin *(N-cad)* Set 2	5' GGATGAAACGGCGGGATAAAGAG 3'	5' GCCTCTCGTCTAGCCGTCTGA 3'	204 bp	NM_007664.4	Yes	Vanselow et al., 2008,	Inqaba Biotechnology
Muscle-segment homeobox *(Msx1)* Set 1	5' GCGGAATTCTCCAGCTCGCTCAGCCTCACC 3'	5' GGCCTCTCTTTTCCTCTTGGCGGTCCTGCA 3'	177 bp	NM_0108352	Yes	Lazzarotto-Silva et al., 2005	Inqaba Biotechnology
Muscle-segment homeobox *(Msx1)* Set 2	a. 5' CCAGAAGATGCTCTGGTGAAG 3' b. 5' CCTCAAGCTGCCAGAAGATG 3'	5' TTGGTCTTGTGCTTGCGTAG 3'	a.137 bp b.147 bp	NM_0108352	Yes	Oka et al., 2005	Inqaba Biotechnology
Green Fluorescent Protein *(GFP)*	5' TGCTTCAGCCGCTACCCCGACCA 3'	5' CGCCGATGGGGGTGTTCTGCTG 3'	361 bp	U55762	No	Sommer et al., 2006	Inqaba Biotechnology
Forkhead box C1 *(Foxc1)*	5' TGGCTTTCCTGCTCATTCGTC 3'	5' TGCAGAAAACGCTGTAGGGG 3'	559 bp	NM_008592.2	No	Sommer et al., 2006	IDT

Prepared PCR reactions were amplified in triplicate under temperature gradient conditions in a BioRad MyCycler™ PCR thermal cycler. Each primer set was subject to optimisation protocols in order to ascertain the specific cycling conditions and primer annealing temperatures; primer specific conditions are outlined in the following sections. Primers targeting an amplicon in the ribosomal protein S12 (*RpS12*) gene were used as an internal reference (housekeeping) gene while primers amplifying a green fluorescent protein (eGFP) amplicon were used to assess successful transfection with the p*Foxc1*-eGFP and p*Foxc1*.neo/gfp plasmid vector. The amplified PCR products were separated out on a 1% (w/v) agarose (Roche, New Jersey, USA) gel, stained, destained and imaged as described in section *3.7.3*.

3.7.2.1. Conventional Polymerase Chain Reaction: N-cadherin

PCR reactions using primers targeting an *N-cadherin* amplicon were prepared as outlined above (*3.7.2*). Reactions were amplified in a BioRad MyCycler™ PCR thermal cycler with a temperature gradient incorporated: an initial 2 minute melting step at 95°C, followed by 39 cycles of 94°C for 15 seconds, 60 - 64°C for 1 minute, 72°C for 1 minute, and a final elongation period of 7 minutes at 72°C. The most optimal primer annealing temperature amplifying *N-cadherin* to show a 205 bp product was determined to be 64.0°C.

3.7.2.2. Conventional Polymerase Chain Reaction: Foxc1

PCR reactions were prepared as outlined in section *3.7.2* using primers to amplify a specific *Foxc1* amplicon. Reactions were amplified in a BioRad MyCycler™ PCR thermal cycler with an initial denaturation step of 94 °C for 2 minutes, followed by 40 cycles of 94 °C for 15 seconds, 60°C for 30 seconds, 72 °C for 1 minute and a single plate read step, followed by a 72°C extension step for 10 minutes. Amplified PCR products were separated out on a 1% (w/v) agarose (Roche, New Jersey, USA) gel, stained, destained and imaged as described in section *3.7.3* to show a 559 bp product.

3.7.2.3. Conventional Polymerase Chain Reaction: Msx1

PCR reactions using primers targeting an *Msx1* amplicon were prepared as outlined above. Reactions were amplified in a BioRad MyCycler™ PCR thermal cycler as per the protocol described by Lazzarotto-Silva et al. (2005), with a temperature gradient incorporated: 1 initial cycle of 94°C for 3 minutes, 80°C for 5 minutes, followed by 39 cycles of 94°C for 1 minute, 58-63°C for 1 minute and 72°C for 1 minute and a final cycle of 72°C for 10 minutes. The most optimal primer annealing temperature amplifying *Msx1* to show a 177 bp product was determined to be 60.4°C.

3.7.3. Agarose gel electrophoresis

3µl of a range-appropriate loading dye (Fermentas, Canada) was added to the amplified PCR products prior to loading. 11µl of each sample was resolved alongside a 100 bp GeneRuler molecular weight marker (Fermentas, Canada) on a 1% (w/v) agarose (Roche, New Jersey, USA) gel by electrophoresis in 1x Tris/Borate/EDTA (TBE) (Appendix 1) for 90 minute at 80V. The resultant bands were visualized by staining with a 0.005% ethidium bromide in 1x TBE solution for 10 minutes followed by destaining in 1x TBE buffer for 5 minutes (Appendix 1). Images captured using the ChemiDoc XRS Imaging System (BioRad, USA) and the Image Lab imaging software (V2.0.1) (BioRad, USA) were analysed to select the most optimal primer annealing temperatures.

3.8. Quantitative Real Time Polymerase Chain Reaction (qPCR)

3.8.1. Overview

Quantitative real time PCR (qPCR) was carried out in order to assess and quantify variability in gene expression between different cell lines and transfection treatments. Primer specificity toward GOI (gene of interest) amplification was confirmed by melt curve analysis after the qPCR amplification cycle. Verification of product-specific melting temperatures (Tm) was carried out by subjecting qPCR products to agarose gel electrophoresis. Data obtained for each run was monitored and assessed using the CFX manager software package (Bio-Rad, USA) installed on a dedicated qPCR desktop computer running the Windows XP operating system.

The threshold cycle (C_T) / quantification cycle (C_q) – the cycle number at which the amount of amplified target reaches a fixed threshold - was used in evaluating data by means of the $2^{-\Delta\Delta C_T}$ method (Livak & Schmittgen, 2001). The relative fold change in gene expression i.e. the change in expression of a target gene in samples normalized against an internal reference gene was compared to a designated control treatment with a consistent basal fold change of 1. The ribosomal sub-unit *Rps12* was used as the internal point of reference. Data were log transformed and gene expression in the form of relative fold change was represented graphically with values indicating standard error of the mean (SEM).

Optimized qPCR (as outlined in the subsequent sections) was carried out on cDNA synthesised from RNA extracted from untreated E12.5 and E13.5 POM cells or cells subjected to transfection with either the psh*Foxc1* or p*Foxc1*-eGFP plasmid vector.

Optimization ensured equal amplification efficiencies for both the *Rps12* reference and experiment genes, thereby allowing for data to be analyzed using the $2^{-\Delta\Delta C_T}$ method as described by Livak and

Schmittgen (2001). Fold changes between wildtype, transfected and treated cells were calculated for each cell type using this method and statistical analyses were carried out on these data.

3.8.2. qPCR: Experimental Design

qPCR experimental design and all subsequent procedures were subject to conformation to the requirements set out in the Minimum Information for Publication of Quantitative Real-Time PCR Experiments (MIQE) guidelines (Bustin *et al*., 2009). The MIQE guidelines ensure that qPCR data is obtained, evaluated and interpreted accurately in a standardized manner. Individual gene analysis experiments were carried out using three biological repeats, with three technical repeats being carried out for each biologically variable sample set. All technical repeats were run in triplicate, with each treatment in a single qPCR experiment having triplicate reactions such that $n = 3$. As per conventional PCR analyses, qPCR experimental runs included no-template (NTCs) and no-Reverse Transcriptase (NRT) controls to verify that results were a true reflection of the experimental treatments on mRNA expression and not influenced by contaminating amplicons. Detected fluorescence in all qPCR experiments was read from a baseline of 0.2 relative fluorescence units (RFU), established by the single threshold setting on the CFX manager analysis software (BioRad, USA).

3.8.3. qPCR: Statistical analyses

Mean fold changes for triplicate experimental runs were subjected to statistical analyses in the form of either a one sample t-test or a single factor Analysis of Variance (ANOVA) in order to compare the statistical significance of any differences between the means using the PASW Statistics 18 statistical analysis program.

3.8.4. Validation the use of the $2^{-\Delta\Delta C_T}$ method in analysis of gene expression

In order for the $2^{-\Delta\Delta C_T}$ method (Livak & Schmittgen, 2001) to be applied in qPCR data analysis, the reaction amplification efficiency of the primers amplifying the target gene of interest must be comparatively close to the amplification efficiency of the primers targeting the selected reference gene used to normalize data against. A serial dilution of the synthesised cDNA was used to assess the qPCR reaction efficiencies of both the *RpS12* reference gene and the target genes (Livak and Schmittegen, 2001).

cDNA synthesised as per section *3.6* was serially diluted to obtain 5-fold template dilutions. These dilutions were subject to qPCR using both the reference and target gene primers. The average C_q (previously C_T) values for each gene was then used to generate ΔC_T value for each dilution. Average ΔC_T values were then plotted against the numeric values of the serial dilutions as data points with the ± SEM. A linear regression was generated passing through the data set, and the absolute value of the

slope (*m*) was evaluated. An *m*-value close to zero was regarded as being the standard required in order for the $2^{-\Delta\Delta C_T}$ method of qPCR data analysis to be applied in assessing data generated during qPCR analysis (Livak and Schmittgen, 2001).

3.8.5. qPCR: General Protocol

qPCR was performed using one of two commercially available mastermixes. SYBR-Green JumpStart® Taq ReadyMix (Sigma-Aldrich®-Aldrich, USA) was used to quantify *Msx1* expression, while FIREPol® EvaGreen® qPCR Mix Plus (no ROX) (Solis BioDyne®, Estonia) was used in reactions assessing *N-cadherin* and *Foxc1* gene expression. Each 25µℓ reaction for *Msx1* incorporated the following reagents: 10.5µl nuclease-free water (Promega, USA), 12.5 µℓ SYBR-Green JumpStart® Taq ReadyMix (Sigma-Aldrich®-Aldrich, USA), 0.5 µℓ 10 µM reverse primer, 0.5 µℓ 10 µM forward primer and 1 µℓ of cDNA template. For *N-cadherin* and *Foxc1* gene amplification, 25µℓ reactions for were set up as follows: 17.5µl nuclease-free water (Promega, USA), 5 µℓ 5x HOT FIREPol® EvaGreen® qPCR Mix Plus (no ROX) (Solis BioDyne®, Estonia), 0.5 µℓ 10 µM reverse primer, 0.5 µℓ 10 µM forward primer and 1.5 µℓ of cDNA template. In order to optimize amplification and determine the most effective annealing temperature, prepared qPCR reactions were amplified in triplicate (with three biological and three technical repeats) under temperature gradient conditions in a Mini Opticon MJ MINI™ Personal Thermal Cycler (Bio-Rad, USA).

3.8.5.1. qPCR: N-cadherin Amplification Protocol

N-cadherin was initially successfully amplified when reactions using SYBR-Green JumpStart® Taq ReadyMix (Sigma-Aldrich®-Aldrich, USA) and primers spanning intro-exon boundaries (designed using Primer3) were exposed to the following cycling conditions: an initial 2 minute melting step at 95°C, followed by 39 cycles of 94°C for 15 seconds, 64°C for 1 minute, 72°C for 1 minute, and an elongation period of 30 seconds at 72°C. A melt-curve analysis to ensure product specificity was carried out on each run as follows: DNA was heated from 50°C to 95°C with a temperature transition rate of 0.5°C every 5 seconds, and a plate read at every 1 °C temperature increment.

However, these primers ceased to amplify the target sequence, and gene analyses had to be carried out using *N-cadherin* primers sourced from literature (Vanselow et *al*., 2008). These primers successfully amplified the target sequence when 5x HOT FIREPol® EvaGreen® qPCR Mix Plus (no ROX) (Solis BioDyne®, Estonia) mastermix was used under the following cycling conditions: an initial 15 minute melting step at 95°C, followed by 39 cycles of 94°C for 15 seconds, 60°C for 1 minute, 72°C for 1 minute, and an elongation period of 30 seconds at 72°C. A melt-curve analysis to ensure product specificity was carried out on each run as follows: DNA was heated from 50°C to 95°C with a

temperature transition rate of 0.5°C every 5 seconds, and a plate read at every 1 °C temperature increment (Appendix 14).

3.8.5.2. qPCR: Msx1 Amplification Protocol

Msx1 was amplified successfully when the conventional PCR protocol described by Lazzarotto-Silva et al. (2005) was modified for use on the Mini Opticon MJ MINI™ Personal Thermal Cycler (Bio-Rad, USA) for qPCR. Product was amplified by an initial cycle of 94°C for 3 minutes, 80°C for 5 minutes, followed by 39 cycles of 94°C for 1 minute, 59°C - 64°C for 1 minute and 72°C for 1 minute and a final cycle of 72°C for 10 minutes. A melt curve analysis was run as per section *3.8.5.1* above.

3.8.5.3. qPCR: Foxc1 Amplification Protocol

Foxc1 qPCR was successfully carried out after optimization trials involving the use of non-DNAse treated cDNA, the synthesis of cDNA by two methods, trials involving several different commercial qPCR mastermixes, as well as the incorporation of a range of substances in the PCR reaction to prevent the GC-rich primers from forming secondary structures and to assist the primers to anneal to the template. The protocol used in the amplification of the target sequence included an initial denaturation step of 95 °C for 15 minutes, followed by 40 cycles of 94 °C for 15 seconds, 60°C for 30 seconds, 72 °C for 1 minute and a single plate read step, followed by a 72°C extension step for 10 minutes. Melt-curve analysis was again carried out as per section *3.8.5.1* above. Curves resulting from qPCR amplification are shown in Appendix 15.

3.8.6. Agarose gel electrophoresis

If necessary, agarose gel electrophoresis of qPCR products was carried out as described in section *3.7.3* above.

3.9. Western Blot Protein Analysis

3.9.1. Protein isolation and sample preparation

Confluent 10cm tissue culture plates (Corning) of wildtype or plasmid-transfected cells were harvested with cell scrapers and transferred to centrifuge tubes (Corning) under sterile tissue culture conditions as previously described in section *3.2*. Cells were pelleted by centrifugation at 4000 x g for 15 minutes at room temperature in an Eppendorf 5810R centrifuge and the supernatant growth medium was completely removed. Total protein was extracted from the cell pellet by cell lysis via resuspension in an appropriate amount of RIPA (RadioImmunoPrecipitation Assay) buffer with protease inhibitors (aprotinin, leupeptin, chymostatin, pepstatin at concentrations of 2mg/ml and 100mM PMSF - all from Sigma, USA) for 5 minutes at room temperature, followed by a 30 minute incubation on ice. Samples were centrifuged at 4000 x g for 15 minutes in an Eppendorf 5810R centrifuge to concentrate nuclei and cellular debris. The supernatant was collected, divided into aliquots and protein concentration of a diluted (1:10) sample was determined using the BCA™ Protein

Assay (Pierce, Rockford, IL, USA) as per the manufacturer's instructions (Appendix 27). Extracted protein was prepared for Western blot analysis by addition of a 2 x Western blot loading dye (Appendix 16) to the protein samples in a ratio of 1:1 followed by incubation at 95°C for 3 minutes to allow for the quaternary structure of the protein to be destabilised. Protein was immediately stored at -80°C until needed.

3.9.2. Western Blot Analysis

Endogenous Foxc1 and N-cadherin were detected in protein isolated from wildtype and transfected E12.5 *Foxc1*$^{+/+}$ and E13.5 *Foxc1*$^{+/+}$ POM cells. Cells were transfected with either the p*Foxc1*-eGFP or psh*Foxc1*-eGFP plasmid vectors as described in section *3.4.* Total protein, isolated and prepared as per section *3.9,* was resolved via SDS-PAGE (sodium dodecyl sulfate polyacrylamide gel electrophoresis) on 10-15% denaturing SDS-polyacrylamide stacking/ resolving gel (Appendix 17). Experiments were carried out using three biological repeats, with three technical repeats being carried out for each biologically variable sample set. All technical repeats were run in duplicate, with each treatment in a single experiment having duplicate reactions. Gels were cast using a Mini-PROTEAN™ 3 Cell kit (BioRad, USA). 45 µg (for N-cadherin blots) or 90 µg (for Foxc1 blots) of each prepared sample was loaded onto gels alongside PageRuler™ Prestained Protein Ladder (Fermentas, Canada) and run with cooling for 30 minutes at 90V, followed by 1 hour at 120V in 1x electrode (running) buffer (Appendix 18). Subsequent to this, gels were transferred to and handled in freshly prepared, cold protein transfer buffer (Appendix 19). The resolved protein was transferred to a Hybond ECL nitrocellulose membrane (presoaked for 5-10 minutes in cold protein transfer buffer to equilibrate) over two days at 10V in a cold room at 15°C (Figure 4).

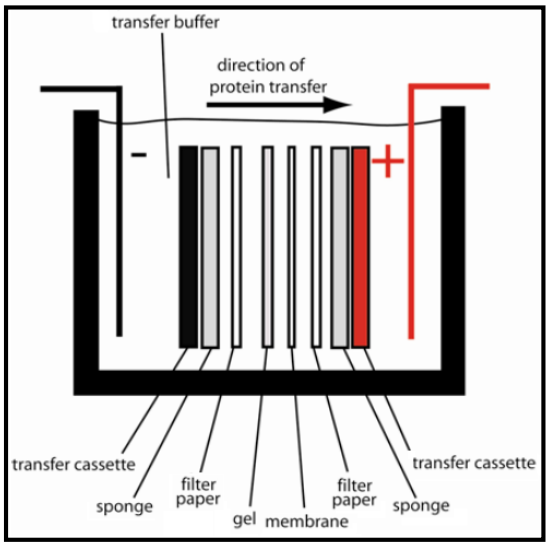

Figure 4: The layout of the protein transfer blotting "sandwich" and mechanism of protein transfer from resolving gel to nitrocellulose membrane. Proteins move from the negative electrode towards the positive electrode and get restrained by the nitrocellulose membrane. Image adapted from *MitoSciences, 2007.*

Nitrocellulose membranes holding transferred proteins were blocked in a 6% skim milk blocking buffer (Appendix 21) for 4 hours at room temperature on an orbital shaker, followed by two 10 second washes in TBS-T wash buffer (Appendix 20) to remove all traces of blocking buffer.

Immunoblot detection of Foxc1 proteins was performed using goat polyclonal anti-Foxc1 primary antibody (Abcam - diluted 1:500 in TBS-T) while N-cadherin protein was detected using mouse polyclonal anti-N-cadherin primary antibody (BD Biosciences, USA - diluted 1:10000 in 6% skim milk blocking buffer) (Appendix 21) with an overnight incubation at 4°C. This was followed by five 10 minute washes in TBS-T wash buffer (Appendix 20) to remove unbound primary antibody the next morning. Membranes were then probed with horseradish peroxidase (HRP)-conjugated secondary antibody (either rabbit anti-goat IgG - Santa Cruz Biotechnology, USA - diluted 1:10 000 in TBS-T OR goat anti-mouse IgG – BD Biosciences, USA – diluted 1:1000 in TBS-T) for 1 hour at room temperature. This was followed by six 10 minute washes in TBS-T wash buffer (Appendix 20) to remove excess secondary antibody. GAPDH was detected as a loading control protein alongside Foxc1 and N-cadherin using rabbit monoclonal anti-GAPDH primary antibody (Cell Signalling, USA - diluted 1:3000 in TBS-T) and a goat anti-rabbit IgG secondary antibody (Cell Signalling – diluted 1:4000 in TBS-T) with treatment as per Foxc1/N-cadherin blots. Finally, immunoreactions were revealed by exposing blots to a 1:1 dilution of the Immun-Star HRP Chemiluminescent Kit (BioRad, USA) followed by imaging using the ChemiDoc XRS Imaging System (BioRad, USA) and the Image Lab imaging software (V2.0.1) (BioRad, USA). Fluorescence intensity of target and reference proteins were assessed in triplicate experimental runs and these values were used to carry out densitometry analysis. Mean densitometry values were further subjected to statistical analyses in the form of a one sample t-test in order to compare the statistical significance of any differences between the means using the PASW Statistics 18 statistical analysis program.

3.10. Microscopy

3.10.1. Sample preparation

3.10.1.1. Monolayer Culture

Cultured wildtype E12.5 and E13.5 POM cells were subjected to standard tissue culture protocols as described in section *3.2*. Confluent cells in 10cm tissue culture dishes (Corning) were trypsinized, microcentrifuged and resuspended in 1mℓ of culture medium. 30µℓ of the cell suspensions were seeded onto 12 mm coverslips (sterilized by immersion in absolute ethanol (Merck, USA)) in clearly labelled 24-well tissue culture plates (Corning), and returned to the tissue culture incubator overnight. Cells were transfected as required the next day, and returned to the culture incubator for a further 24 hours.

3.10.1.2. Fixation and Mounting of Monolayer Cultured Cells

The coverslips with confluent cells were washed in 1 x PBS (Appendix 22) and then fixed for 10 minutes in 4% paraformaldehyde (Merck, USA) (Appendix 23) in serum-free DMEM (Gibco, USA) with 0.15% Triton X-100 (Sigma-Aldrich, USA) at 4°C to allow for permeabilisation. Cells were washed three times (5 minutes per wash) in 1 x PBS (Appendix 22) and blocked in 0.5% BSA in 1 x PBS (Appendix 24) for 1 hour at room temperature. Polyclonal rabbit-anti N-cadherin primary antibody (Santa Cruz Biotechnology, USA) was diluted 1:300 in 0.5% BSA in 1 x PBS (Appendix 24) and incubated overnight at 4°C. Cells were washed with cold 1 x PBS (Appendix 22) the next day (three times, 5 minutes per wash) and incubated with donkey anti-rabbit-Cy3 secondary antibody (Jackson Immunolabs, USA) diluted 1:1000 in 0.5% BSA in 1 x PBS (Appendix 24) for 1 hour at room temperature. Negative control samples were prepared for each experiment – these cells were subject to exposure with 0.5% BSA in 1 x PBS (Appendix 24) without the primary antibody in the case of No-primary antibody controls, or without the secondary antibody with regards to the No-secondary antibody controls (Appendix 28). Cells were washed three times (5 minutes per wash) in 1 x PBS (Appendix 22) and incubated with a 1:50 dilution of DAPI (50 µg/ml) (Appendix 25) in 1 x PBS (Appendix 22) for 5 minutes at room temperature. Coverslips were finally washed once for 5 minutes in 1 x PBS (Appendix 22), lifted off the tissue culture plate, drained of excess PBS and mounted on a single drop of Mowiol with DABCO (both Sigma, USA) (Appendix 26) on a glass slide. Mounted coverslips were sealed in place with nailpolish once the Mowiol had dried.

3.10.1.3. Hanging Drop Culture

Confluent 10 cm plates of wildtype E12.5 POM cells and wildtype E13.5 POM cells were trypsinised, pelleted and then resuspended in 1 ml of culture medium. For each hanging drop, 30 µl of the resuspended cells was pipetted onto the lid of a 35 mm culture dish, which was then placed on the dish itself and returned to culture for 48 – 72 h at 33°C (Figure 5).

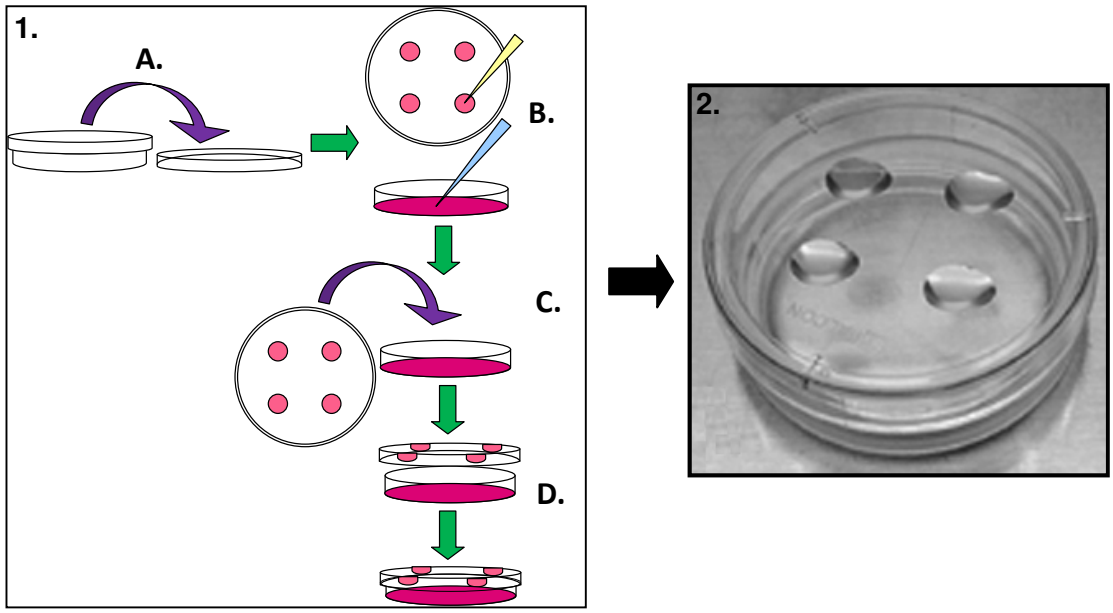

Figure 5: 1. Hanging drop culture technique – A. Invert the top of culture dish B. Pipette cell suspension in individual droplets onto inside of culture dish lid and add culture medium to the dish itself (in order to maintain humidity) C. Carefully invert culture dish lid D. Position lid over culture dish and close without dislodging or disturbing the individual droplets. Return dish to incubator and allow drops to culture. 2. Photo of prepared culture vessel housing hanging drops adapted from *Oshima et al. (2005)*.

3.10.1.4. Fixation and Mounting of Hanging Drop Cultured Cells

Cell aggregates were processed for immuoncytochemistry as described for cells in monolayer culture. Modifications to the protocol for hanging drops were as follows: cells were washed three times in 1 x PBS (Appendix 22) and then left in 0.5% BSA in 1 x PBS for (Appendix 24) 2 hours at 4°C; cell masses were also exposed to more extensive washes after incubation with the N-cadherin primary antibody. The secondary antibody (donkey anti-rabbit-Cy3) was diluted 1:1000 in 0.1% BSA in 1 x PBS and incubated for 1 hour at room temperature. Negative control samples were prepared for each experiment – these cell aggregates were subject to incubation with 0.5% BSA in 1 x PBS (Appendix 24) without the primary antibody in the case of No-primary antibody controls, or without the secondary antibody with regards to the No-secondary antibody controls. Following this, the cell aggregates were washed twice for 5 minutes in 0.5% BSA in 1 x PBS (Appendix 24) and a third wash was carried out for a further hour at room temperature. The aggregates were washed three times (for 5 minutes per wash) in 1 x PBS (Appendix 22) and incubated with a 1:50 dilution of DAPI (50 µg/ml) (Appendix 25) in 1 x PBS (Appendix 22) for 5 minutes at room temperature. Cell aggregates were finally washed once for 5 minutes in 1 x PBS (Appendix 22) before being mounted on a single drop of Mowiol with DABCO (Sigma, USA) (Appendix 26) on a glass slide. Mounted coverslips were sealed in place with nailpolish once the Mowiol had dried.

3.10.2. Image capture

3.10.2.1. Fluorescence Microscopy

Optimization of basic microscopy techniques and antibody concentrations/ applications was carried out at the Electron Microscopy Unit at the University of KwaZulu-Natal (Westville Campus) under the guidance of Dr. James Wesley-Smith. Images were captured from slides prepared as per the protocol laid out above (section *3.10.1.1. - 3.10.1.2*) using a Nikon Eclipse E400 fluorescent compound microscope and the NIS Elements imaging software.

3.10.2.2. Confocal Microscopy

Confocal microscopy imaging was used to assess N-cadherin expression and localization in homozygous wildtype, *Foxc1* knock-down or over-expressed E12.5 and E13.5 POM cells, both in monolayer and hanging drop monoculture and co-culture. Images were captured using the Zeiss LSM 710 laser scanning confocal microscope (Carl Zeiss Meditec GmbH, Oberkochen, Germany) and the ZEN 2009 imaging software at the Center for Electron Microscopy at the University of KwaZulu-Natal (Pietermaritzburg Campus) under the initial guidance of Shirley Mackellar.

Initial fluorescence was detected using traditional epifluorescence emission filters - nuclear staining was viewed using the DAPI filter, while N-cadherin staining was viewed using the

FITC filter and GFP fluorescence was detected under the TRITC filter. A variable spectral detection system was used to detect fluorescence induced by laser excitation. The Argon laser excited the Cy3 antibody (514 nm) used to detect N-cadherin while GFP was detected at 488 nm. A UV diode (405nm) excited the DAPI nuclear stain. The master gain and digital offset settings were initially adjusted using the prepared control slides and these settings were then used to capture images from treatment slides to maintain consistency for comparative analysis. Images were captured in multi-channel mode using a set pinhole aperture of 1 AU and a consistent scanning speed of 4 frames per second. Single optical sections were captured using the EC "Plan-Neofluar" 20x/0.5 multi-immersion DIC M27 and 63x/1.4 oil immersion DIC M27 objectives.

3.10.3. Image Analysis

In order to assess differences in protein expression on confocal images, ImageJ (http://imagej.nih.gov/ij) was used. Total fluorescence intensity of target proteins in single cells was assessed in triplicate experimental runs. Differences in N-cadherin localization were quantified by evaluating the mean grey area occupied by fluorescence in the red-channel at the cell membrane and within the cytoplasm.

Mean grey area analysis along the cell boundary and within the cytoplasm was carried out by randomised measurement of fluorescence in these regions of interest by evaluating a preset volume and maintaining the parameters across sample images and treatments for consistency. 25 measurements were made per image, and 3 images per triplicate biological repeat were assessed for each treatment. Values were subjected to statistical analyses using the PASW Statistics 18 statistical analysis program to determine statistical significance.

CHAPTER 4: RESULTS

A. Verification of methodology & optimization of techniques

4.1. Cell morphology

In order to evaluate morphological differences between cell lines, confluent live cell monolayers were imaged under cell culture conditions. Images showed that the wildtype cells derived from both E12.5 and E13.5 embryos showed no major visibly apparent differences in their morphology with the vast majority of cells having a uniform spindle shaped appearance (Figure 1 A & B).

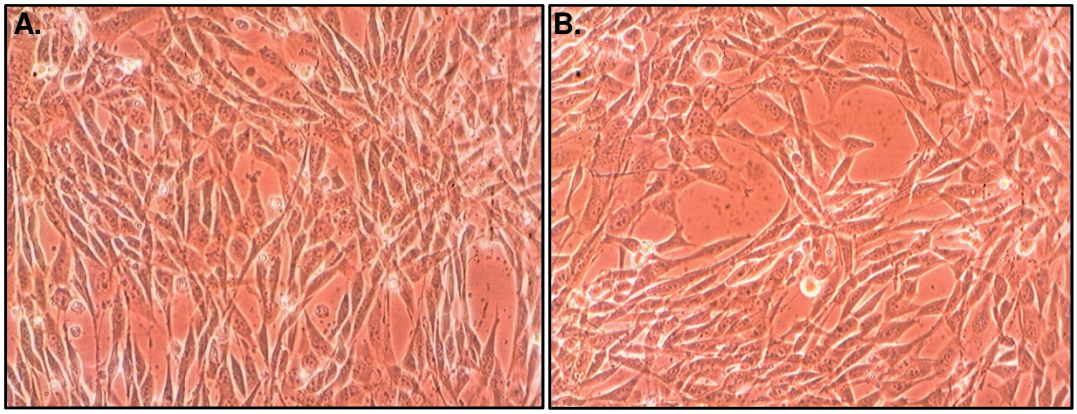

Figure 1: POM cell images captured at passage 8 *(P8)*. A. POM cells from E12.5 wildtype embryo (100x) B. POM cells from E13.5 wildtype embryo (100x).

4.2. p*Foxc1*-eGFP and psh*Foxc1*.neo/gfp Plasmids

4.2.1. Overview

To evaluate the effect of *Foxc1* expression on *N-cadherin* and *Msx1* expression, plasmid expression vectors were designed and developed to either over-express or silence the *Foxc1* gene. Transfected cells either over-expressed Foxc1 protein or had their *Foxc1* gene expression ablated to some substantial degree, if not fully.

4.2.2. Confirmation of transformation and culture of pFoxc1-eGFP plasmid vector

In order to assess the effect of *Foxc1* over-expression on *N-cadherin* and *Msx1* expression in POM cells, the plasmid vector p*Foxc1*-eGFP (full-length *Foxc1* sub-cloned into the plasmid vector pEGFP-N1 in frame with eGFP) was transformed into DH5α competent cells, cultured and purified. The presence of the *Foxc1* gene insert in the plasmid vector was confirmed by conventional PCR amplifying a 559bp amplicon specific to the *Foxc1* gene sequence. All six "positive" clones randomly selected from agar plates with transformed cells showed the robust presence of the *Foxc1* amplicon subsequent to conventional PCR of both 1:100 and 1:1000 dilutions of the purified plasmid (Figure 2). This plasmid was then used to transfect POM cells derived from wildtype E12.5 and E13.5 embryos.

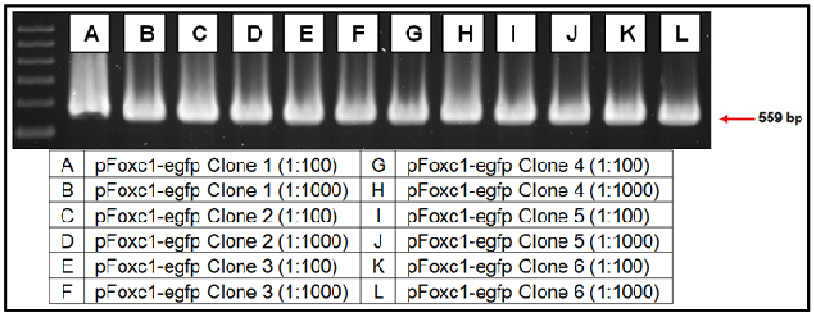

Figure 2: Conventional PCR amplifying *Foxc1* (559bp) from 6 plasmid clones, confirming presence of *Foxc1* gene insert in vector pEGFP-N1.

4.2.3. Confirmation of successful pFoxc1-eGFP plasmid transfection

Following the successful transformation and purification of p*Foxc1*-eGFP plasmid vector, cells seeded onto glass coverslips were transfected with the plasmid in order to assess transfection efficiency. Transfected cell monolayers were processed and imaged for confocal microscopy. Figure 3A shows the successful transfection of POM cells derived from E13.5 wildtype embryos with p*Foxc1*-eGFP. Strong eGFP expression is seen in every cell. Expression is localized perinuclearly in the majority of cells, with faint eGFP fluorescence detected within the cytoplasm. Although *Foxc1* is a transcription factor active in the nucleus, very little *Foxc1* is required to be present in the nucleus for it to effectively transactivate target genes, explaining the deficit of GFP signal in the nuclear region. RNA was extracted from transfected cells and cDNA was synthesized and subject to amplification by qPCR using primers specific to eGFP. Figure 3B shows an agarose gel electrophoresis image of the qPCR product. A band at 361bp indicates the successful amplification of the eGFP target amplicon confirming successful transfection.

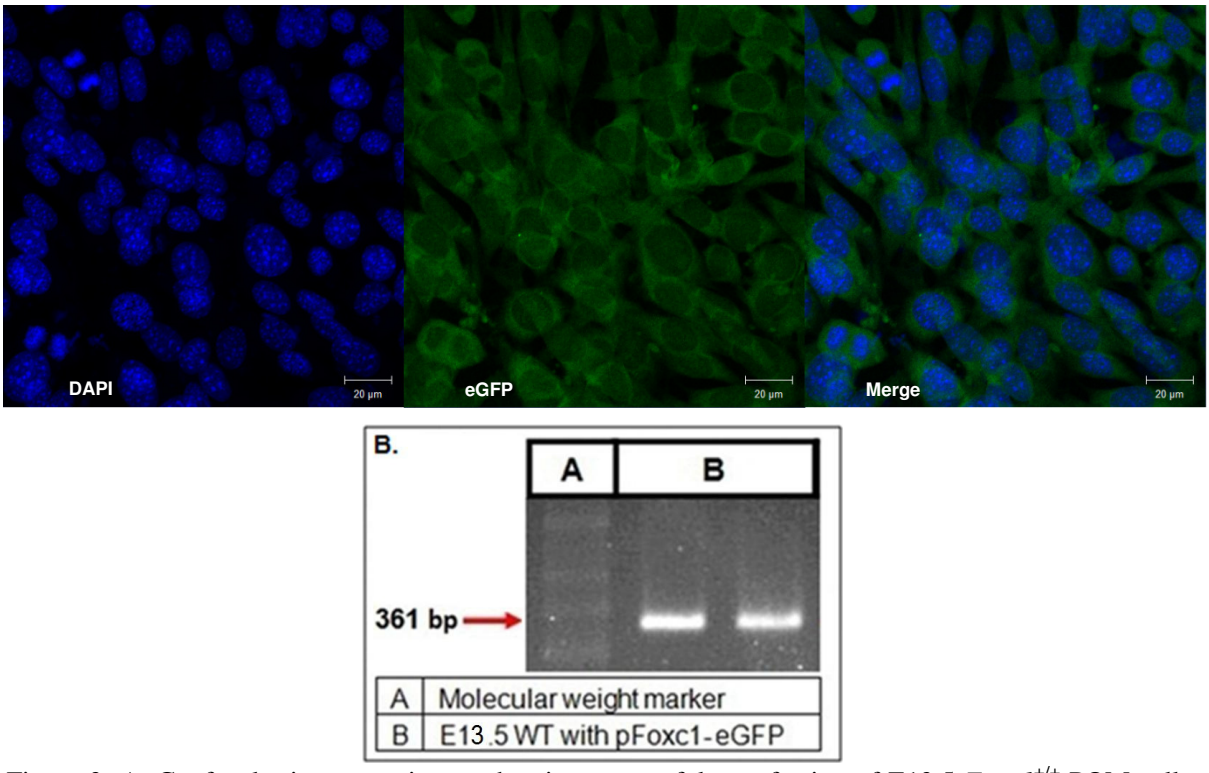

Figure 3: A. Confocal microscopy image showing successful transfection of E13.5 *Foxc1*$^{+/+}$ POM cells with the p*Foxc1*-eGFP plasmid vector. Scale bar = 20µm. B. Gel electrophoresis image of qPCR product upon successful amplification of the eGFP target amplicon of 361bp.

4.2.4. Confirmation of successful development of shRNA Plasmid Vectors

Four (sh*Foxc1*-1 to sh*Foxc1*-4) of five sequences targeting portions of the *Foxc1* sequence were successfully amplified by conventional PCR. These PCR products were cloned into the pGEM-T Easy plasmid vector. Successful incorporation of the hairpin sequence into the plasmid vector was confirmed by *EcoR1* restriction enzyme digest. Figure 4 shows the gel electrophoresis image obtained following *EcoR1* restriction enzyme digest of the four plasmid clones where lanes C, E, G and I show both purified plasmid vector and shRNA sequences (330bp) against *Foxc1* successfully cut by the *EcoR1* restriction enzyme compared to uncut vector in lanes B, D, F and H. These lanes verify the successful incorporation of the selected short hairpin sequences directed against the *Foxc1* gene into pGEM-T Easy. Following this, plasmids confirmed as containing the hairpin were sequenced (Inqaba Biotech, Pretoria) to verify that the sequence incorporated into the plasmid was 100% complementary to the target gene (Appendix 6).

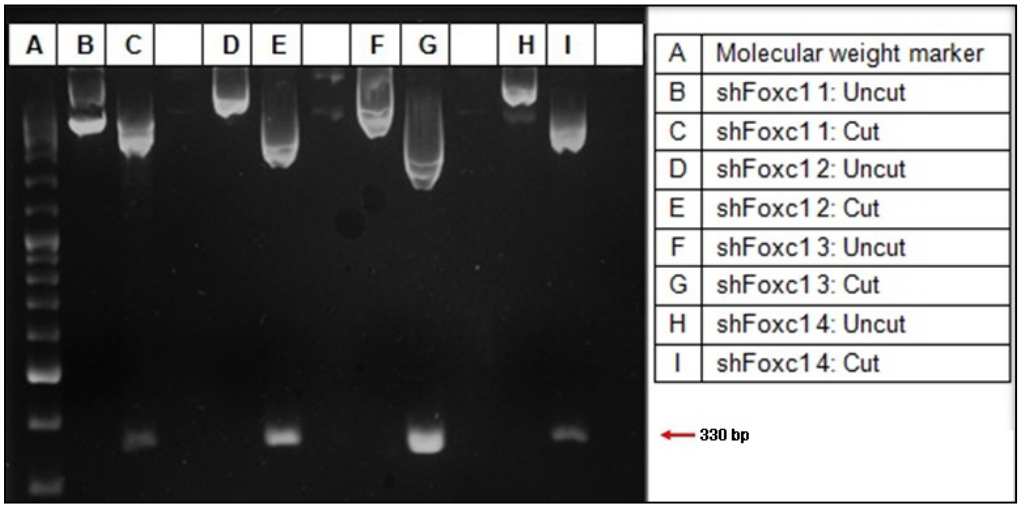

Figure 4: Agarose gel electrophoresis image of *EcoR1* restriction enzyme digest confirming incorporation of shRNA sequences into the pGEM-T Easy plasmid vector.

4.2.5. Functional efficacy of shFoxc1 plasmid vectors

In order to determine the successful activity of the shRNA sequences directed against the *Foxc1* gene, E13.5 POM cells were transfected with the constructs as described in section *3.4*. After 24h, RNA was extracted from the cells, converted to cDNA and subject to qPCR using primers for *Foxc1* and the reference gene, *Rps12*. Figure 5 shows the fold change in *Foxc1* expression relative to the reference gene after transfection with the shRNA constructs.

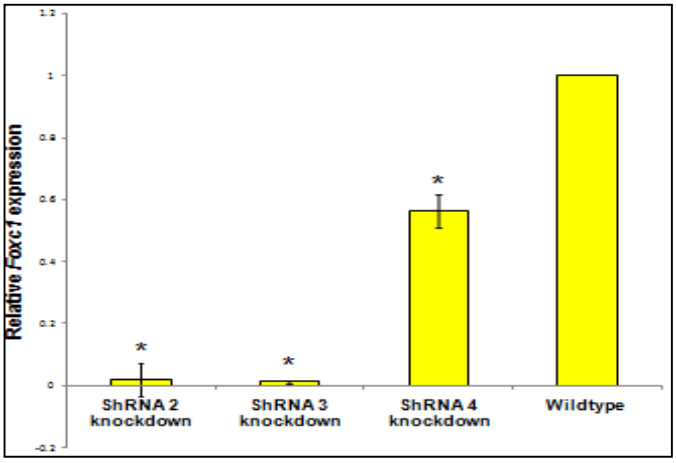

Figure 5: *Foxc1* expression (relative to the internal control, *Rps12*) in E13.5 wildtype POM cells after transfection with shRNA plasmid vector targeting *Foxc1* expression (n=3; $p < 0.05$).

These results indicate that three tested shRNA plasmid vectors successfully and significantly ($p < 0.05$) silenced *Foxc1* gene expression. The plasmid vector incorporating the sh*Foxc1*-3 sequence directed against *Foxc1* was shown to be the most effective at silencing *Foxc1* gene expression relative to the two other shRNA plasmid vectors, ablating *Foxc1* gene expression in these cells by almost 98%. For easy reference, this clone was renamed pshRNA-*Foxc1*, and was used in a number of assays. In order to create stable cell lines in the future, the sequence was cloned into a mammalian expression vector.

4.2.6. Cloning the shRNA sequence into a mammalian expression vector

Due to its efficacy at knocking down the expression of *Foxc1* (as discussed above), the third shRNA sequence was cloned into a mammalian expression vector, pSuper.gfp/neo. Due to the lack of complementary restriction enzyme sites we were unable to sub-clone the shRNA sequence directly from pGEMT-Easy or via an intermediary vector. We therefore purchased oligo sequences (as given in the Materials & Methods, section 3.3.2) with BglII and HindIII restriction sites incorporated into the oligo ends. This sequence was cloned into pSuper.gfp/neo (OligoEngine, USA) as per manufacturer's instructions. Figure 6 shows the gel electrophoresis image obtained when the purified plasmid DNA of three clones was subjected to *EcoR1* and *Hind111* restriction enzyme double digest. The gel image confirms the successful incorporation of the 281bp shRNA sequence into the pSuper.gfp/neo plasmid vector.

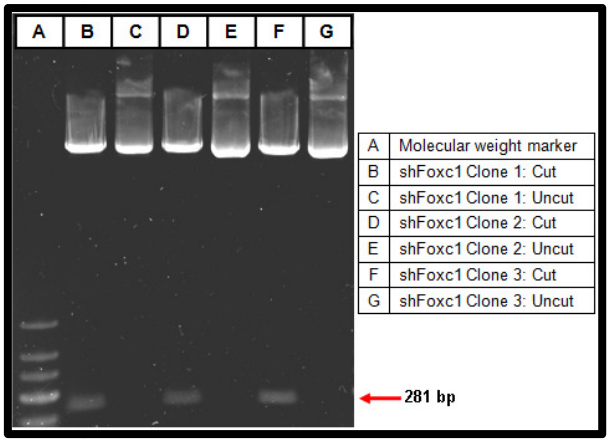

Figure 6: Successful ligation of shRNA sequence into pSuper.gfp/neo mammalian vector.

4.2.7. Confirmation of successful pshFoxc1.gfp/neo *plasmid transfection*

Following the successful transformation and purification of *pshFoxc1*.gfp/neo plasmid vector clones, cells seeded onto glass coverslips were transfected with the plasmid in order to assess transfection efficiency. Transfected cell monolayers were processed and imaged for confocal microscopy. Figure 7A shows the successful transfection of POM cells derived from E12.5 wildtype embryos with *pshFoxc1*.gfp/neo. Strong eGFP expression is seen in every cell. Expression is localized perinuclearly in the majority of cells, with faint eGFP fluorescence detected within the cytoplasm. Figure 7B shows an agarose gel electrophoresis image of qPCR product. A band at 361bp indicates the successful amplification of the eGFP target amplicon confirming successful transfection.

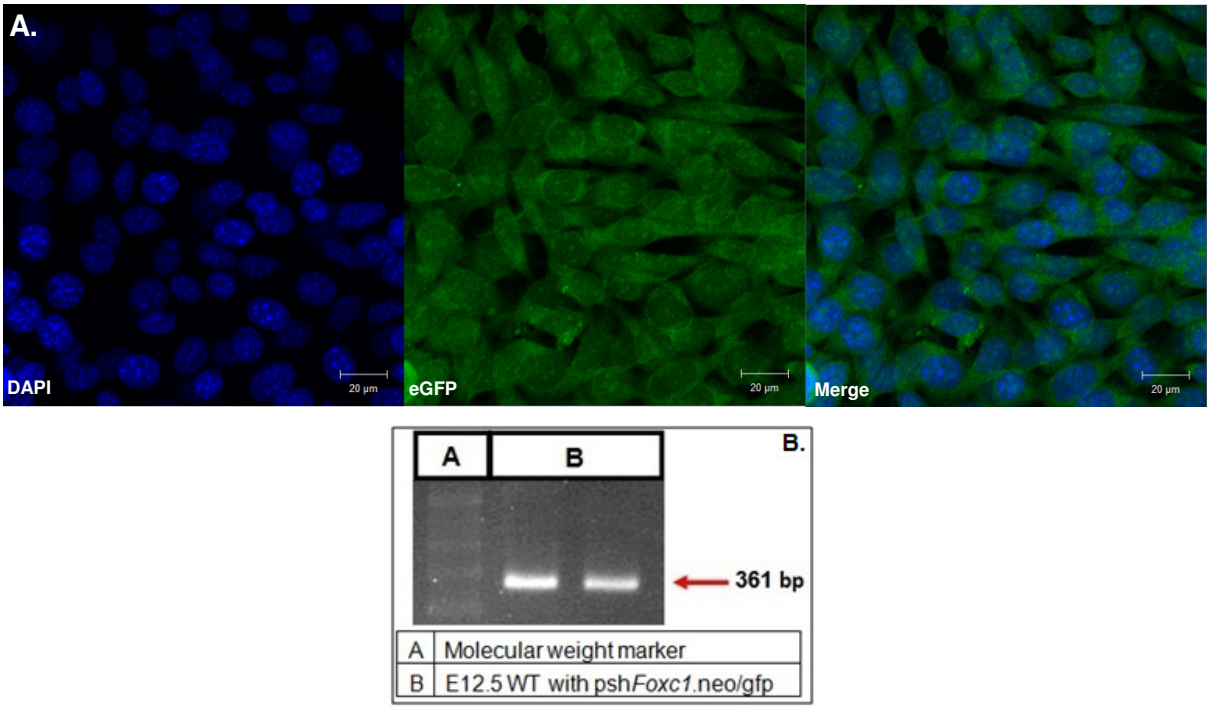

Figure 7: A. Confocal microscopy image showing successful transfection of E12.5 *Foxc1*$^{+/+}$ POM cells with the psh*Foxc1*.neo/gfp plasmid vector. Scale bar = 20µm. B. Gel electrophoresis image of qPCR product showing successful amplification of the 361bp EGFP target amplicon.

4.3. RNA quality

4.3.1. Quantification and A_{260}/A_{280} ratios

The data in Figure 8, imported from the ND-1000 software, was generated from analysis of total RNA isolated from the various samples, 24 hours post-treatment, using UV absorption analysis. The NanoDrop system was used for quantification (to determine the yield) and quality assessment (to determine the purity) of nucleic acid products. The concentration and purity of RNA was determined at an absorbance maximum of 260nm (A_{260}). Upon calculating the $A_{260/280}$ ratio and the $A_{260/230}$ ratio, a reasonable estimate of sample purity can be determined. Relatively pure RNA has an $A_{260/280}$ ratio = 2.0 ± 0.1, while the $A_{260/230}$ ratio should be >2.0 but <2.4. Low $A_{260/280}$ values indicate contamination of the sample with protein while low $A_{260/230}$ ratios may be as a result of carry-over of guanidinium (found in chaotropic cell lysis buffers) or β-mercaptoethanol. As per the values and ratios presented in Figure 8, the quantities and quality of the eluted samples are seen to be of a reasonably good standard, with a high yield and fairly pure, quality eluate. Even though one sample shows a $A_{260/230}$ ratio < 2.0, a value of >1.8 is considered to be acceptably pure when using the QIAGEN RNeasy Mini Kit to carry out RNA isolation.

A

Sample ID	ng/ul	A260	A280	260/280	260/230
E12.5 WT	617.61	15.440	7.039	2.19	2.27
E12.5 pShFoxc1	506.61	12.665	5.788	2.19	2.25
E12.5 +/+ pFoxc1	1276.46	31.912	14.934	2.14	2.20
E12.5 +/+ Dex	911.14	22.778	10.544	2.16	2.17
E12.5 -/-	763.10	19.077	8.850	2.16	2.31
E13.5 WT	1044.08	26.102	12.184	2.14	2.33
E13.5 pShFoxc1	932.32	23.308	10.752	2.17	2.11
E13.5 +/+ pFoxc1	528.87	13.222	6.130	2.16	1.88
E13.5 +/+ Dex	764.00	19.100	8.808	2.17	2.29

B

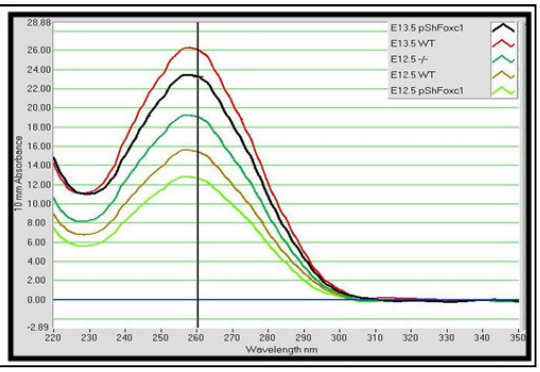

Figure 8: A. Data captured using the NanoDrop ND-1000 Spectrometer and the ND-1000 V3.5.2 software package. Isolated total RNA was analysed for each treatment sample in order to determine the concentration (ng/µl) and purity/quality by means of the $A_{260/280}$ ratio. B. The graph indicate the maximum absorbance at A_{260} of one sample set, indicating that isolated RNA was of good quality.

4.3.2. Denaturing formaldehyde agarose gel electrophoresis

The quality of RNA isolated from POM cells using the QIAGEN RNeasy Plus Mini Kit (QIAGEN, USA) was assessed by running RNA samples on a denaturing agarose-formaldehyde gel. The quality of samples was assessed by visualization of a band approximately 5 kbp in size, the 28S ribosomal subunit, distinctly separated from another band of approximately 2kbp, the 18S ribosomal subunit. The larger 28S subunit should be twice the intensity of the smaller 18S subunit, and separate from its counterpart by a clean space. Any smearing between the two bands is indicative of genomic contamination. Figure 9 shows the results obtained when total RNA isolated from E12.5 wildtype cells, as an example, was run in a formaldehyde denaturing gel.

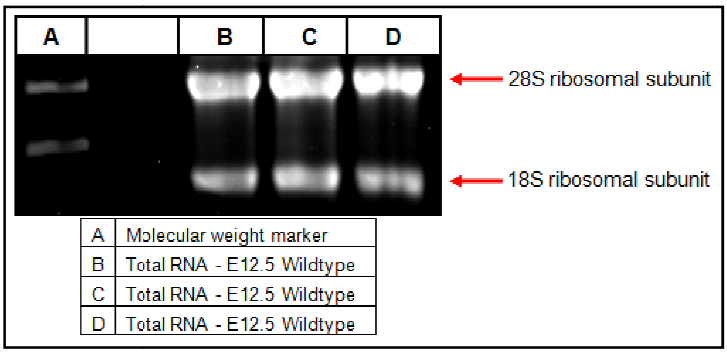

Figure 9: Denaturing formaldehyde agarose electrophoresis of E12.5 wildtype total RNA.

4.4. Validation of the use of *Rps12* as reference gene for gene expression analyses

The ribosomal protein subunit 12 (*Rps12*) was selected as a reference gene against which to normalise relative fold-changes in gene expression of the genes of interest in analyses. Figure 10 below shows the mean C_T values of *Rps12* obtained when the gene was assessed in 5-fold serial dilutions of cDNA synthesized from RNA isolated from the two POM cell lines that were the primary subject of the comparative analyses.

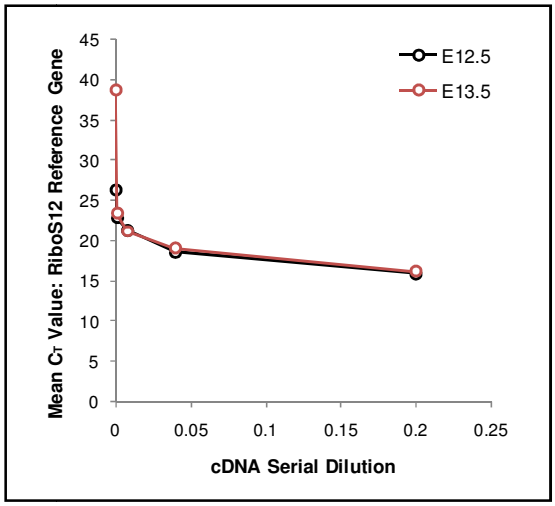

Figure 10: Mean CT values of the *Rps12* reference gene when amplified using cDNA serial dilutions from RNA isolated from wildtype POM cells at E12.5 and E13.5.

Results indicate a distinct overlap in the expression of the reference gene when the target is amplified in serial dilutions of cDNA synthesized from RNA isolated from cell lines derived at two concurrent points in embryonic eye development. This implies that the expression of the prospective reference gene between cell lines remains consistent and does not show variability between the sample sets. As such, *Rps12* may successfully be used as a reference gene against which to normalize target gene expression between samples such that an accurate comparison may be drawn between the two sample sets.

4.5. Validation of the application of the $2^{-\Delta\Delta C_T}$ method in analysis of gene expression

According to Livak & Schmittgen (2001), a main assumption that must be met in order for the calculations applied in the $2^{-\Delta\Delta C_T}$ method of gene expression analysis to be valid is the assumption of approximate equality in the amplification efficiencies of both the target gene of interest (GOI) and the reference gene. In assessing whether such an assumption of equal amplicon efficiency is justified, an assessment of the variability of the ΔC_T ($C_{T_{GOI}}$ - $C_{T_{Rps12}}$) relative to the template dilution can be carried out. In carrying out such an assessment, the stock cDNA template was diluted over a 1,000-fold range. This serial dilution of the cDNA template was used in the RT-qPCR amplification of both the *N-cadherin* and *Foxc1* target genes alongside the *Rps12* reference gene. Mean C_T values of both the target and reference genes were calculated and the ΔC_T value ($C_{T_{GOI}}$ - $C_{T_{Rps12}}$) was calculated. The log cDNA dilution was then plotted against the calculated ΔC_T values and the data generated was fit using a least squares linear regression analysis in Microsoft Office Excel (Microsoft Corporation, 2007).

In assessing the data obtained from such an analysis, the derived slope (*m)* was evaluated. If the absolute value of the gradient generated by the linear regression analysis is close to zero, one can consider the efficiencies of the target and reference genes to be equivalent, such that the relative quantification of target GOI may be determined by application of the $\Delta\Delta C_T$ calculation.

The cDNA concentration curve analysis was applied to two of the three GOI's; namely *N-cadherin* and *Foxc1*. The reaction efficiency for *Msx1* could not be validated as the qPCR failed to amplify when these analyses were being carried out. The reaction efficiency was therefore assumed to be equal to that of *RpS12* for subsequent analyses. The log cDNA dilution versus ΔC_T graph generated for the *Foxc1* gene with the *Rps12* internal reference gene is shown in Figure 11A. Figure 11B shows a similarly generated graph for the target *N-cadherin* again using the *Rps12* reference gene. Results indicated a gradient value very close to zero for both the GOI's ($m_{N\text{-cadherin}}$ = -0.04; m_{Foxc1} = 0.092), indicating that the $2^{-\Delta\Delta C_T}$ for analysis of gene expression by determination of the relative fold change between sample treatments may be successfully applied in the assessment of both *N-cadherin* and *Foxc1* gene expression.

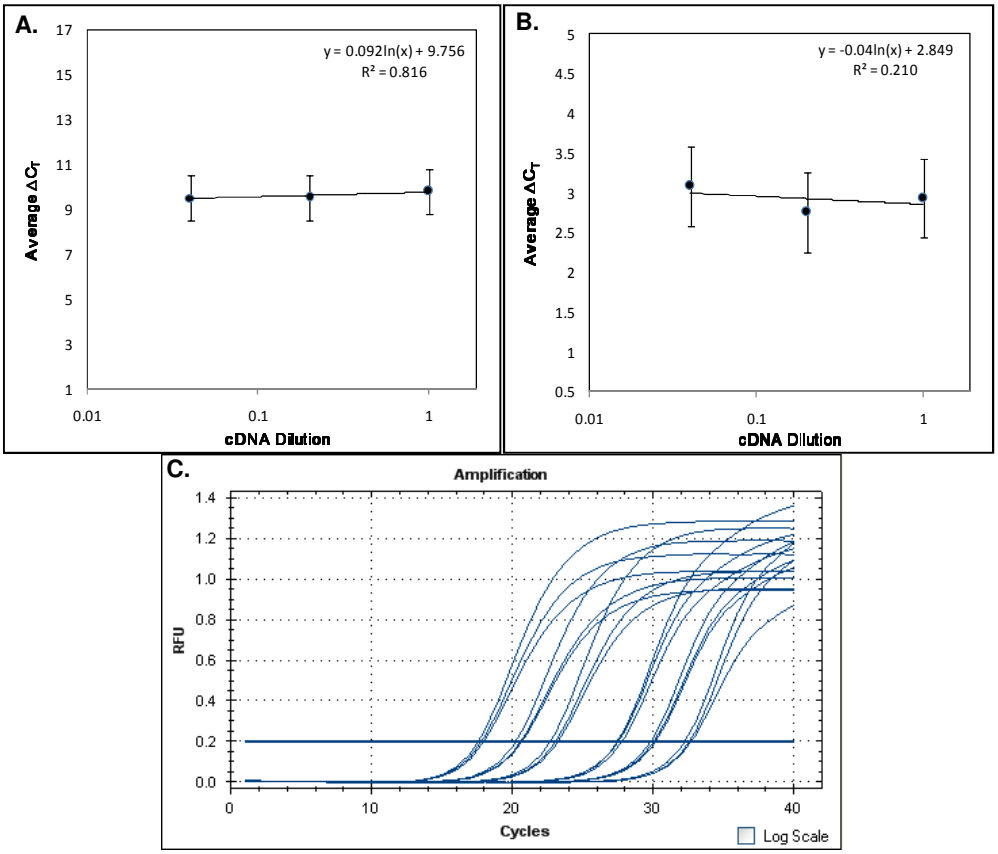

Figure 11: A. Concentration curve analysis for *Foxc1*. The graph shows log cDNA dilution vs. ΔC_T linear analysis in order to assess *Foxc1* qPCR reaction efficiency (n = 3; R^2 = 0.816; m = 0.092). B. Concentration curve analysis for *N-cadherin.* The graph shows log cDNA dilution vs. ΔC_T linear analysis in order to assess *N-cadherin* qPCR reaction efficiency (n = 3; R^2 = 0.210; m = -0.04). C. An example of the fluorescence curve generated when a dilution series of cDNA is used to amplify *Foxc1* and *Rps12* gene targets in order to plot a reaction efficiency linear regression.

4.6. PCR Optimization: *N-cadherin*

Three different primer sets were used to evaluate N-cadherin gene expression. All primers were designed to span intron-exon boundaries such that a single target is amplified during PCR precluding the possibility of contamination from genomic DNA interfering with the robustness of the mRNA gene analysis during PCR. One primer set (set 2) failed to amplified a N-cadherin target in both conventional PCR and qPCR. Primer set 1 was able to amplify N-cadherin in qPCR. Figure 12 shows the successful amplification of N-cadherin primer set 1 confirming the intron-exon boundary primer design. Lane B shows the blank master-mix sample without a cDNA template, while lanes C and D show duplicate samples using genomic DNA. Lanes E & F show samples using cDNA synthesised from an mRNA template. The qPCR amplification confirms the absence of a product when intron-exon boundary primers are used to amplify the target sequence from a genomic DNA template.

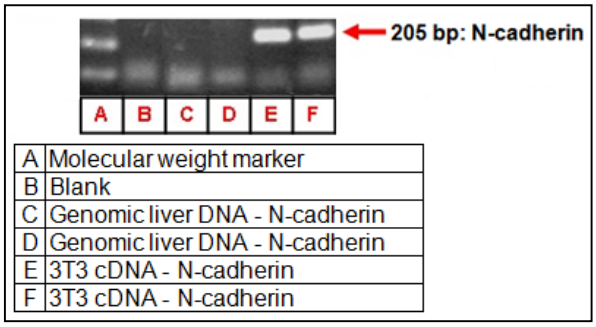

A	Molecular weight marker
B	Blank
C	Genomic liver DNA - N-cadherin
D	Genomic liver DNA - N-cadherin
E	3T3 cDNA - N-cadherin
F	3T3 cDNA - N-cadherin

Figure 12: N-cadherin gene target amplified using intron-exon boundary primers (set 1).

To determine the most successful primer annealing temperature (for primer set 1) at which N-cadherin alone could be amplified to show an electrophoresis band at 205 bp, temperature gradients were carried out. Figure 13 shows an image captured during optimization, distinctly showing a band at 205 bp, however, non-specific amplification was detected during qPCR. Temperature gradients with smaller incremental differences between the annealing temperatures indicated that the primers annealed specifically to yield one product at 64°C.

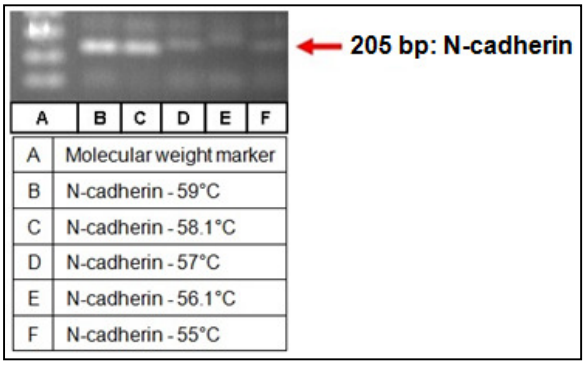

A	Molecular weight marker
B	N-cadherin - 59°C
C	N-cadherin - 58.1°C
D	N-cadherin - 57°C
E	N-cadherin - 56.1°C
F	N-cadherin - 55°C

Figure 13: Agarose gel electrophoresis image of qPCR products from temperature gradient qPCR to optimize N-cadherin primer set 1.

This primer set, although fully optimized, ceased to amplify the N-cadherin amplicon after a period of time. A primer set (primer set 3) sourced from literature (Vanselow et al., 2008) was purchased and used. These intron-exon boundary primers amplified a target amplicon of 204bp successfully at a primer annealing temperature of 60°C (Figure 14).

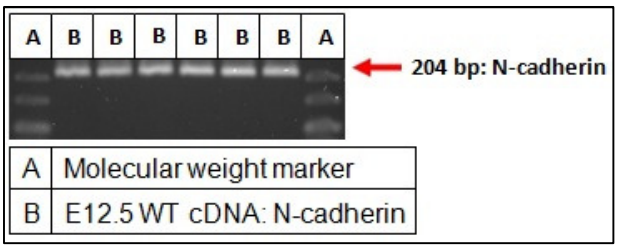

A	Molecular weight marker
B	E12.5 WT cDNA: N-cadherin

Figure 14: Gel electrophoresis image showing successful amplification of N-cadherin target (204 bp) using primers sourced from Vanselow et al. (2008).

4.7. PCR Optimization: *Msx1*

Three primer sets were designed and synthesized in order to amplify a target sequence within the *Msx1* gene. Two of these primer sets failed to amplify target amplicons. However, one primer set was eventually optimized for qPCR to produce a single band at the correct amplicon size. Unfortunately, this optimized primer set stopped amplifying the *Msx1* target whilst gene analyses were being carried out. Primers were then sourced from literature (Oka et al., 2007). These primers were unsuccessful at amplifying the *Msx1* amplicon using a number of different qPCR master mixes and additives.

4.8. PCR Optimization: *Foxc1*

In attempting to amplify a region of the mono-exonic *Foxc1* with primers successfully used by Sommer et al. (2006), a variety of different approaches were undertaken. Fresh primers were purchased, qPCR additives were incorporated into reactions, different RNA isolation techniques were attempted (TriReagent and RNeasy™ Plus Mini Kit), different cDNA synthesis methods were carried out (SuperScript™ III and RNA to cDNA 2-Step MasterMix) and different qPCR mastermixes were used, however, the target could not be amplified. The *Foxc1* target was eventually successfully amplified using cDNA synthesized from non-DNAse treated RNA, PCR water purchased from Promega and the FIREPol® EvaGreen® qPCR Mix Plus (no ROX) (Solis BioDyne®, Estonia) qPCR mastermix. Due to the RNA samples showing a distinct absence of genomic contamination upon denaturing gel electrophoresis and the No-RT controls producing no amplification curves during qPCR, the use of non-DNAse treated cDNA samples to assess *Foxc1* expression was regarded as permissible.

B. Results and data analysis

4.9. Gene expression analyses

In this section, the expression levels of *Foxc1*, *N-cadherin* and *Msx1* were determined at E12.5 and E13.5. The No-RT controls run did not produce amplification curves, indicating the absence of contaminating genomic DNA in RNA samples, allowing the effect of over-expression of *Foxc1* on *N-cadherin* and *Msx1* expression levels to be determined. Unfortunately, due to problems with the *Foxc1* qPCR and the shRNA vectors, the effect of *Foxc1* knock-down on *N-cadherin* and *Msx1* gene expression was not evaluated.

4.9.1. Foxc1 expression in POM cells

4.9.1.1. Foxc1 expression at E12.5 vs. E13.5

qPCR analysis was carried out to determine if there were any differences in *Foxc1* gene expression between E12.5 and E13.5.

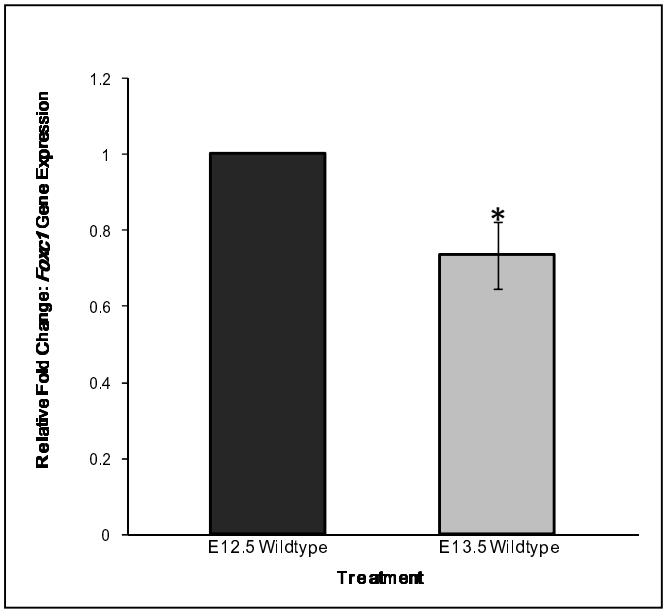

Figure 15: Relative expression of *Foxc1* at E12.5 and E13.5. (* = $p < 0.05$; $n = 3$; P10)

Foxc1 is expressed at both E12.5 and E13.5 in POM cells, however there is slightly (but significantly) less *Foxc1* in POM cells at E13.5 in comparison to cells at E12.5 ($p = 0.039306$; SEM = ±0.087954) (Figure 15). Changes in *Foxc1* expression, although significant, are subtle with E13.5 cells expressing ~26.5% less *Foxc1* relative to E12.5 POM cells.

4.9.1.2. Verification of Foxc1 over-expression in E12.5 and E13.5 POM cells

POM cells were transfected with the p*Foxc1*-eGFP plasmid to evaluate the over-expression of *Foxc1* at E12.5 and E13.5.

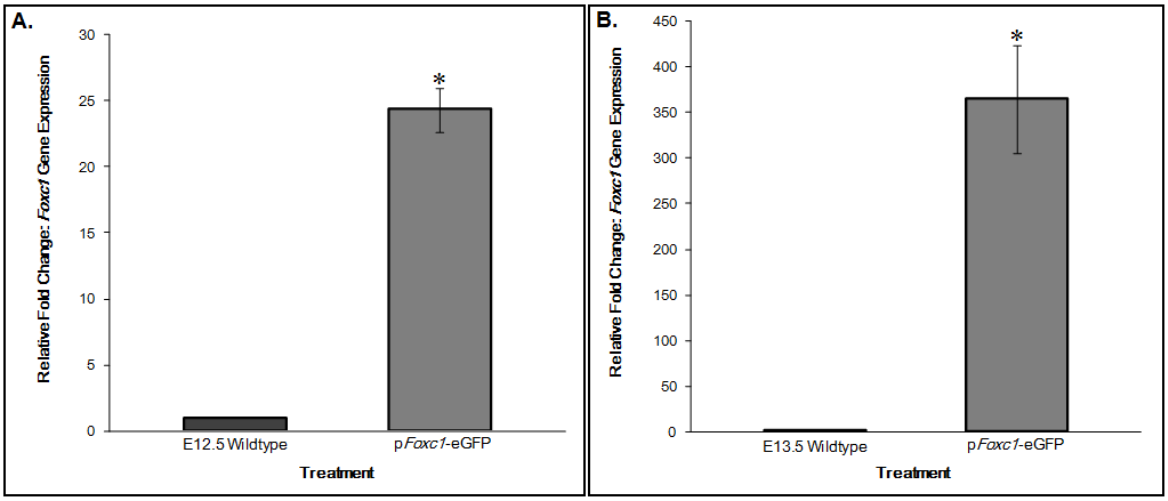

Figure 16: ***A.*** Relative gene expression analysis indicating a significant difference in the expression of *Foxc1* between E12.5 wildtype (control) and p*Foxc1*-eGFP transfected cells. ($n = 3$). B. Relative gene expression analysis indicating a significant difference in the expression of *Foxc1* between E13.5 wildtype (control) and p*Foxc1*-eGFP transfected cells. (* = $p < 0.05$; $n = 3$; P10).

Transfection of POM cells with p*Foxc1*-eGFP resulted in significant over-expression of *Foxc1* in E12.5 POM cells ($p = 0.00015$; SEM = ± 1.661617) (Figure 16A) and in E13.5 POM cells (p =

0.003596; SEM = ± 59.24396) (Figure 16B). *Foxc1* expression upon transfection is considerably higher in both cell lines, with E12.5 and E13.5 cells expressing ~23.31-fold and ~362.97-fold more *Foxc1* than their wildtype counterparts, respectively.

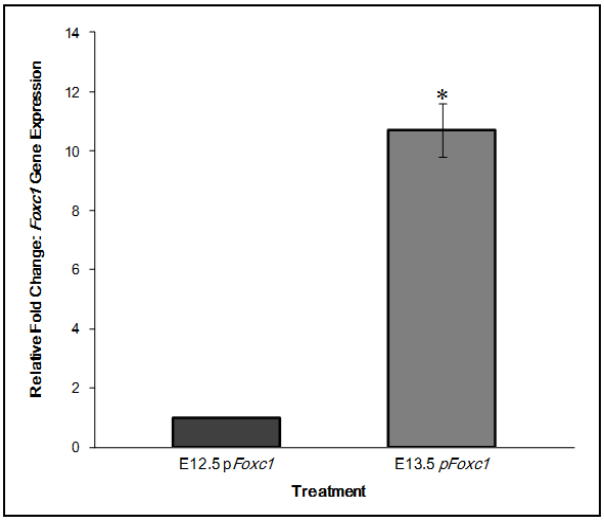

Figure 17: Relative gene expression analysis indicating a significant difference in p*Foxc1*-eGFP transfection efficiency *Foxc1* between E12.5 (control) and E13.5 POM cells. (* = $p < 0.05$; $n = 3$; P10).

POM cells derived at E13.5 showed a significantly greater p*Foxc1*-eGFP transfection efficiency (p =0.000413; SEM = ± 0.896938) relative to POM cells derived from E12.5 embryos. Transfection efficiency in was ~9.71-fold greater in E13.5 POM cells (Figure 17).

4.9.2. N-cadherin expression in POM cells

qPCR analysis was carried out on cDNA synthesized from RNA isolated from POM derived from both E12.5 and E13.5 embryos to assess any differences in *N-cadherin* gene expression during corneal endothelium development. To evaluate whether *Foxc1* had any effect on *N-cadherin* expression in these cell lines, POM cells were transfected with the p*Foxc1*-eGFP plasmid. The following data was generated, showing *Foxc1* to have an effect on the expression of *N-cadherin*, both in its absence or presence.

4.9.2.1. N-cadherin expression at E12.5 vs. E13.5

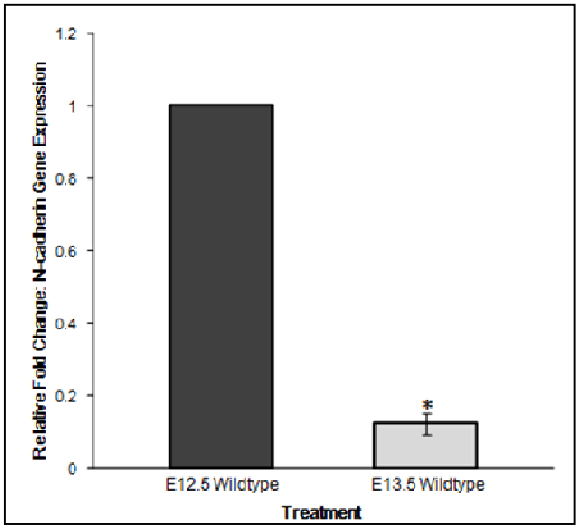

Figure 18: Relative gene expression analysis indicating a significant difference in the expression of N-cadherin between E12.5 (control) and E13.5 (* = $p < 0.05$; $n = 3$; P7).

N-cadherin is expressed at significantly lower levels in E13.5 POM cells relative to E12.5 POM cells (p = 0.020548; SEM = ±0.028302) (Figure 18). E12.5 POM cells express ~8-fold more N-cadherin than E13.5 POM cells.

4.9.2.2. Effect of pFoxc1-eGFP over-expression on N-cadherin expression in E12.5 and E13.5 POM cells

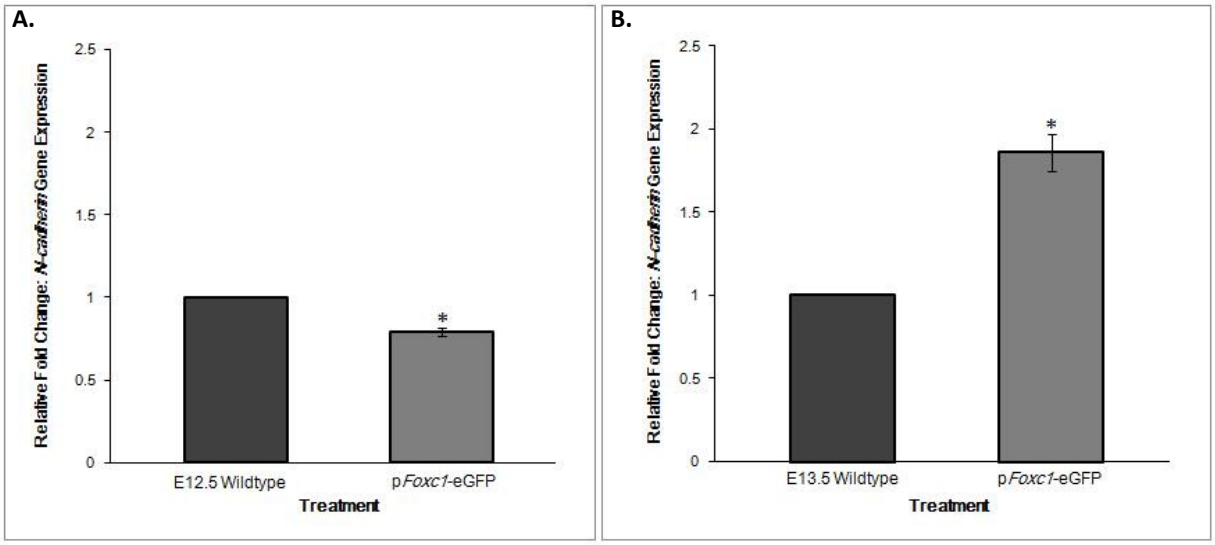

Figure 19: ***A.*** Relative gene expression analysis indicating a significant difference in the expression of *N-cadherin* between E12.5 wildtype (control) and p*Foxc1*-eGFP transfected cells. ($n = 3$). B. Relative gene expression analysis indicating a significant difference in the expression of *N-cadherin* between E13.5 wildtype (control) and p*Foxc1*-eGFP transfected cells. (* = $p < 0.05$; $n = 3$; P10).

Transfection of POM cells at E12.5 and E13.5 with p*Foxc1*-eGFP, resulted in significant differences in relative *N-cadherin* gene expression. Over-expression of *Foxc1* in E12.5 POM cells resulted in a

slight, but significant, (p = 0.001112; SEM = ± 0.024615) decrease in *N-cadherin* (~20.6%) (Figure 19 A). However, in contrast, over-expression of *Foxc1* in E13.5 POM cells significantly (p = 0.001693; SEM = ± 0.114517) increased *N-cadherin* expression by ~85.9% (Figure 19 B).

4.9.3. Msx1 expression in POM cells

In order to evaluate differences in *Msx1* expression in POM cells at E12.5 and E13.5, qPCR analysis was carried out on cDNA synthesized from isolated POM RNA. Cell lines were also subject to transfection with a plasmid over-expressing the transcription factor *Foxc1*. Preliminary data indicates that *Foxc1* exerts an effect on *Msx1* expression. Unfortunately, the *Msx1* target then failed to amplify successfully again and analyses on POM evaluating the effect of *Foxc1* knock-down were unable to be completed.

4.9.3.1. Msx1 gene expression in E12.5 vs. E13.5

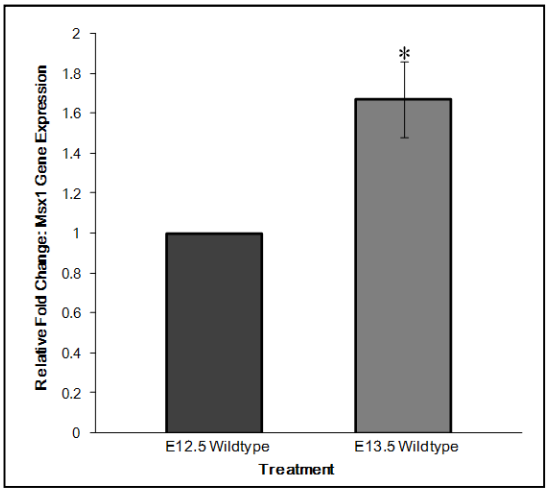

Figure 20: Relative gene expression analysis indicating a significant difference in the expression of *Msx1* between E12.5 (control) and E13.5. (* = $p < 0.05$; $n = 3$; P10).

Msx1 is expressed at significantly higher levels at E13.5 in comparison to E12.5 (p = 0.071545; SEM = ± 0.189097). *Msx1* expression increased at E13.5 by ~66.8% /0.67-fold (Figure 20).

4.9.3.2. Effect of pFoxc1-eGFP over-expression on Msx1 expression in E13.5 POM cells

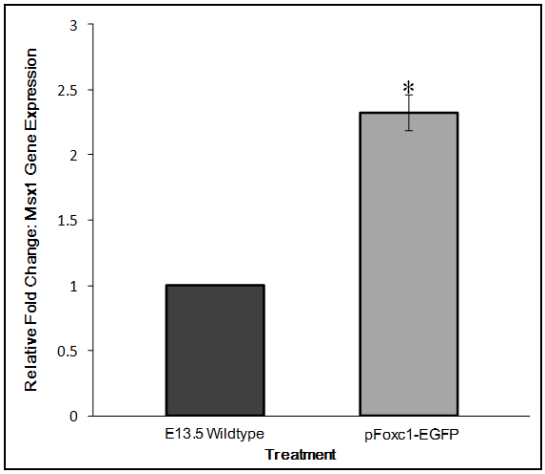

Figure 21: Relative gene expression analysis indicating a significant difference in the expression of *Msx1* between E13.5 wildtype cells (control) and E13.5 cells transfected with p*Foxc1*-eGFP. (* = $p < 0.05$; $n = 3$; P10).

Over-expression of *Foxc1* in E13.5 POM cells increased *Msx1* expression significantly ($p = 0.010402$; SEM = ± 0.136305) by ~137.8% relative to the wildtype control POM cells (Figure 21). *Msx1* qPCR failed repeatedly after these analyses and, despite the design and purchase of two new primer sets, *Msx1* never successfully amplified again.

4.10. *Protein expression analyses*: *Western Blot*

In this section, the expression levels of Foxc1 and N-cadherin protein were analysed at E12.5 and E13.5 by western blot. The effect of over-expression and knock-down of *Foxc1* on N-cadherin expression levels was determined.

4.10.1. Foxc1 protein expression in E12.5 and E13.5 POM cells and the effect of Foxc1 knock-down

Western blot analysis assessed the expression of Foxc1 protein at E12.5 and E13.5. These wildtype cells were subject to transient transfections with plasmid vectors to ablate the expression of the *Foxc1* gene. Figure 22 shows the results of Western blotting using a primary antibody against the Foxc1 protein. Densitometric analysis was carried out on images to quantify band intensity. Intensities of target bands were normalized against the intensity of GAPDH loading controls.

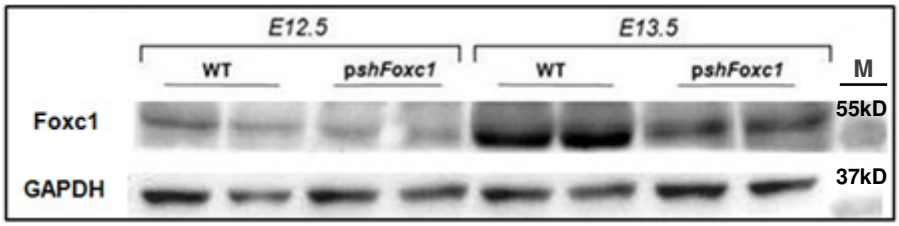

Figure 22: Western blot image captured from nitrocellulose membrane probed with horseradish peroxidase (HRP) –conjugated 2° antibody. Primary antibody directed against Foxc1 protein (WT – wildtype lysate; pshFoxc1 – lysate from cells transfected with psh*Foxc1*.neo/gfp; M - marker).

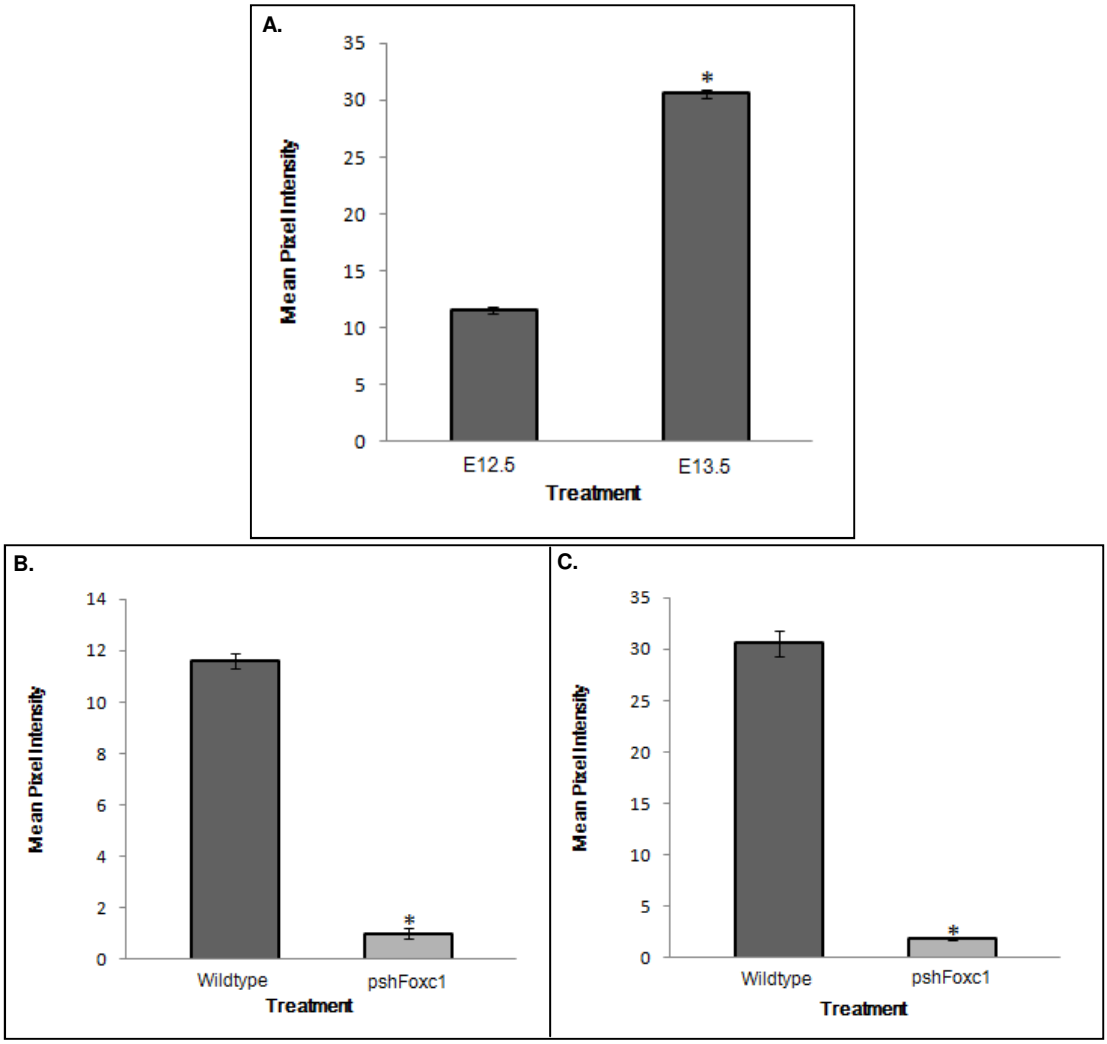

Figure 23: Densitometry results indicate significant changes in Foxc1 protein expression between the cell lines (A), as well as when these wildtype cells are transfected with the shRNA plasmid, psh*Foxc1*.neo/gfp (B – E12.5; C – E13.5) (* = $p < 0.05$; $n = 3$; P10).

There is significantly more Foxc1 protein expression in E13.5 POM cells in comparison to E12.5 POM cells (p = 0.030873) (Figure 22 & 23 A). Foxc1 expression decreases significantly in both E12.5 and E13.5 POM cells (p = 0.006713 and 0.026004 respectively) (Figure 22 & 23 B/C) when POM cells are transfected with a shRNA against *Foxc1*. Foxc1 protein decreases by ~91% in the E12.5 cell line and ~94% in the E13.5 cell line.

4.10.2. N-cadherin protein expression in E12.5 and E13.5 POM cells and the effect of Foxc1 over-expression and knock-down

Western blots were used to evaluate N-cadherin protein levels between E12.5 and E13.5 POM cells. Cells were subjected to transient transfections with plasmid vectors to either over-express or silence *Foxc1* expression. Figure 24 shows Western blot analysis using a primary antibody against N-cadherin proteins. Densitometric analysis was carried out on images to quantify band intensity. Intensities of target bands were normalized against the intensity of GAPDH loading controls.

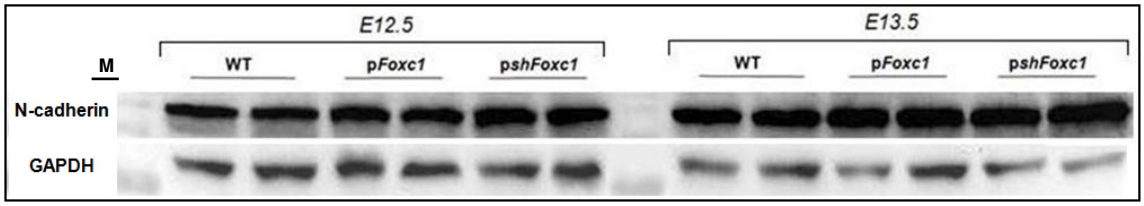

Figure 24: Western blot image captured from nitrocellulose membrane probed with horseradish peroxidase (HRP) –conjugated 2° antibody. Primary antibody directed against N-cadherin protein (WT – wildtype lysate; pFoxc1 - lysate from cells transfected with p*Foxc1*-eGFP; pshFoxc1 – lysate from cells transfected with psh*Foxc1*.neo/gfp; M - marker).

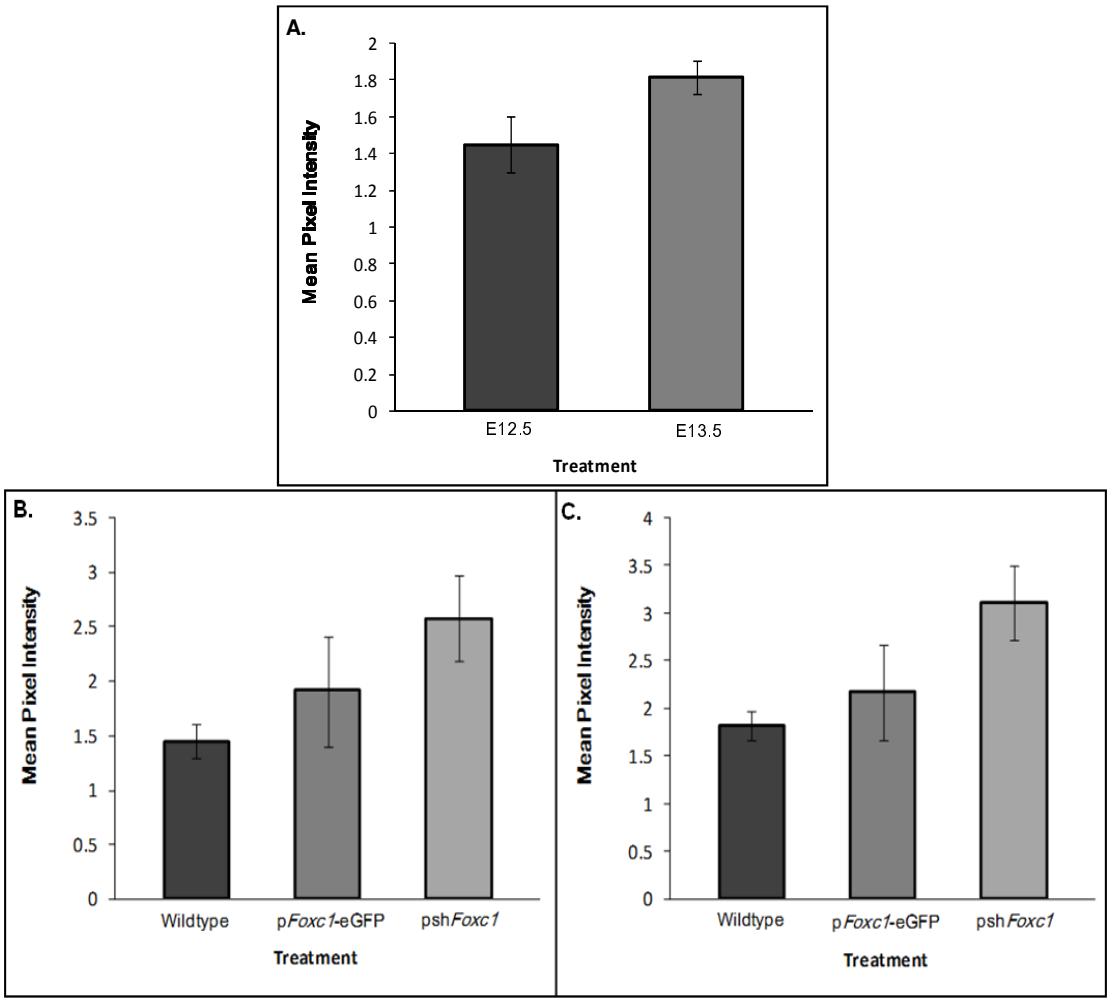

Figure 25: Densitometry showed no significant differences in N-cadherin protein expression between the cell lines (A). Wildtype E12.5 and E13.5 cells transfected with p*Foxc1*-eGFP or psh*Foxc1*.neo/gfp show no significant differences (B – E12.5; C – E13.5) (* = $p < 0.05$; $n = 3$; P10).

There is no significant difference in N-cadherin protein expression between the E12.5 and E13.5 POM cell lines ($p = 0.110258$) (Figure 24 & 25 A). No significant changes in N-cadherin were seen in E12.5 and E13.5 cells upon transfection with either p*Foxc1*-eGFP ($p = 0.477021056$; $p = 0.429961487$) or pshFoxc1.neo/gfp ($p = 0.117432$; $p = 0.156459$) (Figure 24 & 25 B/C).

4.11. Immunocytochemistry and Confocal Microscopy

Confocal microscopy was carried out to assess protein expression and localization in POM cells derived from E12.5 and E13.5 embryos. ImageJ was used to quantify expression and localization in single cells by measuring fluorescence intensity and mean grey area values.

4.13.1. Monolayer cultures

4.13.1.1. N-cadherin expression: E12.5 vs. E13.5

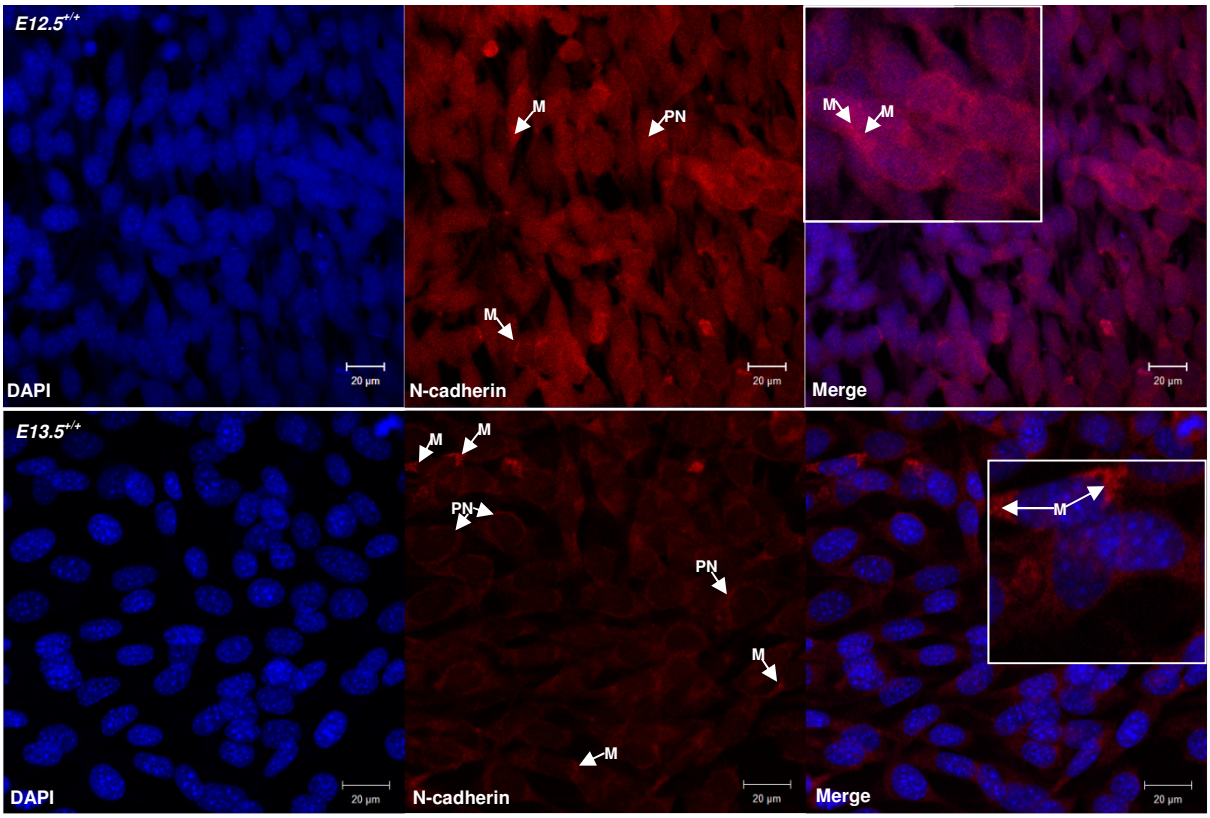

Figure 26: Confocal images of wildtype POM monolayers at E12.5 and E13.5. DAPI stains nuclei blue, and Cy3 detects N-cadherin in the red channel. pn – peri-nuclear N-cadherin; m – membrane localized N-cadherin.

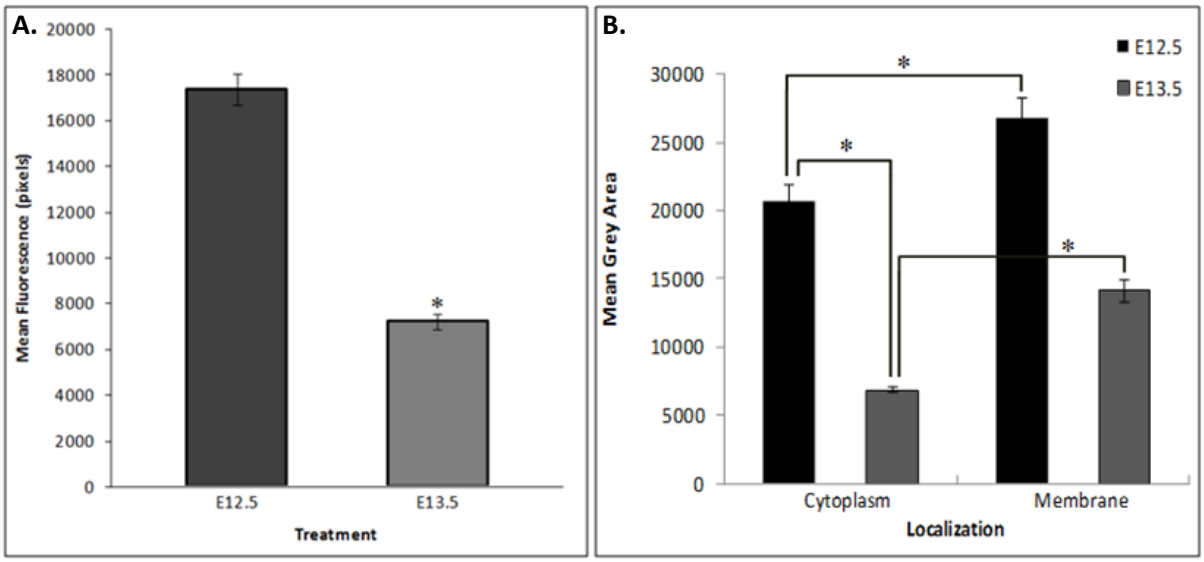

Figure 27: A. Confocal microscopy analysis indicating a significant difference in the expression of N-cadherin between E12.5 (control) and E13.5. B. Mean grey area values indicating N-cadherin expression and localization within the cell. (* = $p < 0.05$; $n = 3$; P10).

Immunohistochemistry results indicate the presence of N-cadherin in both E12.5 and E13.5 wildtype cells. This expression is localized within the cytoplasm and at the cell membrane at contact points between cells (indicated by arrows in Figure 26). There is no localization of N-cadherin within the nucleus (stained blue by DAPI). Total fluorescence intensity indicates significantly more overall (p = 1.37054 x10^{-11}) N-cadherin expression at E12.5 than at E13.5 (Figure 27 A). Grey area analyses indicates that the E12.5 POM cells express significantly more N-cadherin, at both the cell membrane and within the cytoplasm, (p = 3.40871 x 10^{-7}; 1.87175 x 10^{-10}) than the E13.5 POM cells (Figure 27 B). Localization analyses indicates that this N-cadherin localization is slightly, but significantly greater at the cell membranes than in the cytoplasm in E12.5 (p = 0.00775027). In E13.5 POM cells, N-cadherin shifts significantly to the membrane from the cytoplasm (p = 3.88717 x 10^{-9}) (Figure 27 B).

4.13.1.2. Effect of Foxc1 over-expression on N-cadherin expression in E12.5 and E13.5 POM

Transfection of POM cells with the p*Foxc1*-eGFP plasmid (indicated by the robust perinuclear and cytoplasmic expression of green fluorescent protein) results in decreased N-cadherin expression in both E12.5 and E13.5 cells (Figure 28), however this decrease was only significant in E12.5 transfectants (p = 4.12345 x10^{-12}) (Figure 29 A). Increased amounts of N-cadherin are localized at the cell membrane and in excessive amounts within the cytoplasm in E13.5 POM, however, the decrease in N-cadherin caused by *Foxc1* over-expression at E12.5 resulted in a less diffused, perinuclear and peripheral localization of N-cadherin expression (Figure 28). At E12.5, over-expression of *Foxc1* causes decreased N-cadherin presence at both the membrane and in the cytoplasm (p = 2.17745 x10^{-9}; 4.032 x10^{-9}) (Figure 29 C). However membrane expression is significantly greater in comparison to cytoplasmic expression in transfected cells (p = 8.75575 x10^{-7}) (Figure 29 C). N-cadherin increases

slightly but significantly in the cytoplasm in E13.5 POM cells when transfected with pFoxc1-eGFP (p = 0.007969492), but there is no significant change in membrane-localized N-cadherin (Figure 29 D). N-cadherin expression is again greater at the cell membrane relative to the cytoplasm in transfected cells (p = 2.42031 x10^{-5}) (Figure 29 D).

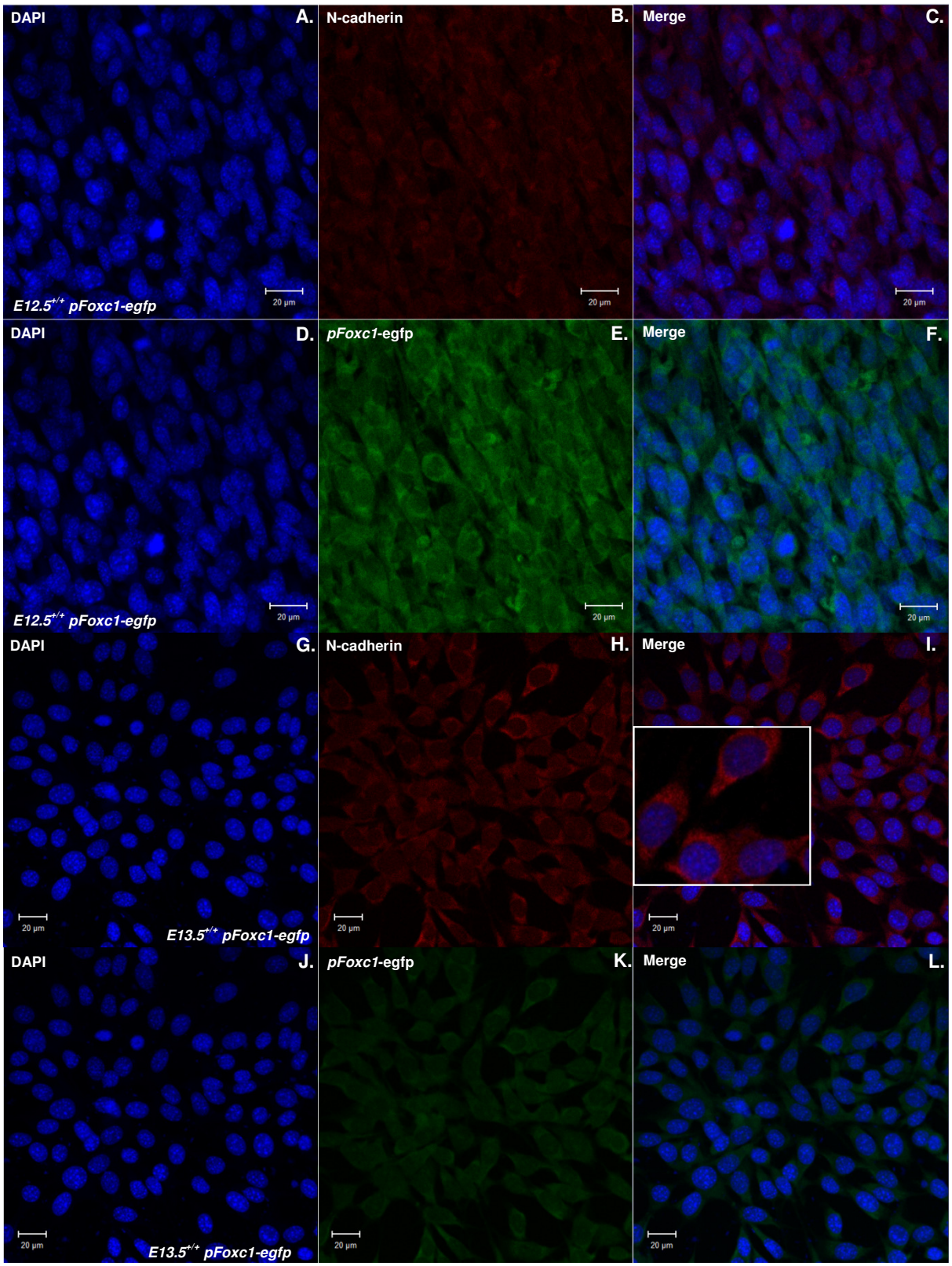

Figure 28: Confocal microscopy images of wildtype POM monolayers indicating localization of N-cadherin when POM cells are transfected with p*Foxc1*-eGFP at E12.5 (Frames A-F) and E13.5 (Frames G-L). DAPI stains nuclei blue, and Cy3 detects N-cadherin in the red channel.

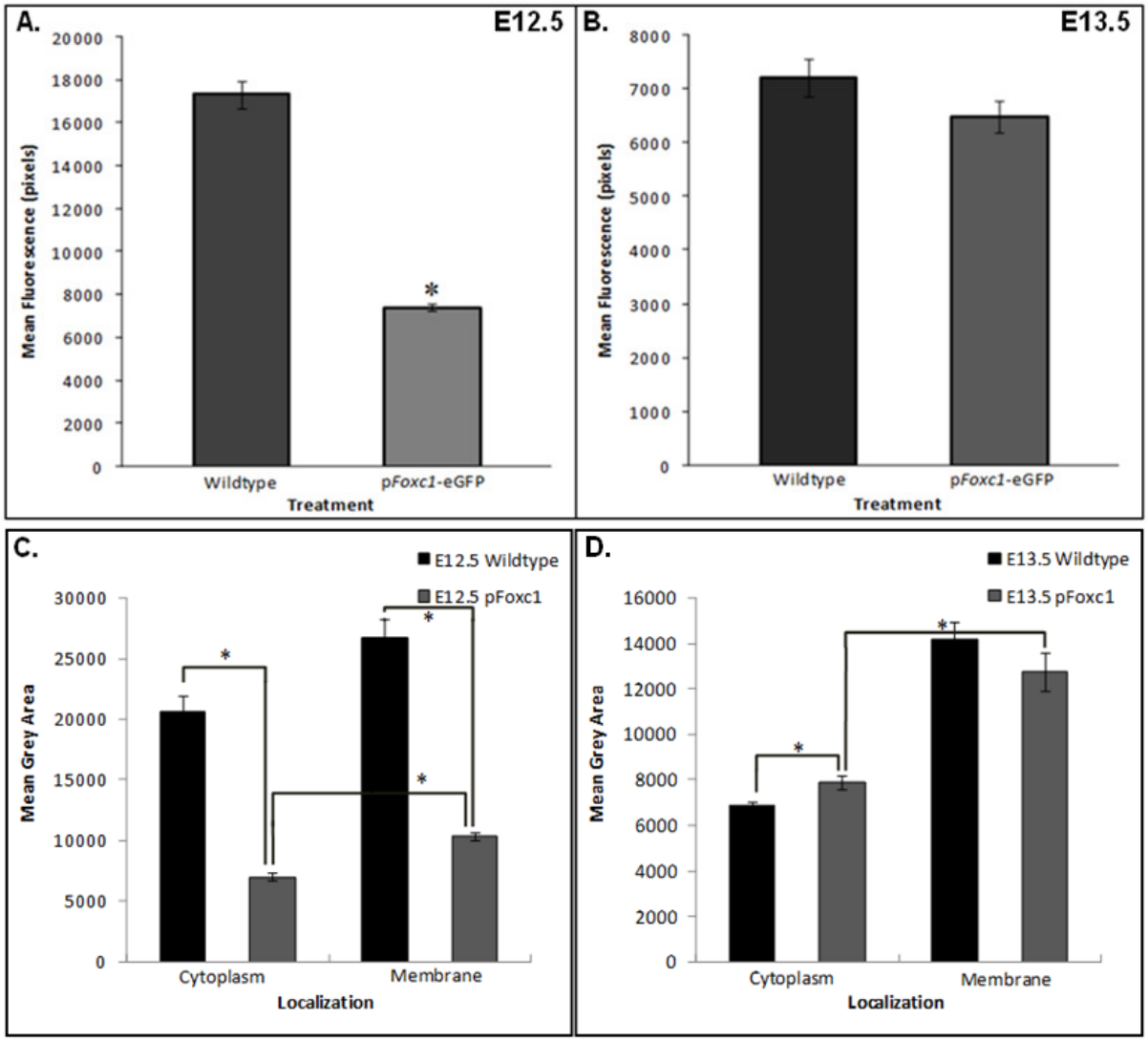

Figure 29: A. Confocal microscopy analysis indicating a significant difference in the expression of N-cadherin between E12.5 wildtype (control) and E12.5 transfected with p*Foxc1*-eGFP. B. No significant differences are seen in N-cadherin expression between E13.5 wildtype (control) and E13.5 transfected with p*Foxc1*-eGFP. C. Mean grey area values indicating N-cadherin expression and localization within wildtype and p*Foxc1*-eGFP transfected E12.5 POM cells. D. Mean grey area values indicating N-cadherin expression and localization within wildtype and p*Foxc1*-eGFP transfected E13.5 POM cells. (* = $p < 0.05$; $n = 3$; P10).

4.13.1.3. Effect of Foxc1 knock-down on N-cadherin expression in E12.5 and E13.5 POM

Successful transfection of POM cells with the *Foxc1* knock-down plasmid vector psh*Foxc1.neo/gfp* is verified by the marked GFP fluorescence localised perinuclearly in the cytoplasm (Figure 30). N-cadherin expression decreased significantly in transfected E12.5 cells (p = 8.10303 x10^{-13}), while N-cadherin expression at cell membranes increased significantly in E13.5 POM cells (p = 1.55867 x10^{-5}) upon knock-down of *Foxc1* expression (Figure 31 A/B). Although N-cadherin expression in transfected E12.5 cells decreased relative to wildtype cells, distinct pooled (sometimes punctuate) expression of N-cadherin was seen at cell membranes at contact points where individual cells overlapped (Figure 30 inset).

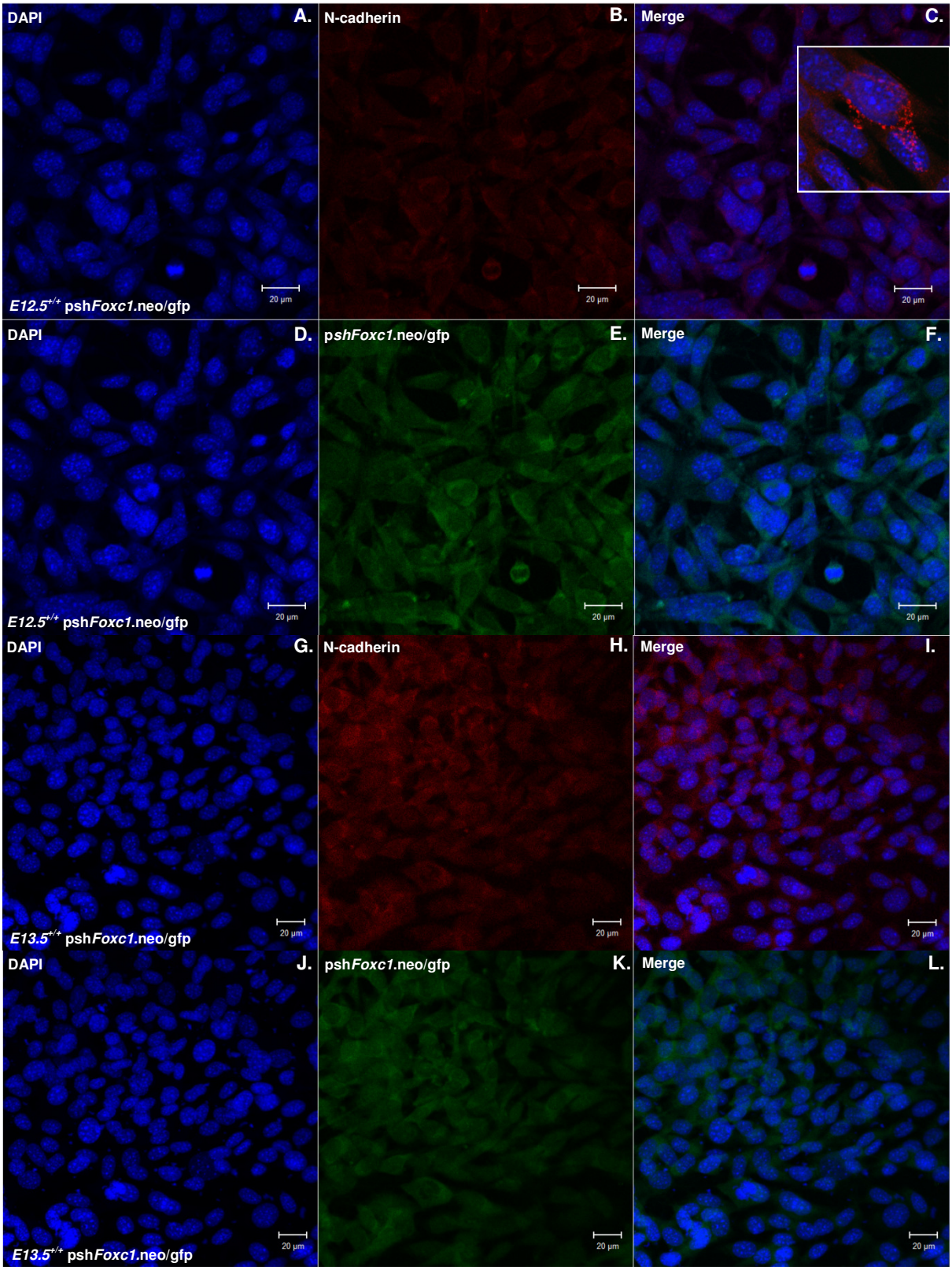

Figure 30: Confocal microscopy images of wildtype POM monolayers indicating localization of N-cadherin when POM cells are transfected with psh*Foxc1*.neo/gfp at E12.5 (Frames A-F) and E13.5 (Frames G-L). DAPI stains nuclei blue, and Cy3 detects N-cadherin in the red channel. GFP is shown in the green channel indicating plasmid location in the cell.

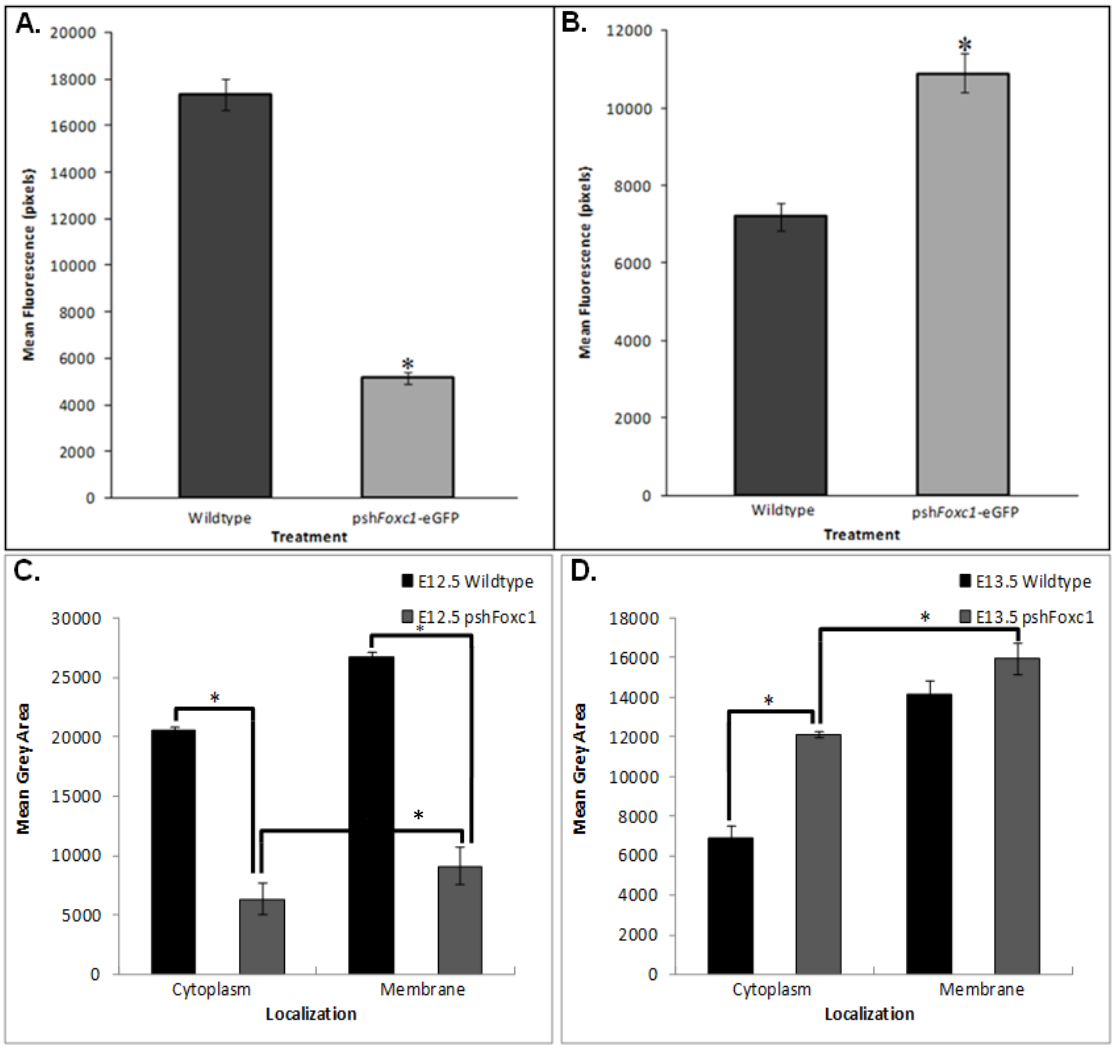

Figure 31*:*A Confocal microscopy analysis indicating a significant difference in the expression of N-cadherin between E12.5 wildtype (control) and E12.5 transfected with psh*Foxc1*.neo/gfp. B. Significant differences are also noted in N-cadherin expression between E13.5 wildtype (control) and E13.5 transfected with p*Foxc1*-eGFP (* = $p < 0.05$; $n = 3$; P10). Mean grey area values indicating N-cadherin expression and localization within psh*Foxc1*.neo/gfp transfected E12.5 (C) and E13.5 (D) POM cells. (* = $p < 0.05$; $n = 3$; P10).

Grey area analysis indicated that E12.5 POM cells transfected with psh*Foxc1*.neo/gfp showed significantly lower N-cadherin levels in the cytoplasm and at the cell membranes ($p = 1.59025 \times 10^{-9}$; 7.92829×10^{-10}), with membrane-bound N-cadherin being maintained at slightly significantly higher levels than cytoplasmic N-cadherin ($p = 2.82735 \times 10^{-5}$) (Figure 31 C). POM cells at E13.5 showed significantly more cytoplasmic N-cadherin ($p = 3.42923 \times 10^{-9}$) upon transfection with psh*Foxc1*.neo/gfp, however there were no significant changes in N-cadherin localization at the cell membranes (Figure 31 D). However, transfected cells had significantly more membrane-bound N-cadherin than cytoplasmic N-cadherin ($p = 0.00040905$) (Figure 31 D).

4.14.2. Hanging drop culture

In order to assess junction formation in a 3D environment, wildtype cells were subjected to hanging drop culture for both 2.5 and 6.5 days. Cells formed distinct spheroid clusters within the drop of culture medium by day 2, and by day 6 had almost tripled in size (Figure 32).

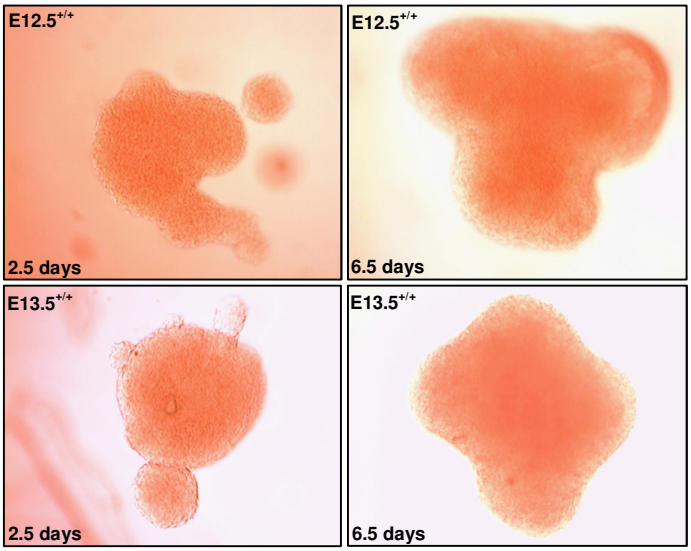

Figure 32: Light microscopy images - E12.5 and E13.5 wildtype hanging drops (100x).

4.14.2.1. N-cadherin protein expression: E12.5 vs. E13.5 hanging drops

In the cell aggregates made using E12.5 wildtype cells, the mass showed a clear lattice work indicative of N-cadherin junction formation (Figure 33) between adjacent cells by day 2.5, however the clarity of the pattern began to decrease by day 6.5, and imaging became difficult due to the accumulative size of the cell mass. At day 6.5 a number of individual cells in the E12.5 spheroid showed robust N-cadherin expression throughout the cell with cells directly adjacent to these cells developing a similar expression pattern. Cell clusters using E13.5 cells showed relatively less expression of N-cadherin at both day 2.5 and day 6.5, however the lattice pattern made by cell boundaries was still clearly visible.

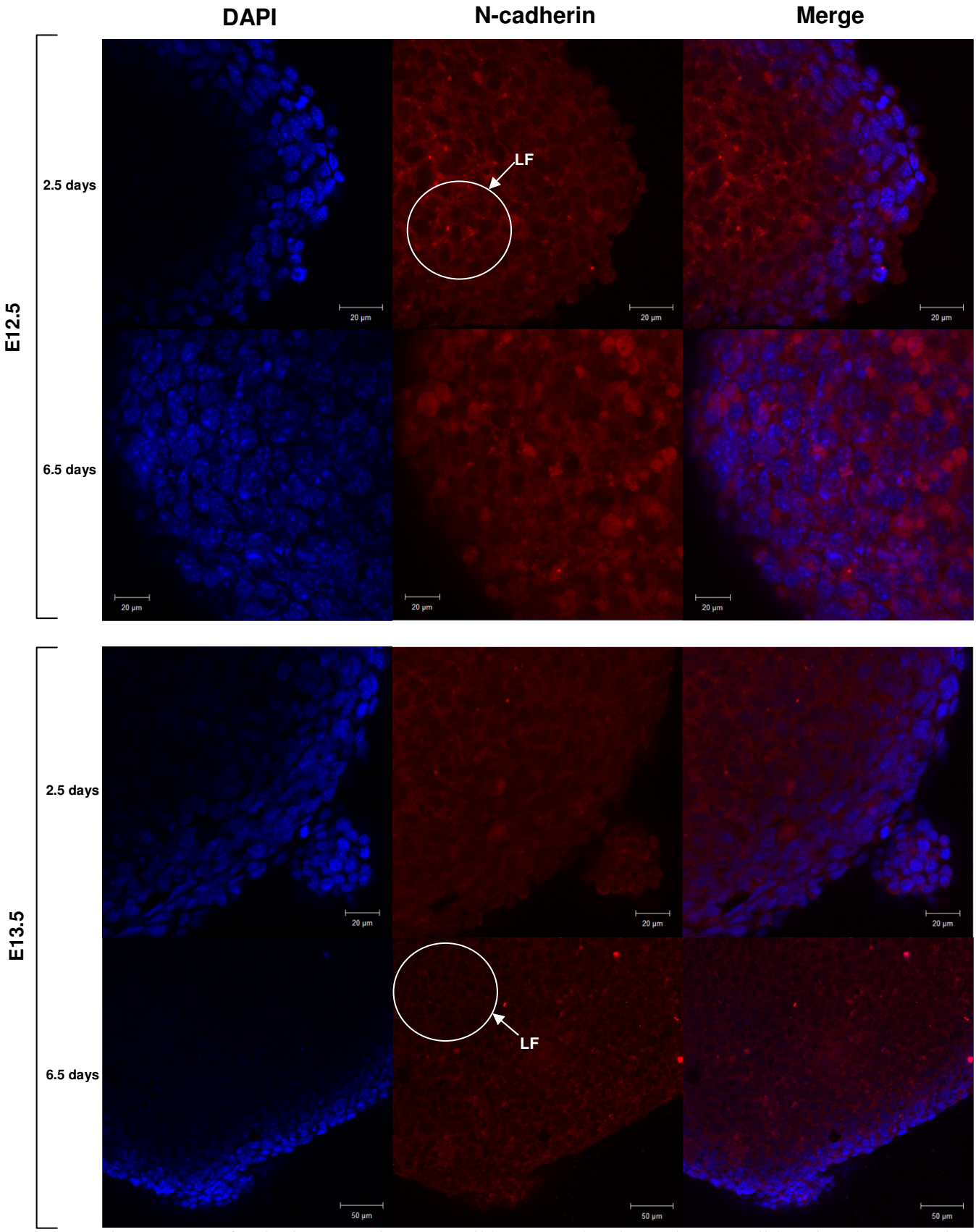

Figure 33: Confocal microscopy images - wildtype E12.5 and E13.5 POM cell hanging drops showing distinct localization of N-cadherin at the cell membrane at contact points between cells in a clear lattice formation (LF). DAPI stains nuclei blue, and Cy3 detects N-cadherin in the red channel.

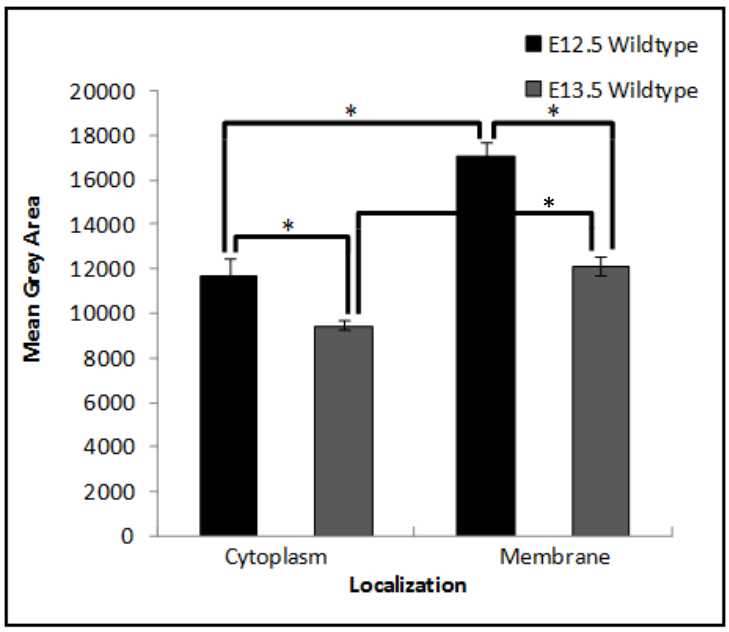

Figure 34: Mean grey area values indicating N-cadherin expression and localization within E12.5 and E13.5 POM cells in hanging drop culture (* = $p < 0.05$; $n = 3$; P10).

Analyses indicated significantly greater amounts of N-cadherin in E12.5 POM cells than in E13.5 POM cells, at both the cell membrane and within the cytoplasm ($p = 2.76363 \times 10^{-6}$; 0.007823414) in hanging drop spheroids (Figure 34). Both E12.5 and E13.5 POM cell lines show significantly more N-cadherin localized at cell membranes at points of contact between adjacent cells than within the cytoplasm ($p = 2.21648 \times 10^{-5}$; 1.98102×10^{-5}).

CHAPTER 5: DISCUSSION

The morphological process referred to as epithelial-mesenchymal transition (EMT) and the reverse process of mesenchymal-epithelial transition (MET) play vital roles during the progression of embryogenesis (Mani et al., 2008). These two processes include a series of cellular conversions whereby the phenotype of cells is changed. The development and generation of most adult tissues and organs arises from the initiation of one of these two key processes (Theiry et al., 2009). It has been postulated that migrating cranial neural crest cells undergo a mesenchyme-to-endothelium (MEndT) conversion (hypothesised to be influenced by lens signalling) once they occupy the space adjacent to the lens epithelium and head surface ectoderm in order to successfully form the corneal endothelium (Kidson et al., 1999).

In order for cells to migrate and proliferate, changes in gene expression are necessary (Zelenka & Arpitha, 2008). These changes are orchestrated by signals generated by epithelial cells or neighbouring cell types and often result in changes in nuclear transcription (Zelenka & Arpitha, 2008). Studies suggest that a number of genes play vital roles and are actively involved in differentiation and patterning of the neural crest cells that give rise to ocular tissues (Lwigale & Bronner-Fraser, 2007). A group of transcription factors have been shown to be able to initiate and carry out EMT programmes during embryonic development and in cancer (Polyak & Weinberg, 2009). These include direct transcriptional repressors of E-cadherin such as *SnAI1*, *SluG* (*SnAI2*), and indirect repressors such as *Foxc2* and Foxc1 (Polyak & Weinberg, 2009).

In the eye, *Foxc1* is expressed in POM cells that give rise to ocular drainage structures such as the iris, cornea, and trabecular meshwork (Kidson et al., 1999; Chakrabarti et al., 2009). In the absence of *Foxc1*, the corneal endothelium fails to develop in mice (Kidson et al., 1999). *Foxc1* is implicated as possibly being part of the downstream signalling cascade of lens secreted factors directing POM cell differentiation into endothelium (Kidson et al., 1999).

In situ hybridization studies indicates that within the developing eye, changes in cadherin expression coincide with cell fate determination and major morphological events, such as lens induction, corneal endothelium differentiation and formation of the retinal pigmented epithelium (Xu et al., 2002). N-cadherin is considered to be a key marker of differentiation in the corneal endothelium and is actively expressed during corneal endothelium development (Ko et al, 2007; Xu et al., 2002). Its expression in the corneal POM is first seen in mice when the corneal endothelium cells begin to differentiate from this mesenchyme cell population, and is maintained in mature corneal endothelial cells (Xu et al., 2002).

Data suggest that any interference in the proper differentiation of the corneal endothelium during early ocular morphogenesis results in the initiation of a cascade of developmental alterations in the anterior segment structures (Reneker et al., 2000). It has been suggested that the expression of N-cadherin may be a key step in initiating the mesenchymal to endothelial transition that results in the correct development of the corneal endothelium (Beebe & Coats, 2000) and that *Foxc1* may target early junction components between corneal endothelial cells (Kidson et al., 1999). However, this theory has yet to been assessed.

This study aimed to comprehensively establish whether *Foxc1* played a role in adherens junction formation in corneal endothelium development by regulating *N-cadherin* expression in POM cells. Vector systems targeting *Foxc1* gene expression were developed and these over-expression and knock-down vector systems were then used in POM cell transfections. Gene and protein expression analyses were carried out to determine the effect of these plasmids on N-cadherin expression at E12.5 and E13.5. The effect of *Foxc1* expression on the expression of the homeobox gene *Msx1* was also assessed in these POM cell lines. Calcium-dependent adhesion molecules are proposed to be targeted by *Hox* genes for regulation (Hatta et al., 1988), and *Msx1* has been shown to decrease cadherin-mediated adhesion *in vitro* (Hartsock and Nelson, 2008). *Msx1* gene expression is down-regulated at E12.5 when adherens junction formation occurs in the periocular mesenchyme (Lincecum et al., 1998), implicating it as a candidate gene for study in the process of corneal endothelium development. N-cadherin protein expression and localization in POM cells was evaluated in a both monolayer and 3-dimentional culture models by confocal microscopy.

5.1. Subtle differences in cell morphology are visible in POM cells at E12.5 and E13.5

Previously described as precursor cells to a number of anterior segment tissues, POM refers to migrant cells predominantly composed of forebrain neural crest cells (Reneker *et al*., 2000; Hsieh et al., 2002; MacDonald et al., 2004, Gage et al., 2005 Ittner *et al*., 2005). These cells give rise to a number of ocular tissues including the corneal endothelium (Reneker *et al*., 2000; Cvekl & Tamm, 2004). POM cells provide a working *in vitro* model to evaluate the processes leading to the corneal endothelium differentiation. In this study, we used primary cultures of murine POM cells derived from wildtype embryos at E12.5 and E13.5. These cells were immortalised by infection with the SV40 Large T-antigen.

Morphologically, cells at these concurrent points in development show minor differences, although not remarkably apparent. At E13.5, the phenotype of migrating cranial neural crest cells in the periocular space changes from stellate to elongated as a result of altered cell-cell and cell-lens interactions (Kidson et al., 1999). However, in culture, cells at E12.5 are distinctly more spindle-like

in appearance, whilst a minor population of cells at E13.5 are beginning to take on a subtle more stellate, cuboidal appearance, and are interspersed amongst cells with spindle morphology. In culture, E12.5 POM cells appeared to adhere more strongly to culture vessel surfaces, and required greater agitation during trypsinization to encourage cells to detach and form a suspension. The two cell lines also showed major differences in transfection efficiencies, with the E13.5 POM cells taking up plasmids with greater ease than the E12.5 POM cell line. This serves as evidence that the two lines are different. Experiments were also performed at the lowest possible passage number to ensure that any variability in the haplotype of the derived cell lines did not confound the data.

5.2. *Foxc1* and *N-cadherin* are concurrently expressed in POM cells

N-cadherin expression is modulated principally by two mechanisms; a decrease in mRNA levels or phosphorylation/dephosphorylation, which determines if N-cadherin remains expressed or is targeted for proteolysis (Van Aken et al., 2000). It is thought that the cadherins require a signal mediated by *Foxc1* to mediate their expression (Kidson et al., 1999). Using *Xenopus* sp. as a model organism, deletion of *Foxc1* was shown to result in a decrease in cadherin expression in the mesoderm, leading to decreased adhesion between these cells (Cha et al., 2007).

Studies show lens signalling to induce differentiation of cranial neural crest cells within the eye (POM cells) to form the corneal endothelium by directing several transcription factors (Kidson et al., 1999; Beebe & Coats, 2000; Ito et al., 2009). Gene analysis experiments carried out using POM cells isolated from embryos at E12.5 and E13.5 show an abundance of *Foxc1* at E12.5 (Figure 15). This expression was slightly, but significantly, down-regulated by E13.5, confirming expression patterns previously seen by Kidson et al. (1999). Beebe & Coats (2000) reported that lens signalling directed transcription factors between E4 and E15 to initiate N-cadherin expression in the presumptive corneal endothelium, confirming Kidson et al.'s (1999) hypothesis that *Foxc1* may target ZO-1 or early junction components such as the cadherins between corneal endothelial cells.

Kidson et al. (1999) proposed that there is an increase in the expression of cadherins resulting in cadherin-mediated cell-cell contact. Indeed, *N-cadherin* expression levels were found to be significantly higher at E12.5 relative to E13.5 (Figure 18). N-cadherin expression in these cells serves not only to maintain the initial structural integrity required for the corneal endothelium to develop at this stage, but the protein is also thought to carry out a transcriptional regulator function (Van Aken et al., 2000; Zhu et al., 2007). Such data imply that *Foxc1* may be a transcriptional regulator of *N-cadherin* and that *N-cadherin* is a downstream target of *Foxc1*. It must be noted that basal levels of both *Foxc1* and *N-cadherin* are higher at E12.5, when these POM cells are transitioning to epithelium, relative to E13.5. *Foxc1* may therefore up-regulate *N-cadherin* gene expression at E12.5 when

adherens junction and their component molecules are actively being to be formed to facilitate corneal endothelium development.

5.3. *Foxc1* expression exerts a regulatory effect on *N-cadherin* expression

The hypothesis that *Foxc1* acts as a transcriptional regulator of *N-cadherin* is supported by transfection experiments in which POM cells were transfected with the p*Foxc1*-eGFP expression vector (Figure 19). *N-cadherin* expression dropped slightly but significantly (20%) in the E12.5 POM cells, but increased significantly (85%) in E13.5 POM cells, indicating that exogenously-induced increases in *Foxc1* expression affect *N-cadherin* expression in POM cells at both these stages. Induced ectopic expression of *Foxc1* has previously been shown to decrease *E-cadherin* expression in cancer cell lines, resulting in these cells undergoing a complete epithelial to mesenchyme transition (Polyak & Weinberg, 2009). Such studies implicate *Foxc1* as a regulator of cell-cell adhesion (Cha et al., 2007). *N-cadherin* decreases upon over-expression of *Foxc1*, indicating that a maximum threshold level may exist for *Foxc1* to exert its transcriptional control over *N-cadherin* at E12.5, which if exceeded, negatively feeds back to decrease *N-cadherin* to acceptable predetermined levels in the cell. Even though the opposite occurs at E13.5, and *Foxc1* over-expression increases *N-cadherin* transcript abundance, it indicates that *Foxc1* directly affects the transcription of *N-cadherin*, as these cells already possess lower levels of both *N-cadherin* and *Foxc1*. It must be mentioned that the differences in *N-cadherin* expression between cell lines cannot be compared following transfection, due to extreme differences in transfection efficiencies between the two cells lines where E13.5 POM cells take up the p*Foxc1*-eGFP plasmid much more effectively than the E12.5 POM cells (transfection efficiency was almost ten-fold greater in E13.5 cells) (Figure 17).

When taken in conjunction with threshold levels of *Foxc1* in wildtype cells at these stages, it implies that there exists a finely balanced threshold range for *Foxc1* to exert its regular effects at both E12.5 and E13.5. These data also imply that the effect of *Foxc1* on *N-cadherin* expression is dose dependent and finely regulated, and that fluctuation out of the tightly specified range, assessed here by increasing *Foxc1* exogenously, results in fluctuating levels of *N-cadherin*. Such fluctuations are hypothesised to result in improper separation of the corneal endothelium from the lens epithelium.

5.4. *Foxc1* a possible downstream target of *Msx1*?

qPCR gene expression analyses also show POM cells at E13.5 to express greater levels of the homeobox gene *Msx1* relative to POM cells derived at E12.5 (Figure 20). *Msx1* is down-regulated at E12.5, when *Foxc1* and *N-cadherin* are up-regulated and junctions are beginning to form, then up-regulated at E13.5 when both these factors are down-regulated. Interestingly, *Msx1* down-regulation is associated with the terminal differentiation of several cell types (Blin-Wakkach et al., 2001; Katerji et

al., 2009). In general, *Msx1* gene expression is restricted to cells that are proliferating (Blin-Wakkach et al., 2001; Chung et al., 2010). Such data implies that *Msx1* may be a downstream target of *Foxc1* that is subjected to transcriptional repression by *Foxc1*. However, signalling molecules such as *Msx1*, *Msx2*, *Dlx5*, *Pax3*, *Pax7*, and *Zic1* are considered to be initiators of a transcription cascade that specify neural crest cells (Morales et al., 2005; Theiry et al., 2009). In fact, *Msx1* expression specifically is considered necessary for the survival and proliferation of cranial neural crest cells (Theiry et al., 2009; Kulesa et al., 2010). Studies have indicated that in the absence of *Msx1*, differentiation of the mesenchyme and establishment of certain craniofacial structures is defective (Katerji et al., 2009). Factors like *Msx1* and *Msx2* are expressed in order to initiate the expression of a variety of other factors including *Foxd3*, *Sox* factors, *Snail1* and *Snail2* that have been implicated in the initiation of different programs in these neural crest derived cells (Morales et al., 2005; Trainor, 2005; Theiry et al., 2009). *Snail1* is thought to facilitate EMT by regulating cadherin expression (as seen in tumors) while *Snail2* is known to trigger EMT in both the chick and amphibian models (Morales et al., 2005). *Foxd3* expression results in cells undergoing EMT and delaminating from the neural tube (Morales et al., 2005). In the neuroepithelium, changes in *Foxd3* expression result in *N-cadherin* being down-regulated (Morales et al., 2005). Such information then implies that, like *Foxd3*, *Foxc1* expression may be a target that is regulated by *Msx1* and that this in turn results in N-cadherin expression being controlled. *Msx1* may hypothetically be a transcriptional regulator of *Foxc1* expression, which in turn regulates *N-cadherin* expression, or it may be that these two EMT/MET factors interact with and regulate expression of each other to synergistically regulate N-cadherin in POM cells. Further studies looking at the effect of *Msx1* gene expression on *Foxc1* expression at both the gene and protein levels need to be carried out to extensively evaluate this theory.

In further experimentation, POM cells at E13.5 subjected to *Foxc1* over-expression resulted in an increase in *Msx1* expression (Figure 21). This increase is may be in response to excess amounts of *Foxc1* that are being produced in POM cells at this stage when basal levels of *Foxc1* transcript are ordinarily lower, in an attempt to repress *Foxc1* expression. Recent data implies that extensive crosstalk does occur between the transcription factors mentioned above, resulting in a signalling network that is able to establish and maintain cell phenotypes (Polyak & Weinberg, 2009).

5.5. Total N-cadherin protein expression is marginally but non-significantly affected by *Foxc1* knock-down

Skarie & Link (2009) showed *Foxc1 k*nockdown to result in defects in vascular endothelial cell fate and differentiation in zebrafish. The cornea of *Foxc1* knockout mice showed disrupted junctional complexes between cells (Kidson et al., 1999), while zebrafish with *Foxc1* knockdown show thickened cornea with fewer corneal endothelial cells and poorly condensing corneal stroma (Skarie

& Link, 2009). A *Foxc1* knock-down plasmid was therefore developed to assess the effect of Foxc1 knock-down on N-cadherin expression in POM cells. Western blot analysis confirmed the functional efficacy of the *Foxc1* knock-down plasmid that was developed, with protein expression showing ~91% and ~94% *Foxc1* knock-down in E12.5 and E13.5 POM respectively (Figure 22/23). This plasmid was then used to assess the effect of *Foxc1* expression knock-down on N-cadherin protein expression using total protein analysis and confocal microscopy. Although western blot analyses showed no significant differences in N-cadherin expression in POM cells transfected with *Foxc1* over-expression or silencing vectors, confocal microscopy analyses substantiated the results of the gene expression analyses. *Foxc1* expression appears to affect N-cadherin protein localization predominantly, with expression being affected to a lesser degree. Discrepancies between the data generated from western blot and those seen in confocal microscopy imaging may possibly be explained by the use of two different antibodies (a different antibody was used in Western analyses since the initial antibody used in ICC targeted an extracellular domain and failed to effectively recognize N-cadherin in total cell lysates when applied to Western blotting), as both techniques are considered to be highly sensitive in the detection of specific target proteins.

5.6. N-cadherin expression and localization differs in E12.5 and E13.5 POM cells

The corneal endothelium monolayer is comprised of polygonal cells, each between 4-6µm thick, arranged in a cohesive monolayer (Joyce, 2003). The patterning of corneal endothelial cell membranes shows similar morphology to mesoderm-derived endothelia of vascular origin and it is due to the morphological homology that this epithelial lining has historically become known as an endothelium (Gordon & Wood, 2009). N-cadherin is considered to be a key marker of differentiation in the corneal endothelium and is actively expressed during corneal endothelium development (Ko et al, 2007; Xu et al., 2002). Migrating neural crest cells weakly initially express N-cadherin at focal contact points between cells (at the tip of cell processes) even though expression must be down-regulated in order for cells to migrate away from the neural tube (Luo et al., 2006). N-cadherin expression in the corneal POM is first seen in mice when the corneal endothelium cells begin to differentiate from this mesenchyme cell population (Xu et al., 2002). Immunohistochemistry shows N-cadherin to cluster in adherens junctions, with staining resulting in a distinct honey-comb pattern (Van Aken et al., 2000). Images captured using POM cells at E12.5 and E13.5 in this study clearly report this phenomenon.

Data taken from confocal microscopy imaging corroborated data from gene expression analyses, with wildtype POM cells showing decreased N-cadherin protein expression at E13.5 relative to cells at E12.5. N-cadherin showed over-all higher expression levels at cell membranes than in the cytoplasm in both cell lines. N-cadherin was abundant in E12.5 cells, with slightly more protein at the membrane than in the cytoplasm. In E13.5 POM cells, the total N-cadherin was less than that seen in E12.5

POM, but expression is proportionally more at the membrane than in the cytoplasm. This can be explained by the fact that E13.5 POM cells are at a later differentiation stage than E12.5 POM cells, with these later stage cells assembling the membrane junctions required for the formation of a cohesive monolayer. Expression in wildtype cells, although abundant and present in excessive amounts, appeared diffused and dispersed in pools throughout the cytoplasm and peri-nuclearly in E12.5 POM, with increased amounts of N-cadherin at points of contact between cells. N-cadherin showed a more specific expression pattern in E13.5 cells with distinct localization at the cell periphery. There is no localization of N-cadherin within the nucleus (stained blue by DAPI) in both E12.5 and E13.5 POM cells.

In order to assess junction formation in a more 3-dimensional setting, cell spheroids were prepared by means of the hanging drop technique. The hanging drop method is based on the natural behaviour of cells to aggregate without the assistance of polymer scaffolds such as Matrigel or any form of microporous support. This form of culture also avoids the use of additives to increase mobility or enhance affinity, precluding possible material artifacts (Kelm et al., 2003). Spheroid culture such as this allows for the processes that occur during differentiation to be evaluated whilst conserving morphogenic capacities and maintaining functional activity and gene expression patterns (Kelm et al., 2003).

The aggregates cultured using E12.5 and E13.5 POM cells showed a similar picture to monolayer cells in terms of N-cadherin expression, with significantly more N-cadherin in E12.5 cells than in E13.5 cells at both the cell membrane and within the cytoplasm. However, there was significantly more N-cadherin localized at cell membranes in both E12.5 and E13.5 POM cell hanging drops. The gravitational force exerted on cells in suspension may be a driving force in encouraging contact between individual cells as they fall to the bottom of the droplet of medium and aggregate in a cluster, allowing for junction formation to be assessed more clearly. Cell aggregates comprised of E12.5 POM cells showed marked N-cadherin expression by day 2.5 with a clear lattice pattern formed by junctions between adjacent cells. The clarity of this lattice pattern began to decrease by day 6.5 due to the increased size of the cell mass; however, a number of individual cells in the spheroid were showing robust N-cadherin expression across the entire exposed surface. Cells directly adjacent to these cells were gradually beginning to showing a similar expression pattern. Cell clusters using E13.5 cells showed a similar expression pattern to monolayers, with relatively less expression of N-cadherin at both day 2.5 and day 6.5, however the lattice pattern made by cell boundaries was still clearly visible.

Over all, N-cadherin appears to be found within the cytoplasm and abundantly at the cell membranes in both E12.5 and E13.5 POM cells, with subtle differences in cytoplasmic N-cadherin between the cell lines. Monolayers show that N-cadherin appears to have been synthesised in excess by E12.5

POM cells in preparation for the assembly of adhesion junctions. These protein molecules are already being shuttled to the cell boundaries by E12.5, and have been assembled into functional junctional complexes by E13.5, evident by the distinct honeycomb, lattice pattern seen in the 3-dimensional hanging drop cultures. Excess cytoplasmic pools of N-cadherin protein are scarce at E13.5 (both in monolayers and hanging drops), implying that free molecules not shuttled to the cell membrane and sequestered by the junctional complexes may have been targeted for proteolysis by the cell. Differential cadherin expression is proposed to mediate cell sorting – switching cadherin expression results in the aggregation of cells into specific, different cell populations (Pontoriero et al., 2009). Such differential expression is thought to occur during POM cell differentiation, and is noted to occur between the E12.5 and E13.5 stages when the corneal endothelium is being formed by the assembly of N-cadherin based adhesion junctions. The maintained expression of N-cadherin in the corneal endothelium that follows junction formation is not only considered vital in maintaining the specific physiological functions of the corneal endothelium, but is also thought to contribute to the eventual successful formation of a cohesive cell monolayer (Reneker et al., 2000; Ramachandra & Srinivas, 2010).

5.7. N-cadherin protein synthesis and localization is affected by *Foxc1* expression

The number of N-cadherin molecules expressed in a cell directly influences its adhesive ability, in turn modulating the overall morphology of a group of cells; in this way, by control of cadherin expression, selective adhesion is conferred to a specific subset of cells (Takeichi, 1991). Such predetermined modulation of cadherin expression may function in cell segregation during morphogenesis and is thus an important determinant in tissue morphology (Takeichi, 1991). Our data suggests that cadherin expression and localization is affected by changes in *Foxc1* expression.

Over-expression of *Foxc1* decreased total N-cadherin expression at E12.5 while expression was not significantly altered at E13.5. E12.5 cells showed a less diffused, perinuclear and peripheral N-cadherin localization, with higher membraneous expression than cytoplasmic. E13.5 cells showed excessive, increased cytoplasmic expression while membrane-localized expression remained fairly stable.

Silencing Foxc1 expression by means of a knock-down plasmid resulted in significant decreases in N-cadherin expression (both membrane and cytoplasmic) at E12.5 with distinct, pooled protein expression at cell membranes at points where individual cells overlapped and made contact. Total N-cadherin expression increased significantly in cytoplasm of E13.5 POM cells, with N-cadherin appearing to be scattered in dense pools, however, there were no significant changes in expression at the membrane. No real changes in N-cadherin distribution were noted in either cell line.

The data from *Foxc1* over-expression/knock-down studies on E12.5 and E13.5 POM cells together suggests that N-cadherin is transcriptionally regulated by *Foxc1*. The results collectively suggest a threshold level required for *Foxc1* to exert its effects on N-cadherin in POM cells, corroborating the theorized dose dependant effect of *Foxc1*. *Foxc1* activity is thought to have strict upper and lower thresholds in place to drive the normal development and functioning of the eye. This dose-dependent effect is supported by studies showing that both mutations causing reduced *Foxc1* activity and chromosome duplications creating an extra copy of *Foxc1* result in debilitating ocular defects (Huang et al, 2008).

This study suggests that whilst *Foxc1* exerts regulatory control over N-cadherin expression, the regulation appears to be finely modulated by very specific amounts of *Foxc1*. *Foxc1* is maintained at a specific threshold level in each cell line and not down-regulated to complete absence in E13.5 POM cells. These data suggest that *Foxc1* regulation of N-cadherin is very dose-specific/dose dependent and that there exists a threshold level at which *Foxc1* exerts its specific effects on N-cadherin. If this level is exceeded or if the levels of *Foxc1* fall below this threshold, N-cadherin levels become disregulated, and the cell initiates mechanisms to ensure that N-cadherin is maintained at a predetermined basal level. N-cadherin may have a self-regulating negative feedback mechanism in place to maintain expression levels at a basal level if *Foxc1* expression is disregulated at E12.5. Any excess cytoplasmic N-cadherin may become sequestered and targeted for ubiquitination if *Foxc1* levels are not at the required threshold. In E13.5 POM cells, which usually express lower levels of N-cadherin, fluctuations in *Foxc1* result in N-cadherin levels increasing, again re-iterating the dose-dependent effect of *Foxc1*.

5.8. Conclusions

Previous studies suggest that elevated/decreased levels or enhanced/reduced activity of FOXC1 are equally detrimental during development (Huang et al, 2008). The precise control of FOXC1 activity is thus considered paramount for this transcription factor to carry out its proper function and for the prevention of ocular disease phenotypes. The results of this study substantiate this idea.

Experiments with *Foxc1* over-expression indicate that a maximum threshold level may exist for *Foxc1* to exert its transcriptional control over N-cadherin. Taken together, these results suggest a negative feedback mechanism for control of N-cadherin protein expression in POM cells at E12.5, whereby N-cadherin may be self-regulated and targeted for proteolysis to decrease proteins to acceptable predetermined levels when levels within the cell become excessive. Silencing of *Foxc1* at E12.5 appears to affect the shuttling of N-cadherin. This is most likely through the regulation of other intermediate factors participating in the shuttling and membrane junction assembly processes.

The data also points towards an interaction between *Foxc1* and *Msx1* in POM cells, with preliminary data suggesting that *Foxc1* may be a target regulated by *Msx1*, modulating N-cadherin expression indirectly. *Msx1* may transcriptionally repress Foxc1 expression, in turn repressing N-cadherin expression. All three elements play major roles in the neural crest cell specification and differentiation, and even though the two transcription factors are organized in a specific functional hierarchy alongside other factors, the idea has been suggested that factors involved in EMT/MET are able to regulate expression of each other in certain instances (Theiry et al., 2009). *Msx1* has previously been described as a transcriptional repressor which impedes terminal differentiation, explaining its down-regulation at E12.5 (Petit et al., 2009), but is also known to enhance proliferation, which then clarifies its up-regulation at E13.5. Further studies evaluating *Msx1* gene and protein expression alongside *Foxc1* with the aid of expression vectors need to be carried out in POM cells to assess this hypothesis fully.

The hanging drop culture method has also proven to be a novel and viable method with which to assess junction formation in POM cells. However, incubation times and their effect on spheroid growth and cell mass must be carefully considered. Studies in which human mesenchymal stem cells (hMSC) were subject to hanging drop culture have shown that a greater number of cells become apoptotic/ necrotic in larger spheroids, and this becomes a factor to contend with during longer incubation times (Bartosh et al., 2010). Taking such knowledge into consideration, future studies should look into transfection of cells with *Foxc1* expression or knock-down vectors prior to spheroid culture, as this method presents an excellent mechanism with which to view junction formation in a more structurally realistic way. The interactions between *Snail1*, N-cadherin and *Foxc1* should also be evaluated in order to elucidate their functional relationship in junction formation during corneal endothelium development.

CHAPTER 6: APPENDICES

Appendix 1: 10 x TBE / 1 x TBE

To make 500ml of a 10 x TBE stock solution, add 53.89g Tris base (0.89M), 27.51g boric acid (0.89M) and 1.861 EDTA (0.01M) to 400ml of distilled water. Adjust the pH of the solution to 8.3 and make the solution up to a final volume of 500ml with distilled water. Autoclave the solution and store at 4˚C.

To make 1l of a 1 x TBE working solution, add 900ml distilled water to 100ml of 10 x TBE stock solution.

Appendix 2: Ligation of ShRNA Sequences into the pGEM-T Easy Plasmid Vector

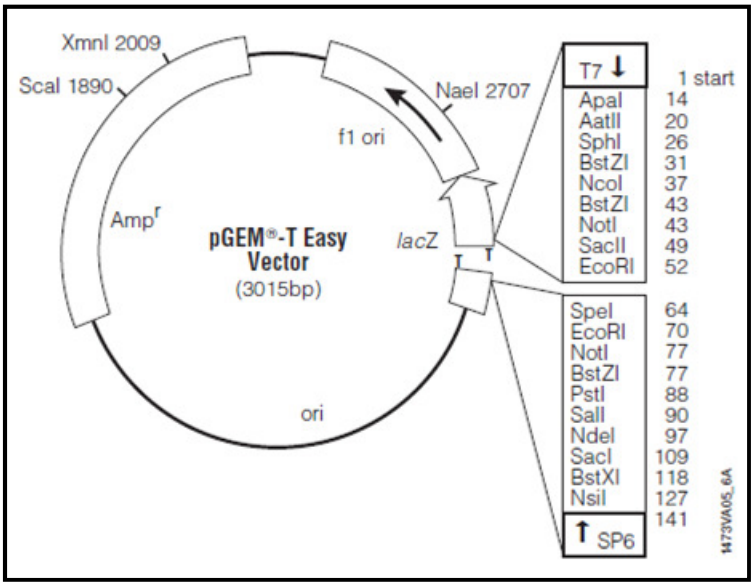

Figure 1: Plasmid vector map – pGEM- T Easy.

Ligation reactions were set up for each ShRNA sample, as well as for a positive control, as per the table below. Reactions were triturated with a pipette and incubated overnight at 4°C to ensure a maximum number of transformants.

	Positive Control	**ShRNA**
Deionized H_2O (to bring volume to 10)	1 µℓ	x µℓ
2x Rapid Ligation Buffer	5 µℓ	5 µℓ
PCR Product DNA Insert		x µℓ (15ng)
Control Insert DNA	2 µℓ	
pGEM-T Easy Vector	1 µℓ	1 µℓ
T4 DNA Ligase	1 µℓ	1 µℓ
Final Reaction Volume	**10 µℓ**	**10 µℓ**

Appendix 3: Transformation of DH5α Competent Cells with Plasmid Vectors

A sufficient amount of LB broth was heated to room temperature in a centrifuge tube. Ligation reaction tubes were centrifuged and 2µℓ of each ligation reaction was transferred to microcentrifuge tubes on ice. DH5α cells were thawed in an ice bath for 5 minutes and flicked gently to resuspend. 50µℓ of the competent cell suspension was transferred into each prepared ligation reaction microcentrifuge tube. Tubes were gently flicked to mix and placed on ice for 20 minutes. Cells were heat-shocked for 45-50 seconds in a heating block maintained at 42°C, and plunged into ice for 2 minutes. 950µℓ of LB broth at room temperature was added to the transformed cell suspension, and incubated at 37°C for 1.5 hours in a shaking incubator. Cells were centrifuged at 1000 x g for 10 minutes to pellet and 800µℓ of the supernatant was removed to ensure a high colony number. The pellet was reconstituted and cells were plated onto prepared antibiotic agar plates. Prepared plates were incubated overnight at 37°C and transferred to 4°C after this overnight incubation in order to facilitate development of blue colonies. White colonies contain plasmid insert.

Appendix 4: Preparation of Agar plates

500mℓ Luria agar growth medium (Sigma-Aldrich, USA) was prepared as per manufacturer's instructions, and autoclaved to sterilize. Once agar cooled to "baby temperature" 100mg/µℓ Ampicillin Ready Made Solution (Sigma, USA) was added on a microliter:milliliter basis, e.g. if making 500mℓ of agar, add 500 µℓ of ampicillin. The liquid agar was swirled to mix, poured into plates, and allowed to set on the benchtop. Once set, prepared plates were stored in the fridge at 4°C until needed. When plates were required, An X-gal and IPTG master mix was prepared to screen for resistance and plasmid uptake as per the table below:

Antibacterial Master Mix (for 1 plate)*	
IPTG	50 µℓ
X-gal	20 µℓ
H_2O	50 µℓ
Total volume per plate	**120 µℓ**

***Adjust master mix as required if using more than one plate**

120 µℓ of antibacterial master mix was pipetted onto each agar plate and spread across plate surface using a sterilized glass spreader (coat spreader in ethanol and hold over open flame to sterilize). Plates were set aside with lids ajar to allow surface to dry, and closed until needed. Close plates and place aside until needed.

Appendix 5: EcoR1 Restriction Enzyme Digest

Using the MiniPrep-extracted plasmid DNA (approximately ~1µg of DNA) make up reaction mixes in eppendorfs for each sample as outlined in the table below:

Gel Electrophoresis Mix (for each MiniPrep DNA sample)	
MiniPrep DNA (1µg)	x µℓ
Eco-RI	1 µℓ
Eco-RI Buffer	2 µℓ
H_2O	x µℓ**
Final total reaction volume	**20 µℓ**

Reactions in microcentrifuge tubes were incubated in a dry bath incubator maintained at 37°C for 1-2 hours to facilitate restriction digest.

Appendix 6: Plasmid sequencing

ShRNA3

gtgacactatagaatactcaagctatgcatccaacgcgttgggagctctcccatatggtcgacctgcaggcggccgcgaattcactagtgatt
gatctcgagaaggtcgggcaggaagagggcctatttcccatgattccttcatatttgcatatacgatacaaggctgttagagagataattagaattaatt
tgactgtaaacacaaagatattagtacaaaatacgtgacgtagaaagtaataatttcttgggtagtttgcagttttaaaattatgttttaaaatggactatca
tatgcttaccgtaacttgaaagtatttcgatttcttggctttatatatcttgtggaaaggacgaaacaccgcccggacaagaagatcactctcctgaccc
aagagtgatcttcttgtccaatcgaattcccgcggcc**gccatggcggccgggagcatgcgacgtcgggcccaattcgccctatagtgagtcgt
attacaattcactggccgtcgttttacaac**

Accession	Description	Max score	Total score	Query coverage	E value	Max ident
14285		130	130	13%	2e-35	100%

```
Query  346  TTGTGGAAAGGACGAAACACCGCCCGGACAAGAAGATCACTCTCCTGACCCAAGAGTGAT  405
            ||||||||||||||||||||||||||||||||||||||||||||||||||||||||||||
Sbjct  79   TTGTGGAAAGGACGAAACACCGCCCGGACAAGAAGATCACTCTCCTGACCCAAGAGTGAT  20

Query  406  CTTCTTGTCC  415
            ||||||||||
Sbjct  19   CTTCTTGTCC  10
```

Appendix 7: Annealing buffer – pSuper.neo/gfp

To make up annealing buffer, 100 mM NaCl was added to 50 mM HEPES buffer and the solution was pH'ed to 7.4. Nuclease-free water was added to the final volume. The solution was alliquoted and stored at 4˚C until needed.

Appendix 8: Ligation of Oligonucleotides into pSuper.neo/gfp Vector

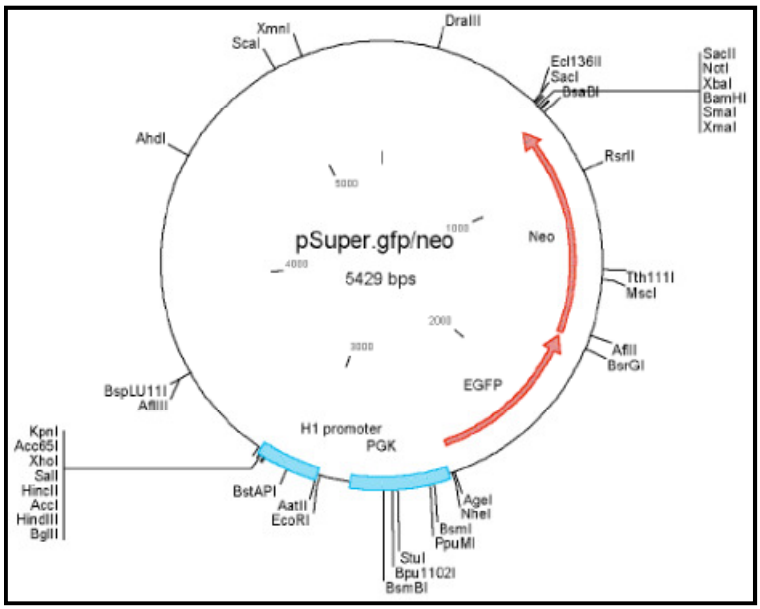

Figure 2: Plasmid vector map – pSuper.neo/gfp.

Deionized H_2O (to bring volume to 10)	5 µℓ
2x T4-DNA Rapid Ligation Buffer	1 µℓ
Annealed oligos (3mg/ml)	2 µℓ
pSUPER Vector (0.5 mg/ml)	1 µℓ
T4 DNA Ligase enzyme	1 µℓ
Final Reaction Volume	**10 µℓ**

Reactions were incubated overnight at room temperature. A negative control cloning reaction should be performed with the linearized vector alone and no insert.

Appendix 9: BglII Restriction Enzyme treatment

1.0 µl of BglII was added to the ligated plasmid vector, and the reaction was incubated for 30 minutes at 37°. This will ensure that only plasmids containing the insert will be available for transformation - the BglII site is destroyed upon successful cloning of the oligo pair, so those vectors cut by the enzyme will NOT contain the insert fragment.

Appendix 10: EcoR1 and Hind111 Restriction Enzyme Double Digest

Reaction mixes were made in eppendorfs for each sample using the MiniPrep-extracted plasmid DNA (approximately ~1µg of DNA) as outlined in the table below:

Gel Electrophoresis Mix (for each MiniPrep DNA sample)	
MiniPrep DNA (1µg)	x µℓ*
Eco-RI	1 µℓ
Hind111	1 µℓ
Buffer R	2 µℓ
H_2O	x µℓ**
Final total reaction volume	**20 µℓ**

Microcentrifuge tubes were incubated in a dry bath incubator maintained at 37°C for 1-2 hours to facilitate restriction digest.

Appendix 11: BamH1 and Eco-R1 Restriction Enzyme Double Digest

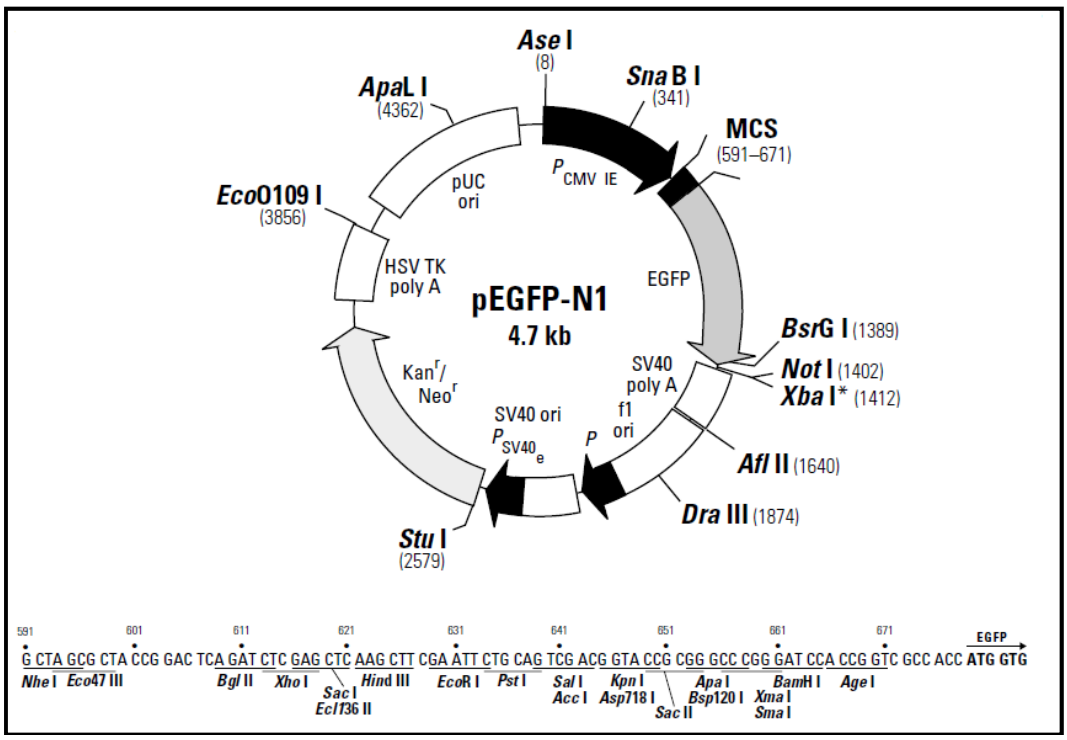

Figure 3: Plasmid vector map – peGFP-N1.

Reaction mixes were made in eppendorfs for each sample using the MiniPrep-extracted plasmid DNA (approximately ~1µg of DNA) as outlined in the table below:

Gel Electrophoresis Mix (for each MiniPrep DNA sample)	
MiniPrep DNA	x µℓ*
Eco-RI	1 µℓ
BamH1	2 µℓ
Buffer R	2 µℓ
H_2O	x µℓ**
Final total reaction volume	**20 µℓ**

Microcentrifuge tubes were incubated in a dry bath incubator maintained at 37°C for 1-2 hours to facilitate restriction digest.

Appendix 12: RNA isolation – TriReagent method

Trypsinised cells were pelleted by centrifugation at 3000rpm for 1 minutue and the medium was carefully removed. 750µl Tri-Reagent (Sigma, USA) was added to the cell pellet which was then reconstituted by vortexing and incubated at room temperature for 5 minutes. 200 µl

chloroform was added to the suspension which was then shaken vigorously for 15 seconds.This suspension was centrifuged at 12000 rcf for 15 minutes, following which the top layer of precipitated RNA was removed and transferred into a new eppendorf. 500µl isopropanol was added to this precipitated RNA, mixed and incubated at room temperature for 7 minutes. RNA was centrifuged at 12000 rcf for 8 minutes to pellet RNA. The supernatant was removed, and the pellet was immersed in 1ml 75% ethanol in RNAse-free water. The pellet was vortexed to dislodge it from the wall of the eppendorf and centrifuged at 6000 rpm for 5 minutes. The supernatant was removed and the pellet was air dried for 5 minutes. The RNA pellet was diluted in 15µl of RNAse-free water by pipetting up and down slowly, follwed by heating at 50-55°C for 10 minutes in a heating block to fully dissolve the pellet.

Appendix 13: Denaturing RNA gel electrophoresis

Note: All apparatus (gel casting tray and comb, electrophoresis gel sub, as well as staining vessels) is to be treated with 10% hydrogen peroxide to ensure that they are RNase-free.

10 x MOPS buffer stock solution was prepared by combining 0.2M MOPS (3-(4-Morpholino)propane sulfonic acid) , 0.05M sodium acetate and 0.1M EDTA in DEPC-treated water (0.1% DEPC water – add 100 µl Diethylpyrocarbonate to 1 ℓ distilled water and incubate at 37˚C without stirring, followed by autoclaving) and pH to 7.0. Buffer was filter-sterilized and stored in an amber bottle at room temperature. If solution turns yellow, discard.

To prepare a 15mℓ RNA gel, 1.5 mℓ 10 x MOPS, 0.17g agarose and 12.75 mℓ DEPC water was added to an autoclaved conical flask tared on a balance. The flask was weighed with the chemicals and the contents were dissolved in a microwave. The conical flask with dissolved agarose was weigh, and the volume was adjusted to the original weight with DEPC-treated water. Once agarose cooled, 750 µℓ of 40% paraformaldehyde (to allow the RNA to denature) was added to the flask. The agarose was swirled to mix and 11 mℓ was pipetted into the gel casting tray. The gel was allowed to set for 30 minutes at room temperature.

The electrophoresis gel sub was filled with 1 x MOPS buffer (dilute 10 mℓ 10 x MOPS with 90 mℓ DEPC-treated water). 10 mℓ DEPC-treated water was added to the volume present in the tank and the cast gel was placed into the prepared tank. Equal volumes of RNA (~20µg) incorporating 2 µℓ of loading dye per sample was loaded into each lane. The gel was run at 80V for an hour and a half or until the dye front was 1.5cm from the end of the gel.

The gel was stained for 2 minutes in ethidium bromide in the MOPS buffer used to run the gel followed by immediate destaining in 1 x MOPS buffer. Bands were visualized immediately. Eukaryote RNA should show 2 bands – one at 5.1kbp (the 28S fragment) and one at 2.0kbp (the 18S fragment).

Appendix 14: N-cadherin expression: Fluorescence, Melt and Amplification Curves

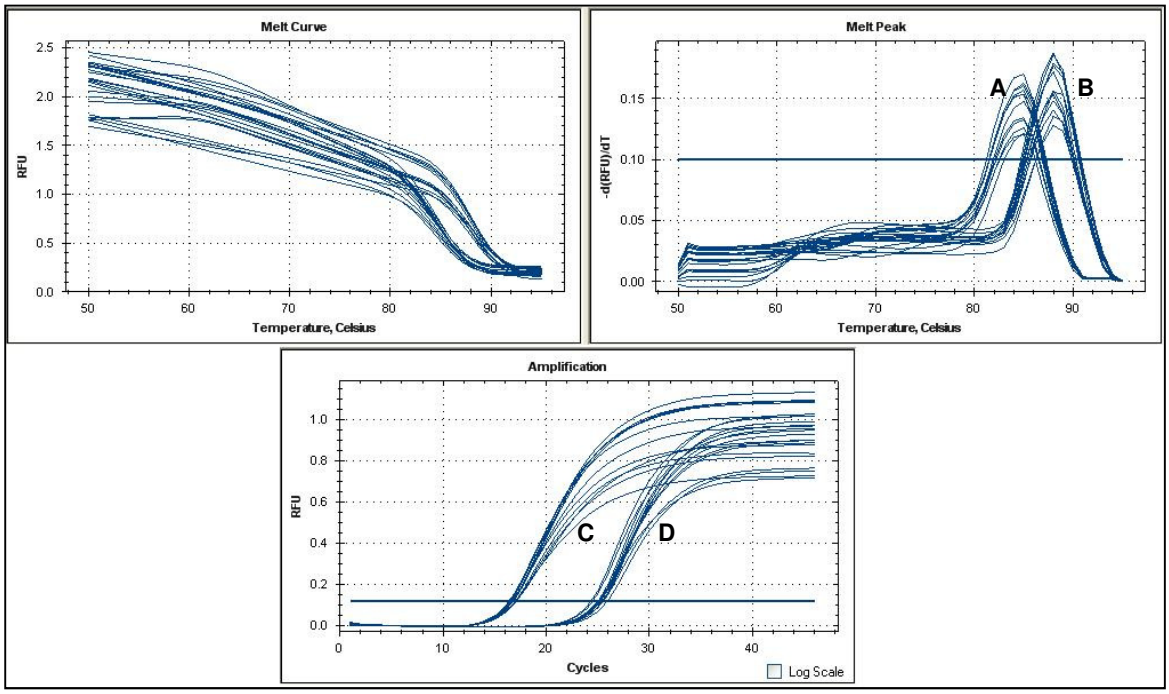

Figure 4: Melt and fluorescence curves – A. *N-cadherin* (T_m = 85); B. *Rps12* (T_m = 88); C. *Rps12* amplification in the FAM fluorescence channel; D. *N-cadherin* amplification in the FAM fluorescence channel.

Appendix 15: Foxc1 expression: Fluorescence, Melt and Amplification Curves

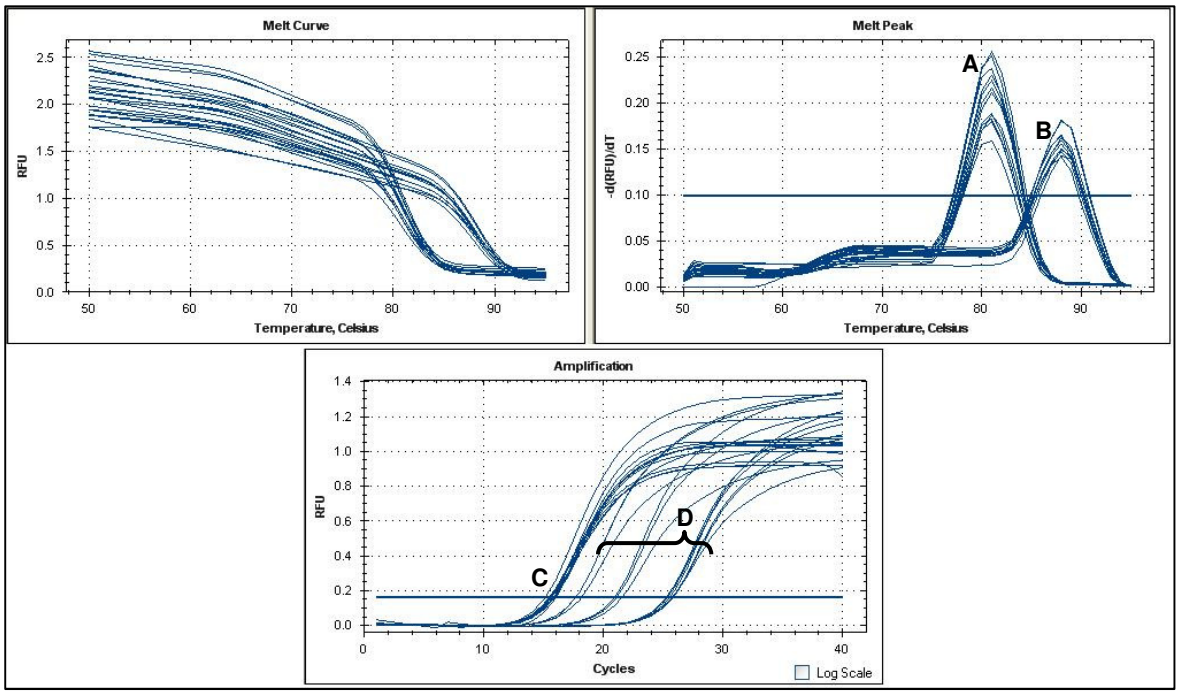

Figure 5: Melt and fluorescence curves – A. *Foxc1* (T_m = 81); B. *Rps12* (T_m = 88); C. *Rps12* amplification in the FAM fluorescence channel; D. *Foxc1* amplification in the FAM fluorescence channel.

Appendix 16: 2x Western Blot Protein Loading Dye (Reducing Sample Treatment Buffer)

2.5 mℓ 4 x SDS-PAGE stacking gel buffer (1.5 M Tris-HCℓ, pH 8.8), 4 mℓ SDS stock solution (10% m/v SDS), 2 mℓ glycerol and 1 mℓ β-mercaptoethanol were combined. The solution was made up to 10 mℓ with deionized water. A sufficient amount of bromophenol blue powder was added to the mixture to turn the solution dark (opaque) blue. The loading buffer was aliquotted and stored at 4˚C

Appendix 17: 12.5% SDS–Polyacrylamide Stacking & Resolving gels

Prepare the following reagents:

4 x Resolving gel buffer (1.5 M Tris-HCℓ, pH 8.8: filter sterilize and stored at 4˚C)

4 x Stacking gel buffer (500 mM Tris-HCℓ, pH 6.8: filter sterilize and stored at 4˚C)

10% (m/v) SDS stock solution (filter sterilize and store at room temperature)

20% (m/v) Ammonium persulfate (APS) initiator solution

To prepare running gel for 1 x 12.5% gel (7.5 mℓ), 3.125 mℓ BioRad 30% Acrylamide/Bis solution, 1.875 mℓ resolving gel buffer, 2.375 mℓ deionized water and 75 µℓ SDS stock solution were added to a 15 mℓ centrifuge tube and inverted to mix. 40 µℓ of APS initiator

solution and 3.75 µℓ TEMED was added and the gel was cast immediately. Cast gel was immediately overlayed with a thin layer of deionized water and allowed to set.

Once resolving/running gel was set, the water was decanted off and excess water was blotted away with filter paper.

To prepare stacking gel for 1 x 12.5% gel (7.5 mℓ), add 0.47 mℓ BioRad 30% Acrylamide/Bis solution, 0.8475 mℓ stacking gel buffer, 2.15 mℓ deionized water and 35 µℓ SDS stock solution and invert to mix. Add 20 µℓ of APS initiator solution and 3.75 µℓ TEMED and cast immediately. Carefully overlay cast resolving running gel with this stacking gel (making sure to place comb in gel to form wells) and allow to set.

Appendix 18: 1x Electrode (Running) Buffer

Note: Prepare freshly on day of use. Do not re-use.

Add 3g Tris-HCℓ, 14.4g glycine and 10 mℓ 10% SDS stock solution to 800 mℓ deionized water. pH to 8.3 and make up to 1ℓ with deionized water.

Appendix 19: Protein Transfer Buffer

Note: Cold buffer is to be prepared freshly each time. Do not re-use buffer.

To prepare 800mℓ of buffer, add 2.424g Tris-base, 11.53g glycine and 0.8g SDS to 160 mℓ methanol and add 440 mℓ deionized water; pH to 8.3 and make up to a final volume of 800 mℓ. Refrigerate until needed.

Appendix 20: 0.05% Tris-Buffered Saline with Tween-20 (TBS-T) Wash Buffer Solution

To prepare 1ℓ, add 8 g NaCℓ, 0.2 g KCℓ and 3 g Tris-base to 800 ml of deionized water. Adjust pH to 7.5 and make up to 1 ℓ. Add 0.5 mℓ Tween-20 to make 0.05% TBS-T.

Appendix 21: 6% Skim Milk Blocking Buffer

Dissolve 3g skim milk powder in 50 mℓ TBS-T buffer solution by gentle agitation on and elliptical orbital shaker.

Appendix 22: 1 x Phosphate Buffered Saline Buffer

To prepare 1ℓ, add 8 g NaCℓ, 0.2 g KCℓ, 1.44 g Na2HPO4 and 0.24 g KH2PO4 to 800 ml of deionized water. Adjust pH to 7.5 and make up to 1 ℓ.

Appendix 23: 16% m/v Paraformaldehyde

Dissolve 16g of paraformaldehyde in 100mℓ deionized water. Filter sterilize, aliquot and store at -20°C until needed.

Appendix 24: 0.5% BSA in 1 x PBS

Add 0.5 g BSA to 10 mℓ 1 x PBS buffer and agitate gently to mix.

Appendix 25: 1:50 dilution of DAPI (50 μg/ml)

Add 1 μℓ of the 50 μg/ml DAPI solution to 49 μℓ of 1 x PBS buffer for each coverslip/well.

Appendix 26: 10% (m/v) Mowiol and 23M glycerol in Tris (0.1M, pH8.5) with DABCO

Dissolved 2.4 g Mowiol in 0.2 M Tris (12 ml) in a closed container, wrapped in foil,and stir over night. Add 6g glycerol and 6 ml d. H_20 and stir over night. Clarify the solution by centrifugation (500 x g, 15 minutes) and add DABCO to 2.5% for to reduce fading during fluorescence detection. Store aliquots in eppendorfs at -20°C.

Appendix 27: Protein Quantification: BCA Protein Assay

Upon isolation, total cellular protein was quantified by means of the BCA Protein Assay. Protein samples were assayed at a 1:10 sample dilution from which the final stock concentration of the protein was derived. Figure shows an example of the standard curve derived from the known concentration of serial dilutions of bovine serum albumin protein (BSA) standards plotted against their absorbance at 526nm (A_{526}). This standard curve produced a linear regression equation (refer to Figure 6) from which the unknown concentrations of the experimental protein samples was calculated.

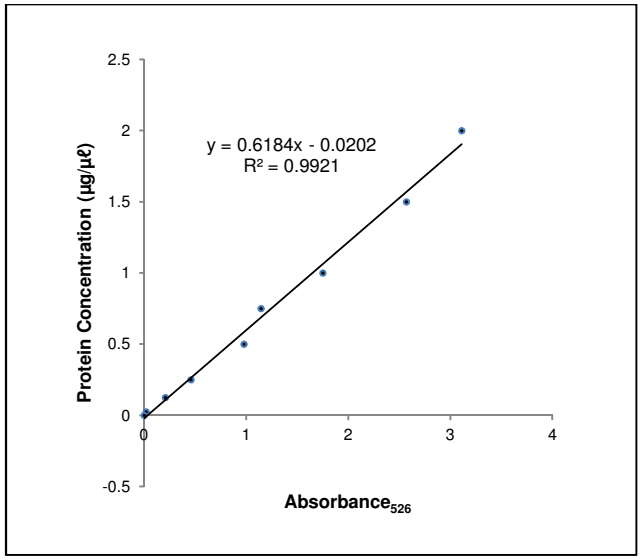

BSA Standard	Concentration (µg/µL)	Absorbance$_{526}$ 1	Absorbance$_{526}$ 2	Mean Absorbance$_{526}$	Mean Absorbance-Blank Absorbance
A	2	3.447	3.007	3.227	3.111
B	1.5	2.507	2.863	2.685	2.569
C	1	1.946	1.788	1.867	1.751
D	0.75	1.262	1.26	1.261	1.145
E	0.5	1.04	1.148	1.094	0.978
F	0.25	0.583	0.566	0.5745	0.4585
G	0.125	0.323	0.324	0.3235	0.2075
H	0.025	0.132	0.137	0.1345	0.0185
I	0	0.108	0.124	0.116	0

Figure 6: BCA Protein Assay standard curve – known protein concentration is plotted against the A_{526}, generating a linear regression equation that may be used to extrapolate the unknown concentrations of samples for which the A_{526} value is known.

The example shows the graph generated in order to assay total protein samples isolated from two confluent 10cm culture dishes per sample treatment for use in Western blots assessing N-cadherin protein expression. Using the linear regression equation generated when the concentration of the standards is plotted against the standardized mean absorbance of the BSA standards at 526nm, the concentration for the unknown samples can be extrapolated using the mean absorbance values detected at A_{526}. The R^2-value of 0.992 associated with the above standard curve indicates that, given the A_{526} of a sample, the concentration of the sample can be accurately predicted. Figure 7 below shows the derived final stock concentrations of two total protein samples.

Sample	A_{526} 1	A_{526} 2	A_{526} 3	Mean	Mean-Standard Blank	µg/µL (1:10)	µg/µL (stock)
POM E12.5$^{+/+}$	2.961	3.031	2.869	2.953666667	2.837666667	4.559331176	45.59
POM E13.5$^{+/+}$	2.778	2.519	2.645	2.647333333	2.531333333	4.06364617	40.63

Figure 7: Derived sample stock concentrations using regression equation from the standard curve generated using BSA standards with known concentration read at A_{526}.

Appendix 28: Confocal Microscopy Antibody Controls

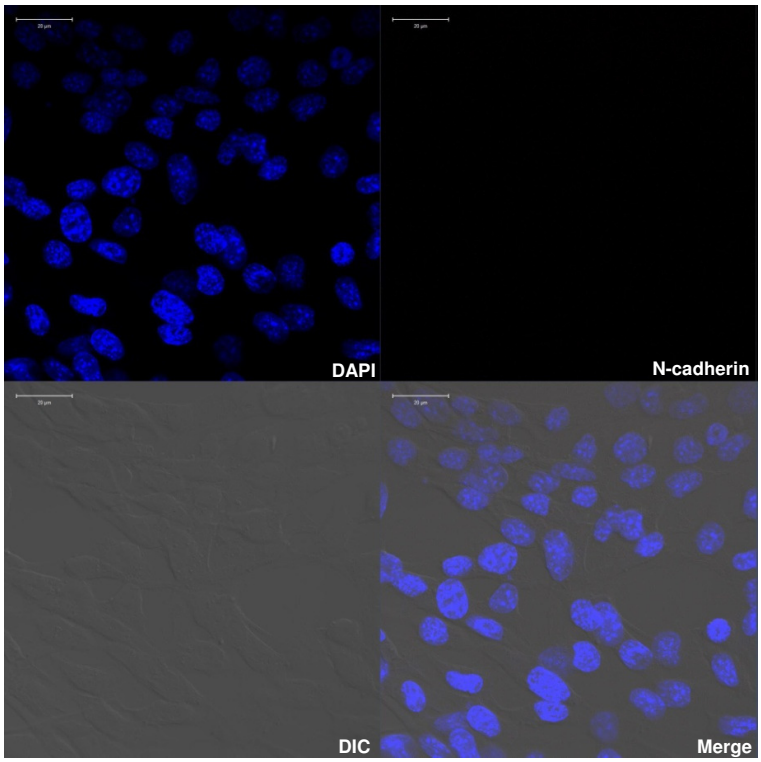

Figure 8: Confocal microscopy images – no-primary antibody control. Dilution of N-cadherin primary antibody optimized to prevent non-specific background from being detected by laser scanning confocal microscopy. DAPI stains nuclei blue, Cy3 detects N-cadherin in the red channel and DIC image shows cell boundaries.

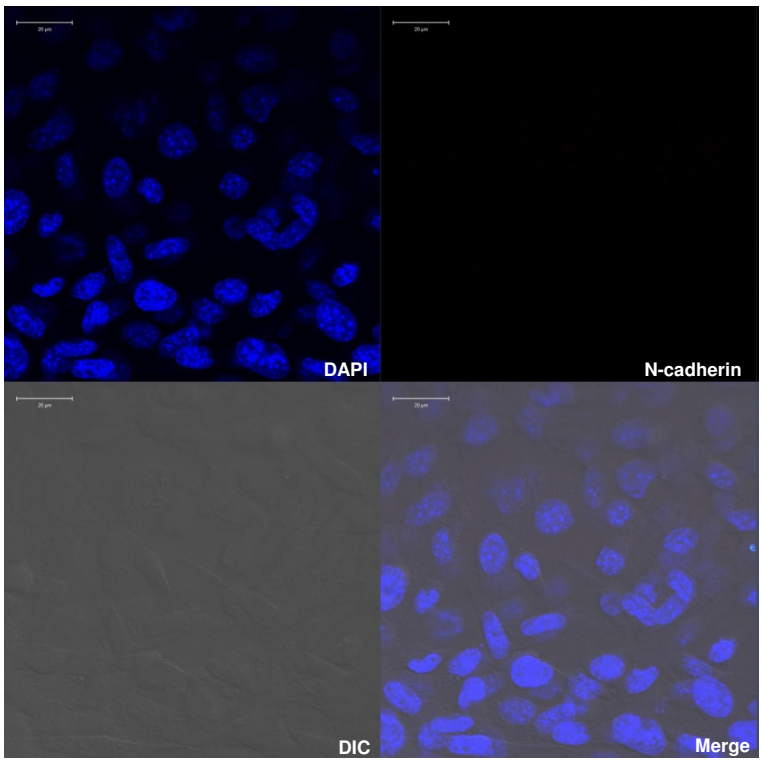

Figure 8: Confocal microscopy images – no-secondary antibody control. Dilution of N-cadherin secondary antibody optimized to prevent non-specific background from being detected by laser scanning confocal microscopy. DAPI stains nuclei blue, Cy3 detects N-cadherin in the red channel and DIC image shows cell boundaries.

CHAPTER 7: REFERENCES

Balda, M.S. and Matter, K. 2009. Tight junctions and the regulation of gene expression. Biochim. Biophys. Acta. – Biomembranes. 1788 (4): 761-767.

Barth, A.I.M., Näthke, I.S. and Nelson, W.J. 1997. Cadherins, catenins and APC protein: interplay between cytoskeletal complexes and signaling pathways. Curr. Opin. Cell Biol. 9:683-690.

Bartosh, T.J., Ylöstalo, J.H., Mohammadipoor, A., Bazhanov, N., Coble, K., Claypool, K., Lee, R.H., Choi, H. and Prockop, D.J. 2010. Aggregation of human mesenchymal stromal cells (MSCs) into 3D spheroids enhances their anti-inflammatory properties. Proc. Natl. Acad. Sci. 107(31): 13724–13729.

Baulmann, D.C., Ohlmann, A., Flügel-Koch, C., Goswami, S., Cvekl, A. and Tamm, E.R. 2002. *Pax6* heterozygous eyes show defects in chamber angle differentiation that are associated with a wide spectrum of other anterior eye segment abnormalities. Mech. Dev. 118: 3–17.

Beebe, D.C. and Coats, J.M. 2000. The lens organizes the anterior segment: specification of neural crest cell differentiation in the avian eye. Dev. Biol. 220:424-31.

Berdal, A., Lezot, F., Pibouin, L., Hotton, D., Ghoul-Mazgar, S., Teillaud, C., Robert, B., MacDougall, M. and Blin, C. 2002. *Msx1* Homeogene antisense mRNA in mouse dental and bone cells. Connect. Tissue Res.43: 148–152.

Blin-Wakkach, C., Lezot, F., Ghoul-Mazgar, S., Hotton, D., Monteiro, S., Teillaud, C., Pibouin, L., Orestes-Cardoso, S., Papagerakis, P., Macdougall, M., Robert, B. and Berdal, A. 2001. Endogenous *Msx1* antisense transcript: *In vivo* and *in vitro* evidences, structure, and potential involvement in skeleton development in mammals. Proc. Natl. Acad. Sci. 98(13): 7336–7341.

Blixt, Å., Landgren, H., Johansson, B.R. and Carlsson, P. 2007. *Foxe3* is required for morphogenesis and differentiation of the anterior segment of the eye and is sensitive to *Pax6* gene dosage. Dev. Biol. 302: 218–229.

Boogerd, C.J.J., Moorman, A.F.M. and Barnett, P. 2010. Expression of muscle segment homeobox genes in the developing myocardium. Anat. Rec. 293:998–1001.

Braga, V.M.M. 2002. Cell–cell adhesion and signalling. Curr. Opin. Cell Biol.14:546–556.

Cain, S., Martinez, G., Kokkinos, M. I., Turner, K., Richardson, R. J., Abud, H. E., Huelsken, J., Robinson, M. and de Iongh, R. 2008. Differential requirement for beta-catenin in epithelial and fiber cells during lens development. Dev. Biol. 321: 420–433.

Castro, C.H., Shin, C.S., Stains, J.P., Cheng, S.L., Sheikh, S., Mbalaviele, G, Szeinfeld, V.L. and Civitelli, R. 2004. Targeted expression of a dormant negative N-cadherin *in vivo* delays peak bone mass and increases adipogenesis. J. Cell Sci. 117(13): 2853-64.

Catron, K.M., Zhang, H., Marshall, S.C., Inostroza, J.A., Wilson, J.M. and Abate, C. 1995. Transcriptional repression by *Msx1* does not require homeodomain DNA-binding sites. Mol. Cell. Biol. 861–871.

Cha, J.Y., Birsoy, B., Kofron, M., Mahoney, E., Lang, S., Wylie, C. and Heasman, J. 2007.The role of *FoxC1* in early *Xenopus* development. Dev. Dynam. 236:2731–2741.

Chaffer, C.L., Thompson, E.W. and Williams, E.D. 2007. Mesenchymal to epithelial transition in development and disease. Cells Tissues Organs. 185: 7–19.

Chakrabarti, S., Kaur, K., Rao, K.N., Mandal, A.K., Kaur, I., Parikh, R.S. and Thomas, R. 2009. The Transcription factor gene *FOXC1* exhibits a limited role in primary congenital glaucoma. Invest. Ophthalmol. Vis. Sci. 50: 75– 83.

Chakravarti, S. 2001. The cornea through the eyes of knockout mice. Exp. Eye Res. 73: 411-419.

Chen, Q., Chen, T., Letourneau, P.C., Costa, L. D.F and Schubert, D. 2005. Modifier of cell adhesion regulates N-cadherin-mediated cell–cell adhesion and neurite outgrowth. J. Neurosci. 25(2):281–290.

Chen, H. and Ma, Z. 2007. N-cadherin expression in a rat model of retinal detachment and reattachment. Invest. Ophthalmol. Vis. Sci. 48:1832–1838.

Christofori, G. 2006. New signals from the invasive front. Nature. 441(7092): 444-450.

Chung, I., Han, J., Iwata, J. and Chai, Y. 2010. *Msx1* and *Dlx5* function synergistically to regulate frontal bone development. Genesis. 48(11): 645-655.

Collinson, JM., Quinn, J.C., Buchanan, M.A., Kaufman, M.H., Wedden, S.E., West, J.D. and Hill, R.E. 2001. Primary defects in the lens underlie complex anterior segment abnormalities of the *Pax6* heterozygous eye. Proc. Natl. Acad. Sci. 98 (17): 9688–9693.

Cvekl, A. and Tamm, E.R. 2004. Anterior eye development and ocular mesenchyme: New insights from mouse models and human diseases. Bioessays. 26(4): 374–386.

O'Day, D.H. 2010. Cell Adhesion Molecules (Internet). Available from: http://www.utm.utoronto.ca/~w3bio315/pdf/Cell%20Adhesion%20Molecule%20Types.pdf. Accessed: 20-05-2009.

Davis-Silberman, N. and Ashery-Padan, R. 2008. Iris development in vertebrates; genetic and molecular considerations. Brain Res. 1192:17-28.

Faber, S.C., Dimanlig, P., Makarenkova, H.P., Shirke, S., Ko, K. and Lang, R.A. 2001. Fgf receptor signaling plays a role in lens induction. Development. 128: 4425-4438.

Frederiksen, K., Jat, P.S., Valtz, N., Levy, D., McKay, R. 1988. Immortalization of precursor cells from the mammalian CNS. Neuron. 1: 439–448.

Fuse, N., Takahashi, K., Yokokura, S. and Nishida, K. 2007. Novel mutations in the *FOXC1* gene in Japanese patients with Axenfeld-Rieger syndrome. Mol. Vis. 13:1005-9.

Gould, D.B., Smith, R.S. and John, S.W.M. 2004. Anterior segment development relevant to glaucoma. Int. J. Dev. Biol. 48: 001-015.

Gage, P.J., Rhoades, W., Prucka, S.K. and Hjalt, T. 2005. Fate maps of neural crest and mesoderm in the mammalian eye. Invest. Ophthalmol. Vis. Sci. 46(11): 4200–4208.

Gage, P.J. and Zacharias, A.L. 2009. Signaling "cross-talk" is integrated by transcription factors in the development of the anterior segment in the eye. Dev. Dynam. 238:2149–2162.

Ganong, W.F. 2003. [Chapter Eight: Vision] in: Review of Medical Physiology. McGraw Hill. Twenty-first edition. Pp 150-151. Lange Medical Publications. India (2001).

Gordon, S.R. and Wood, M. 2009. Soybean agglutinin binding to corneal endothelial cell surfaces disrupts in situ monolayer integrity and actin organization and interferes with wound repair. Cell Tissue Res. 335(3): 551-563.

Gumbiner, B.M. 2005. Regulation of cadherin-mediated adhesion in morphogenesis. Nat. Rev. Mol. Cell Bio. 6: 622-634.

Han, J., Mayo, J., Xu, X., Li, J., Bringas, P., Maas, R.L., Rubenstein, J.L.R. and Chai, Y. 2009. Indirect modulation of Shh signaling by *Dlx5* affects the oral-nasal patterning of palate and rescues cleft palate in *Msx1*-null mice. Development. 136(24): 4225-4233

Hartsock, A. and Nelson, W.J. 2008. Adherens and tight junctions: structure, function and connections to the actin cytoskeleton. Biochim. Biophys. Acta. 1778(3): 660-669.

Harada, T., Harada, C. and Parada, L.F. 2007 Molecular regulation of visual system development: more than meets the eye. Genes Dev. 21: 367-378.

Hatta, K., Okada, T.S. and Takeichi, M. 1985. A monoclonal antibody disrupting calcium.dependent cell-cell adhesion of brain tissues: possible role of its target antigen in animal pattern formation. Proc. Nat. Acad, Sci. USA 80: 1038-1042.

Hatta, K., Nose, A., Nagafuchi, A. and Takeichi, M. 1988. Cloning and expression of cDNA encoding a neural calcium-dependent cell adhesion molecule: its identity in the cadherin gene family. J. Cell. Biol. 106: 873-881.

Hjalt, T.A. and Semina, E.V. 2005. Current molecular understanding of Axenfeld-Rieger syndrome. Expert Rev. Mol. Med. 7: 1-17.

Hsieh, Y., Zhang, X., Lin, E., Oliver, G. and Yang, X. 2002. The homeobox gene *Six3* is a potential regulator of anterior segment formation in the chick eye. Dev. Biol. 248: 265–280.

Huang, L., Chi, J., Berry, F.B., Footz, T.K., Sharp, M.W. and Walter, M.A. 2008. Human p32 is a novel *FOXC1*-interacting protein that regulates *FOXC1* transcriptional activity in ocular cells. Invest. Ophthalmol. Vis. Sci. 49(12): 5243-5249.

Hulpiau, P., van Roy, F. 2009. Molecular evolution of the cadherin superfamily. Int. J. Biochem. Cell Biol. 41: 349–369.

Idrees, F., Vaideanu, D.,Fraser, S.G., Sowden, J.C. and Khaw, P.T. 2006. A Review of Anterior Segment Dysgeneses . Surv Ophthalmol. 51(3):213- 231.

Ito, Y.A., Footz, T.K., Berry, F.B., Mirzayans, F., Yu, M., Khan, A.O. and Walter, M.A. 2009. Severe molecular defects of a novel *FOXC1* W152G mutation result in aniridia. Invest. Ophthalmol. Vis. Sci. 50(8): 3573-3579.

Itoh, M., Nagafuchi, A., Yonemura, S., Kitani-Yasuda, T., Tsukita, S. and Tsukita, S. 1993. The 220-kD protein colocalizing with cadherins in non-epithelial cells is identical to ZO-1, a tight junction-associated protein in epithelial cells: cDNA Cloning and Immunoelectron Microscopy. J. Cell. Biol. 121(3):491-502.

Ittner, L.M., Wurdak, H., Schwerdtfeger, K., Kunz, T., Ille, F., Leveen, P., Hjalt, T.A., Suter, U., Karlsson, S., Hafezi, F., Born, W. and Sommer, L. 2005. Compound developmental eye disorders following inactivation of TGFβ signaling in neural-crest stem cells. J. Cell. Biol. 4(11): 1-16.

Jat, P.S., Sharp, P.A., 1989. Cell lines established by a temperature-sensitive simian virus 40 large-T-antigen gene are growth restricted at the nonpermissive temperature. Mol. Cell Biol. 9: 1672–1681.

Jowett, A.K., Vainio, S., Ferguson, M.W.J., Sharpe, P.T. and Thesleff, I. 1993. Epithelial-mesenchymal interactions are required for *msx 1* and *msx 2* gene expression in the developing murine molar tooth. Development.117: 461-470.

Joyce, N.C. 2003. Proliferative capacity of the corneal endothelium. Prog. Retin. Eye Res. 22: 359–389

Katerji, S., Vanmuylder, N., Svoboda,M., Rooze, M. and Louryan, S. 2009. Expression of *Msx1* and *Dlx1* during Dumbo rat head development: Correlation with morphological features. Genet. Mol. Biol.32(2): 399-404.

Kelm, J.M., Timmins, N.E., Brown, C.J., Fussenegger, M. and Nielsen, L.K. 2003. Method for generation of homogeneous multicellular tumor spheroids applicable to a wide variety of cell types. Biotechnol. Bioeng. 83(2): 173-180.

Kidson, S.H., Kume, T., Deng, K., Winfrey, V. and Hogan, B.L.M. 1999. The Forkhead/Winged-Helix gene, *Mf1*, is necessary for the normal development of the cornea and formation of the anterior chamber in the mouse eye. Dev. Biol. 211:306–322.

Kim, J. and Lauderdale, J.D. 2008. Over-expression of pairedless *Pax6* in the retina disrupts corneal development and affects lens cell survival. Dev. Biol. 313: 434–454.

Ko, S.O., Chung, I.H., Xu, X., Oka, S., Zhao, H., Cho, E.S., Deng, C. and Chai, Y. 2007. *Smad4* is required to regulate the fate of cranial neural crest cells. Dev. Biol. 312(1): 435-447.

Komatireddy, S., Chakrabarti, S., Mandal, A.K., Reddy, A.B.M., Sampath, S., Panicker, S.G. and Balasubramanian, D. 2003. Mutation spectrum of *FOXC1* and clinical genetic heterogeneity of Axenfeld-Rieger anomaly in India. Mol. Vis. 9:43-48.

Kulesa, P.M., Bailey, C.M., Kasemeier-Kulesa, J.C. and McLennan, R. 2010. Cranial neural crest migration: New rules for an old road. Dev. Biol. 344: 543–554

Kume, T., Deng, K. and Hogan, B.L.M. 2000. Murine forkhead/ winged helix genes *Foxc1* (*Mf1*) and *Foxc2* (*Mfh1*) are required for the early organogenesis of the kidney and urinary tract. Development. 127:1387-1395.

Kume, T., Jiang, H.Y., Topczewska, J.M. and Hogan, B.L.M. 2001. The murine winged helix transcription factors, *Foxc1* and *Foxc2*, are both required for cardiovascular development and somitogenesis. Genes and Dev. 15: 2470-2482.

Lazzarotto-Silva, C., Bemvenuti, A., de Castro Silva, T.M. and Abdelhay, E. 2005. Possible role of *Msx1* in murine hematopoiesis. Braz. J. Morphol. Sci. 22(1): 9-17.

Lehmann, O.J., Ebenezer, N.D., Jordan, T., Fox, M., Ocaka, L., Payne, A., Leroy, B.P., Clark, B.J., Hitchings, R.A., Povey, S., Khaw, P.T. and Bhattacharya, S.S. 2000. chromosomal duplication involving the forkhead transcription factor gene *Foxc1* causes iris hypoplasia and glaucoma. Am. J. Hum. Genet. 67:1129–1135.

Libby R.T., Smith, R.S., Savinova, O.V., Zabaleta, A., Martin, J.E., Gonzalez, F.J., John, S.W. 2003. Modification of ocular defects in mouse developmental glaucoma models by tyrosinase. Science. 299:1578–1581.

Lincecum, J.M., Fannon, A., Sassoon, D.A., Song, K., Wang, Y., 1998. *Msh* homeobox genes regulate cadherin-mediated cell adhesion and cell-cell sorting. J. Cell. Biochem. 70: 22-28.

Livak, K.J. and Schmittgen, T.D. 2001. Analysis of relative gene expression data using real-time quantitative PCR and the 2(-Delta Delta C(T)) Method. Methods. 25(4): 402-408.

Luo, Y., High, F.B., Epstein, J.A. and Radice, G.L. 2006. N-cadherin is required for neural crest remodeling of the cardiac outflow tract. Dev. Biol. 299: 517–528.

Lwigale, P.Y. and Bronner-Fraser, M. 2007. Lens-derived Semaphorin3A regulates sensory innervation of the cornea. Dev. Biol. 306: 750–759.

Macdonald, I.M., Tranand, M. and Musarella, M.A. 2004. Ocular Genetics: Current Understanding. Surv. Ophthalmol. 49(2):159-196.

Mani, S.A., Guo, W., Liao, M., Eaton, E.N., Ayyanan, A., Zhou, A.Y., Brooks, M., Reinhard, F., Zhang, C.C., Shipitsin, M., Campbell, L.L., Polyak, K., Brisken, C., Yang, J. and Weinberg, R.A. 2008. The epithelial mesenchymal transition generates cells with properties of stem cells. Cell. 133(4): 704–715.

Mattiske, D., Kume, T. and Hogan, B.L. 2006. The mouse forkhead gene *Foxc1* is required for primordial germ cell migration and antral follicle development. Dev Biol. 290:447–458.

Matsuda, T., Fujio, Y., Nariai, T., Ito, T., Yamane, M., Takatani, T., Takahashi, K. And Azuma, J. 2006. N-cadherin signals through Rac1 determine the localization of connexin 43 in cardiac myocytes. J. Mol. Cell. Cardiol. 40: 495–502.

Morales, A.V., Barbas, J.A. and Nieto, M.A. 2005. How to become neural crest: From segregation to delamination. Semin. Cell. Dev. Biol. 16(6): 655-662.

Oka, K., Oka, S., Sasaki, T., Ito, Y., Bringas Jr., P., Nonaka, K. and Chai, Y. 2007. The role of TGF-β signaling in regulating chondrogenesis and osteogenesis during mandibular development. Dev. Biol. 303(1): 391-404.

Oshima, Y., Watanabe, N., Matsuda, K., Takai, S., Kawata, M. and Kubo, T. 2005. Behavior of transplanted bone marrow–derived gfp mesenchymal cells in osteochondral defect as a simulation of autologous transplantation. J. Histochem. Cytochem. 53(2): 207–216.

Packer, A.I., Elwell, V.A., Parnass, J.D., Knudsen, K.A. and Wolgemuth, D.J. 1997. N-cadherin protein distribution in normal embryos and in embryos carrying mutations in the homeobox gene *Hoxa-4*. Int. J. Dev. Biol. 41:459-468.

Panicker, S.G., Sampath, S., Mandal, A.K., Reddy, A.B.M., Ahmed, N. and Hasnain, S.E. 2002. Novel mutation in *FOXC1* wing region causing Axenfeld-Rieger anomaly. Invest. Ophth. Vis. Sci. 43 (12): 3613-3616.

Petit, S., Meary, F., Pibouin, L., Jeanny, J., Fernandes, I., Poliard, A., Hotton, D., Berdal, A. and Babajko, S. 2009. Autoregulatory loop of *Msx1* expression involving its antisense transcripts. J. Cell. Physiol. 220: 303–310.

Pirity, M.K., Wang, W., Wolf, L.V., Tamm, E.R., Schreiber-Agus, N. and Cvek, A. 2007. Rybp, a polycomb complex-associated protein, is required for mouse eye development. BMC Dev. Biol. 7:39.

Polyak, K. and Weinberg, R.A. 2009. Transitions between epithelial and mesenchymal states: acquisition of malignant and stem cell traits. Nat. Rev. Cancer. 9: 265-273.

Pontoriero, G.F., Smith, A.N., Miller, L.D., Radice, G.L., West-Mays, J.A. and Lang, R.A. 2009. Co-operative roles for E-cadherin and N-cadherin during lens vesicle separation and lens epithelial cell survival. Dev. Biol. 326: 403–417.

Radice, G.L., Rayburn, H., Matsunami, H., Knudsen, K.A., Takeichi, M. and Hynes, R.O. 1997. Developmental defects in mouse embryos lacking N-cadherin. Dev. Biol. 181: 64–78.

Ramachandran, C. and Srinivas, S.P. 2010. Formation and assembly of adherens and tight junctions in the corneal endothelium: Regulation by actomyosin contraction. Invest. Opthalmol. Vis. Sci. 51(4): 2139-48.

Reneker, L.W., Silversides, D.W., Xu, L. and Overbeek, P.A. 2000. Formation of corneal endothelium is essential for anterior segment development – a transgenic mouse model of anterior segment dysgenesis. Development. 127: 533-542.

Rice, R., Rice, D.P., Olsen, B.R. and Thesleff, I. 2003. Progression of calvarial bone development requires *Foxc1* regulation of *Msx2* and *Alx4*. Dev. Biol. 262: 75–87.

Rozen, S., Skaletsky, H.J. 2000. Primer3 on the WWW for general users and for biologist programmers. In: Krawetz S, Misener S (eds) Bioinformatics Methods and Protocols: Methods in Molecular Biology. Humana Press, Totowa, NJ, pp 365-386.

Saleem, R.A., Banerjee-Basu, S., Berry, F.B., Baxevanis, A.D. and Walter, M.A. 2003. Structural and functional analyses of disease-causing missense mutations in the forkhead domain of *FOXC1*. Hum. Mol. Gen. 12(22): 2993–3005.

Saleem, R.A., Banerjee-Basu, S., Murphy, T.C., Baxevanis, A. and Walter, M.A. 2004. Essential structural and functional determinants within the forkhead domain of FOXC1. Nucleic Acids Res. 32(14): 4182–4193.

Seo, S., Fujita, H., Nakano, A., Kang, M., Duarte, A. and Kume, T. 2006. The forkhead transcription factors, *Foxc1* and *Foxc2*, are required for arterial specification and lymphatic sprouting during vascular development. Dev Biol. 294:458–470.

Skarie, J.M. and Link, B.A. 2009. FoxC1 Is Essential for Vascular Basement Membrane Integrity and Hyaloid Vessel Morphogenesis. Invest. Ophthalmol. Vis. Sci. 50: 5026–5034.

Smith, R.S., Zabaleta, A., Kume, T., Savinova, O.V., Kidson, S.H., Martin, J.E., Nishimura, D.Y., Alward, W.L., Hogan, B.L., John, S.W. 2002. Haploinsufficiency of the transcription factors FOXC1 and FOXC2 results in aberrant ocular development. Human Mol. Genet. 9: 1021-1032.

Sommer, P., Napier, H.R., Hogan, B.L. and Kidson, S.H. 2006. Identification of *Tgfβ1i4* as a downstream target of *Foxc1*. Develop. Growth Differ. 48, 297–308.

Strungaru, M.H., Dinu, I. and Walter, M.A. 2007. Genotype-phenotype correlations in Axenfeld-Rieger malformation and glaucoma patients with *FOXC1* and *PITX2* Mutations. Invest. Ophthalmol. Vis. Sci. 48(1): 228-237.

Takeichi, M., 1991. Cadherin cell adhesion receptors as a morphogenetic regulator. Science. 51: 1451–1455.

Tamimi, Y., Lines, M., Coca-Prados, M. and Walter, M.A. 2004. Identification of target genes regulated by *FOXC1* using nickel agarose–based chromatin enrichment. Invest. Ophthalmol. Vis. Sci. 45(11): 3904-3913.

Tamimi, Y., Skarie, J.M., Footz, T., Berry, F.B., Link, B.A. and Walter, M.A. 2006. FGF19 is a target for FOXC1 regulation in ciliary body-derived cells. Mol. Genet. 15(21): 3229–3240.

Thiery, J.P., Acloque, H., Huang, R.Y.J. and Nieto, M.A. 2009. Epithelial-Mesenchymal Transitions in Development and Disease. Cell. 139: 871-890.

Trainor, P.A. 2005. Specification of neural crest cell formation and migration in mouse embryos. Semin. Cell Dev. Biol. 16: 683–693.

Troyanovsky, S.M. 1999. Mechanism of cell–cell adhesion complex assembly. Curr. Opin. Cell Biol. 11:561–566.

Van Aken, E., Papeleu, P., De Potter, P., De Laey, J.J., Mareel, M. 2000. Cadherin expression in the eye. Bull. Soc. Belge. Ophtalmol. 278: 55-59.

Vanselow, J., Nürnberg, G., Koczan, D., Langhammer, M.,Thiesen, H. and Reinsch, N. 2008. Expression profiling of a high-fertility mouse line by microarray analysis and qPCR. BMC Genomics. 9(1):307.

Vieira, A.R. 2008. Unraveling Human Cleft Lip and Palate Research. J. Dent. Res. 87: 119-125.

Vincent, A., Billingsley, G., Priston, M., Glaser, T., Oliver, E., Walter, M., Ritch, R., Levin, A. and Héon, E. 2006. Further support of the role of *CYP1B1* in patients with Peter's anomaly. Mol.Vis. 12:506-510.

Wang, W., McNatt, L.G., Shepard, A.R., Jacobson, N., Nishimura, D.Y., Stone, E.M., Sheffield, V.C. and Clark, A.F. 2001. Optimal procedure for extracting RNA from human ocular tissues and expression profiling of the congenital glaucoma gene *FOXC1* using quantitative RT-PCR. Mol.Vis. 7:89-94.

Wu, F., Lee, S., Schumacher, M., Jun, A. and Chakravarti, S. 2008. Differential gene expression patterns of the developing and adult mouse cornea compared to the lens and tendon. Exp. Eye Res. 87: 214–225.

Wurm, A., Sock, E., Fuchshofer, R., Wegner, M. And Tamm, E.R. 2008. Anterior segment dysgenesis in the eyes of mice deficient for the high-mobility-group transcription factor *Sox11*. Exp. Eye Res. 86: 895–907.

Xu, L., Overbeek, P.A. and Reneker, L.W. 2002. Systemic analysis of E-, N- and P-cadherin expression in mouse eye development. Exp. Eye Res. 74: 753-760.

Zarbalis, K., Siegenthaler, J.A., Choe, Y., May, S.R., Peterso, A.S. and Pleasure, S.J. 2007. Cortical dysplasia and skull defects in mice with a *Foxc1* allele reveal the role of meningeal differentiation in regulating cortical development. Proc. Natl. Acad. Sci. 104 (35): 14002–14007.

Zelenka, P.S. and Arpitha, P. 2008. Coordinating cell proliferation and migration in the lens and cornea. Semin. Cell Dev. Biol. 19:113–124.

Zhang, Y., Burgess, D., Overbeek, P.A. and Govindarajan, V. 2008. Dominant inhibition of lens placode formation in mice. Dev. Biol. 323: 53–63.